E-20-E76

Mercury Methylation and Fate in *Spartina* Saltmarsh Systems – Assessment of Fundamental Processes Determining Production and Fate of Methylmercury in Natural and Contaminated Sediments

Saunders, F. M., Frischer, M., Kostka, J., King, J., Sauer, R., Fu. T., Genzler, S., and Healy, M.,
of
Georgia Institute of Technology,
Skidaway Institute of Oceanography, and
Florida State University

Final Report
to
HSRC/South-Southwest
LSU, Baton Rouge LA

September 2002

TABLE OF CONTENTS

LIST OF FIGURES

LIST OF TABLES

SUMMARY

Sediments from a coastal Georgia Superfund site were investigated in a specially-designed mesocosm facility, the Bioremediation and Environmental Research Mesocosms (BERM), as working-scale models of contaminated saltmarsh. The BERM was unique in that sediment could be placed into a controlled, contained mesocosm environment for study of variables affecting sediment and contaminant chemistry under a simulated tidal cycle. Three sediment cells were used for this study: one vegetated with *Spartina* in Hg-contaminated sediment, one unvegetated in Hg-contaminated sediment, and one vegetated in pristine sediment, which served as the control cell.

This project sought to quantitatively elucidate roles of chemical variables and *Spartina* plants in Hg transformation (primarily microbially-mediated methylation and demethylation) and availability in saltmarsh sediments. An integrated study of factors affecting mercury methylation and demethylation, incorporating geochemistry, rate measurements, plant influence, and contaminant chemistry, has not previously been conducted. Such a study is necessary in order to understand the controls on mercury methylation in saltmarsh sediments and is the subject of this thesis.

The saltmarsh mesocosms were observed to equilibrate and mimic the native marsh environment. Sediments studied to a depth of 10 cm exhibited stratification of geochemical parameters while *Spartina* plants were observed to acclimate to the mesocosm environment. Sulfate reduction rates (SRRs), an indicator of microbial

metabolism, peaked in the top two cm of sediment in each mesocosm and were higher in contaminated LCP site sediments relative to pristine Groves Creek (GC) sediments. Higher organic matter content in the LCP sediments may have contributed to this. Also, SRR were quicker to recover from winter minimums in the vegetated mesocosms.

Chemical variables monitored in mesocosm porewaters included: pH, dissolved inorganic carbon, ammonium, reduced sulfide, reduced iron, and sulfate. Similar to the natural marsh, sulfate levels decreased with depth for the most part in each of the mesocosms and sulfide levels accumulated to a slight degree in the LCP mesocosms. The GC mesocosm showed nearly no sulfide; this may be explained by the consistent presence of reduced iron in the porewaters of this mesocosm. Iron, in oxidized or reduced form, may have precipitated available sulfides and dampened sulfate reduction since iron reduction is more energetically-favorable. Reduced iron was barely evident in the LCP mesocosms; this may be explained by the different origin of the sediments.

In addition to sediment geochemistry, mercury concentrations (methylmercury and total mercury) were determined in the solid phase and in porewater of mesocosm sediment. With these measurements, controls of methyl mercury (MeHg) formation over a seasonal growth cycle of *Spartina* in the mesocosms were investigated. Data indicated that the LCP vegetated mesocosm showed lower levels of MeHg than the LCP unvegetated mesocosm during the active growing season of *Spartina*, perhaps due to oxidative demethylation stimulated by the plants. This was especially evident in average MeHg porewater measurements, which exhibited linear relationships with integrated

SRR. This relationship was negative for the vegetated mesocosms and positive for the unvegetated mesocosm. Total Hg, both in solid phase and porewater, remained fairly unchanged in the mesocosms. Surprisingly high levels of THg in porewaters may have been due to sulfide controls on Hg speciation and bioavailability. It was also found that relative abundance of MeHg in sediment was inversely correlated to the total mercury content in those sediments.

The growth of *Spartina* appeared to be only slightly affected by the Hg-contaminated sediment. Above-ground biomass measurements (survival rate, plant height, and additional sprouting) were shown to be higher, but not to a great degree, in GC sediments relative to sediments derived from the LCP mesocosm. Sulfide may have hindered plant growth more than Hg did since sulfide levels were higher in the LCP mesocosm and sulfide is a known phytotoxin.

The mesocosms were also evaluated on the effectiveness of the design and simulated tidal cycle, i.e. how the influent water flushed through the mesocosm sediments. Using sulfate concentration as the chief mass-balance parameter, it was found that sulfate levels in surface sediments exceeded levels found in influent water and re-oxidation processes near the surface were substantial.

CHAPTER I

INTRODUCTION

Project Background

A southeastern Georgia saltmarsh, adjacent to an industrial site and dominated by cordgrass (*Spartina alterniflora*), was designated a Superfund site (LCP site) in 1994. As a result of 80 years of industrial activities and discharges, saltmarsh sediments were highly-contaminated with mercury, ranging in the parts-per-thousand levels near the site to the low (less than 100) parts per million (μg/g) in the surrounding estuary. Mercury was used at LCP in cathodes as part of chlor-alkali chemical production.

Sediment toxicity attributed to Hg has been confirmed at the site using bio-assays and specimens. This is of concern in that the LCP saltmarsh is part of the lower Turtle River - Brunswick Estuary, an environmentally-sensitive area that provides important habitat for endangered species and supports an important sport and commercial fishery (Winger *et al.*, 1993).

The health hazards of mercury are well-documented. The lipophilic nature of organic mercury, CH_3Hg^+ (methyl mercury) in particular, leads to enhanced bioaccumulation in the food chain (Mason *et al.*, 1996; Watras, 1994; Kannan *et al.*, 1998). The EPA concluded that consumption of contaminated fish and shellfish is the primary route of human exposure to Hg (EPA, 1997). However, a limited amount of

information is available on the fate and transport of Hg in estuarine environments where Hg enters the food chain (Mason and Fitzgerald, 1991; Gilmour and Henry, 1991; Gagnon *et al.*, 1996).

Three saltmarsh mesocosms were set up to provide an accessible, controlled environment for scientific study of LCP saltmarsh sediments. Mercury-contaminated sediments were placed in two mesocosms, while pristine sediment was placed into a third mesocosm. Prior to mercury analysis, the work of Gentzler (1999) validated the equilibration and usefulness of these mesocosms. Additionally, Frischer *et al.* (2000) found that the relative distribution of sulfate-reducing bacteria was similar to that observed in natural marsh systems. This project also built on findings of King (1999), who confirmed in laboratory studies of sediment slurries that mercury methylation rate and sulfate reduction rate occur in direct proportion and the relationship was dependent on mercury availability, growth substrates, temperature, and oxygen.

Objectives

The research summarized in this report was for a project entitled, "*Interactive Roles of Microbial and Spartina Populations in Mercury Methylation Processes in Bioremediation of Contaminated Sediment in Saltmarsh Systems.*" The project was funded by the Hazardous Substance Research Center, South & Southwest, and included construction of three mesocosms to simulate both pristine and contaminated saltmarsh

ecosystems. Due to the difficulties associated with sampling at Superfund sites, mesocosms were chosen as the basis for this study.

Before mercury methylation research could begin, the mesocosms were set up and monitored to assess system equilibration. In the Gentzler (1999) study, equilibration was monitored and measured as the stratification of sediment geochemistry and microbial process rates. Determination of mesocosm equilibration was essential since the basis for this research was to gain a better understanding of mercury methylation in natural saltmarsh ecosystems.

Data from Georgia saltmarshes were used for comparison during equilibrium assessment. The top 10 cm of sediment were studied since a significant portion of saltmarsh biogeochemical processes occurs in this interval (Hines *et al*, 1989). Gentzler (1999) reported on a five-month period of mesocosm analysis. Mercury analysis was not performed in this period.

In this research, direct measurements in the three mesocosms were made in order to determine the roles of master chemical variables and microbial activity in mercury methylation and demethylation. Several studies have been carried out to delineate factors affecting methylation of mercury in marine sediments (King, 1999; Weber *et al.*, 1998; Compeau and Bartha, 1984; Compeau and Bartha, 1985). The geochemical effects of the *Spartina* growth cycle have also been studied (Hines *et al.*, 1989; Kostka and Luther, 1995). Currently, the controls of mercury methylation and demethylation are being further studied to determine nutrient requirements, the role of enzymes, and specific bacterial species involved. Demethylation is significant because it counters methylation

and converts toxic MeHg to Hg(II), which can then bind with products of microbial metabolism or be further reduced to volatile Hg(0). An integrated study of factors affecting methylation and demethylation, incorporating geochemistry, rate measurements, plant influence, and contaminant chemistry, has not been conducted. Such a study is necessary in order to understand the controls on mercury methylation in saltmarsh sediments and is the subject of this thesis.

Specific objectives of this thesis were to:

1) Ensure that equilibration of the simulated saltmarsh environment had occurred in the mesocosms using measurements of pertinent geochemical parameters and microbial process rates. Compare the results to field observations of stratified redox zones.

2) Measure and compare mercury levels in contaminated and pristine sediments over a *Spartina* growing season. This was accomplished for total mercury and methyl mercury with state-of-the-art ultra-trace-level analytical techniques.

3) Ascertain relationships among sediment geochemistry, microbial process rates, mercury levels and mercury speciation, and *Spartina* vegetation in the saltmarsh ecosystem. This was accomplished by comparing depth profiles and integrated measurements of chemical variables with *Spartina* biomass data over a growing season in the pristine-vegetated, contaminated-vegetated, and contaminated-unvegetated mesocosms.

4) Assess the effectiveness of the BERM mesocosms at simulating a natural system, both in design and in mimicking the natural tidal cycle. This was accomplished with measurements of flow rates and comparisons of biochemical variables with field data.

5) Determine why sulfate levels in surficial porewaters are higher than levels in influent waters. This was accomplished by mathematically assessing sulfide re-oxidation and input of oxygen in a mass balance.

CHAPTER II

LITERATURE REVIEW

History of Mesocosms

Experimental ecosystems, or mesocosms, provide engineers and scientists with an effective tool for gaining knowledge about particular ecosystems and for testing hypotheses concerned with factors that control ecosystems. Inputs and outputs can be controlled and monitored and potential impacts of ecosystem changes can be assessed. However, extrapolation to the natural environment must be made with caution and the extent of mesocosm equilibrium must be considered. Differences in physical, chemical, and biological conditions between mesocosms and the natural environment have to be taken into account.

Mesocosms were defined on the basis of size at the Symposium on Enclosed Marine Experimental Ecosystems, sponsored by the U.S. National Science Foundation and the Canadian Research Council. The definition specified a size range larger than bench-top containers but smaller than, and isolated from, any sub-unit of the natural environment (Grice and Reeve, 1982).

British Columbia's Controlled Ecosystem Pollution Experiment (CEPEX), San Diego State University's Pacific Estuarine Research Laboratory (PERL), and three other

mesocosm facilities summarized below are mesocosms that have been used over the past two decades for research purposes.

Kiel Plankton Tower

The Kiel Plankton Tower was used to study plankton-sediment interactions in the western Baltic Sea. Four nylon-coated polyethylene bags, each two meters in diameter, were secured to a tower consisting of a rectangular grid of steel. This structure was placed in the Kiel Bight in the western Baltic Sea. The bags extended from above the water surface to the bottom sediment surface and their transparent nature allowed for simulation of temperature and light variations experienced in the Baltic Sea (Grice and Reeve, 1982). No equilibration studies were conducted in the mesocosms.

MERL Mesocosms

The Marine Ecosystem Research Laboratory (MERL) of the University of Rhode Island uses land-based tanks containing sediment and seawater from Narragansett Bay for examining eutrophication and biological and chemical responses of ecosystems when exposed to petroleum hydrocarbons and trace metals (Grice and Reeve, 1982). These 15,000-L mesocosms, 1.8 m in diameter and 5.4 m in height, have a sediment depth of 0.3 m and can operate in a batch or flow-through mode.

Experiments have shown that annual nutrient cycles and trace metal behavior in the MERL tanks mimic those of Narragansett Bay (Santschi *et al.*, 1982; Hunt and Smith,

1982). Results from MERL have been instrumental in showing the importance of nitrogen in eutrophication. It was previously thought that eutrophication processes in coastal marine ecosystems paralleled those in lakes and depended on phosphorus, but experiments indicated that N inputs, independent of P, caused large increases in both rates of algal production and abundance of phytoplankton (Webb, 1998).

MLI Benthic Mesocosm Facility

Four benthic mesocosms were constructed at Maurice Lamontagne Institute (MLI) of Quebec, Canada in 1990. These mesocosms provided a research environment for study of biogeochemistry of sediment recovered from depths of 300-400 m in the Laurentian Trough of the Gulf of St. Lawrence, off the coast of Canada. Comparisons were made with macrofaunal and meiofaunal numbers, various microbiological parameters, and respiration rates in benthic mesocosm sediments weeks (Silverberg *et al.*, 1995).

The 1.0-m x 1.0-m x 0.7-m basins featured an independent overlying water circulation system for each mesocosm. In order to limit the build-up or loss of nutrients and unidentified metabolic by-products and other chemicals, one third of the overlying water was replaced every two weeks.

Equilibration was assessed by observation of surface appearance and visible activity, measurements of macrofauna and meiofauna survival, measurements of oxygen uptake for the whole sediment, and analysis of ammonia, nitrate, phosphate, and silicate from overlying water. All of these parameters were compared to field data from the

sediment collection area. The MLI basins, while unable to replicate the immense pressure at 300-400-m depths and low overlying dissolved oxygen concentrations, did manage to maintain species composition and principal macrofaunal abundances of the Laurential Trough benthos for periods exceeding a year (Silverberg *et al.*, 1995).

Saltmarsh Ecosystems

Saltmarshes ecosystems occupy the intertidal zone of many marine coastlines. These marshes are particularly dominant along the Eastern Seaboard and Gulf Coast of North America, where they cover vast expanses behind barrier islands and in bays. Saltmarshes represent one of the most productive ecosystems on the planet, providing structure, habitat, and food for developing fish and shellfish, as well as many other animals and plants. Saltmarshes also lessen impacts of floods, storm surges, and coastal erosion and are able to filter out nutrients, pollutants, and pathogens (Alongi, 1998).

Physically, saltmarshes are low-elevation areas regularly flooded by brackish or saltwater tides. Slopes of most marshes are relatively flat and their mean elevation is near or slightly below the mean high tide level. This allows for the rising tidal waters to inundate the saltmarsh sediments. Along much of the Eastern Seaboard and Gulf Coast of North America, tides flood over much of the surface of marsh sediments twice each day, although tides of lower amplitude result in less frequent flooding in some areas (Howarth, 1993).

Spartina alterniflora

Saltmarshes are often identified by the vascular plants that dominate the ecosystem. The diversity of saltmarsh grass species is low. Along the east coast of North America, the dominant macrophyte is *Spartina alterniflora*, also known as smooth cord grass. Generally, *Spartina* will take one of two growth forms. Nearest the creek bank, where tidal drainage is greatest, the tall form of *Spartina* is present. The short form can be found further away from the intertidal creeks, where drainage occurs mostly along the sediment surface as the tide recedes. Figure 2.1 shows a typical *Spartina* saltmarsh transect.

Spartina growth is dominated by oxygen supply. Marsh grasses translocate necessary oxygen to their roots via air-space tissue, oxidizing the sediment proximate to their roots and rhizomes (Mendelssohn *et al.*, 1981). However, the surrounding sediment substrate may be reduced to a point where aerobic respiration can not occur. Mendelssohn *et al.* (1981) presented data demonstrating that root oxygen deficiencies may produce variations in height and productivity. Measurements of plant vigor, such as plant height and density, at inland sites were lowest compared to sites closer to intertidal creeks. The lower elevation and reduced interstitial (pore) water movement of inland sites result in waterlogging, minor turnover of water, and consequently a highly-reduced environment. At creek bank sites, regular tidal fluxes readily supply root zones with oxygen-rich water, whereas inland sites remain stagnant. Inland plants accumulate phytotoxins and eventually create the "dieback" or "ponded marsh" commonly seen in saltmarshes.

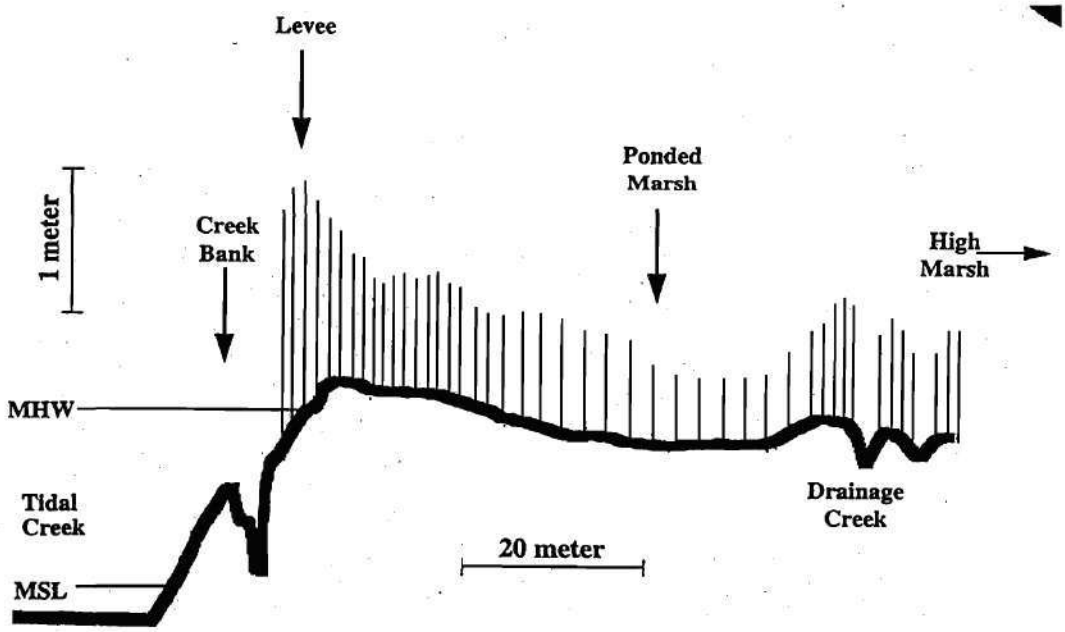

Figure 2.1 Transect of a saltmarsh, illustrating gradient in above-ground biomass and tidal height. MSL = mean sea level; MHW = mean high water (Koretsky *et al.*, 2000).

In Figure 2.1, the lower elevation and reduced plant growth of the ponded marsh are shown. Mendelssohn *et al.* (1981) found *Spartina* height reduced by as much as 45 percent and density reduced by as much as 70 percent at inland sites when compared to plants on creek banks. Wiegart (1978) artificially increased drainage within a stand of *Spartina* and observed an increase in plant height. The enhanced growth was attributed to increased oxygen supply and removal of phytotoxins.

The seasonal growth cycle of *Spartina* begins with vegetative growth in the spring. Plants remain vigorous through the summer months and enter reproductive growth in late summer. Senescence usually begins in October and, by November, *Spartina* lose color and are fairly dormant in growth until the seasonal cycle resets in spring.

Besides oxygen deficiency, other factors affect *Spartina* growth. The optimal temperature for *Spartina* is 30-35°C (Alongi, 1998); climate changes thus give rise to a seasonal growth cycle. Hydrogen sulfide in porewater is a phytotoxin and can inhibit energy generation (Koch *et al.*, 1990). Further, *Spartina* grows best at a salinity of 10 parts-per-thousand (ppt), but survives in salinities up to 70 ppt. However, at high levels, salt upsets water balance in the plant cells (Alongi, 1998).

Organic Matter Inputs in Saltmarshes

High rates of primary production from marsh grasses and surface algae are mainly responsible for large amounts of organic matter present in the marsh sediments, which in turn supports high rates of heterotrophic activity. Net primary production by dominant

grasses and surface algae range from 540-3400 g/m^2-yr as carbon. In addition, in some marshes, production by chemoautotrophic sulfur-oxidizing bacteria may provide another 275-500 g/m^2-yr (Howarth, 1993).

It is believed that at least half of all net primary production of marsh grasses occurs as below-ground production from roots and rhizomes (Pomeroy *et al.* 1981), with rates ranging from 220-1680 g/m^2-yr (Good *et al.*, 1982). *Spartina* roots have been shown to produce low-molecular-weight organic compounds such as ethanol and malate when roots metabolize anaerobically (Mendelssohn *et al.*, 1981). Anaerobic fermentation during organic matter remineralization, mediated by microorganisms, also produces alcohols and low-molecular-weight fatty acids, such as acetate (Howarth, 1993). These relatively labile organic materials diffuse into surrounding sediments, fueling high rates of microbial processes. Microbes such as sulfate-reducing bacteria (SRB) can utilize an array of electron donors, including hydrogen, low-molecular-weight organic acids (e.g. lactate, acetate, and propionate), and long-chain fatty acids (Widdel, 1988).

Aerobic Respiration in Saltmarsh Sediments

The depth to which oxygen penetrates into saltmarsh sediment systems varies from marsh to marsh. Differences in frequency of tidal flooding, porosity of sediments, and distance from intertidal creeks can influence the rate and extent that oxygen diffuses into sediments. In general, when saturated with water, marsh sediments are anoxic below the top few millimeters (King, 1988). The small oxic zone in these sediments can be

attributed to high rate of oxygen consumption by surface sediments and the slow rate of oxygen diffusion through water-saturated pores of low-permeability sediments.

Most saltmarshes on the east coast of North America are flooded twice daily by tides. In these areas, water lost from sediments due to drainage or evapotranspiration at low tide is replenished relatively quickly the same day. Therefore, saltmarsh sediments tend to stay saturated with water and anoxic to within a centimeter of the surface (Howarth, 1993).

Although the bulk of aerobic respiration tends to occur on the surface of these sediments, there are circumstances that lead to the presence of oxygen and its availability as an electron acceptor at lower depths. Low-tide drainage and diffusion provide an opportunity for oxygen to enter sediment pore spaces; high-porosity sediments are vulnerable to these two situations. In addition, air-space tissue in vascular saltmarsh grasses and other plants allow oxygen diffusion from the atmosphere into the rhizosphere. Bioirrigation by fiddler crabs and other macrofauna also brings in oxygen and is important to biogeochemical exchange. Quantification of oxygen diffusion occurring through the plant rhizosphere has been difficult due to the fact that oxygen is consumed both in aerobic respiration and in chemical oxidation of reduced species such as sulfides.

Anaerobic Respiration in Saltmarsh Sediments

Anaerobic respiration dominates below the thin oxic zone at surfaces of saltmarsh sediments. In the absence of oxygen, bacteria utilize alternate electron acceptors for

respiration in the order in which free energy is obtained from their reduction, as depicted in Figure 2.2. Bacteria can use nitrate, manganese, iron, sulfate, and carbon dioxide as electron acceptors, with nitrate being the most energetically favorable and carbon dioxide the least favorable. Thus, in saltmarsh sediment systems, nitrate reduction is expected to dominate in anoxic sediment, followed by manganese and iron reduction, and then sulfate reduction and methanogenesis. A hypothetical depth profile of porewater chemical constituents resulting from bacterial respiration is shown in Figure 2.3. However, in natural settings, other factors can affect or dictate which respiration process dominates.

It is believed that only limited denitrification (or nitrate reduction) occurs in saltmarshes due to a low supply of nitrate (Howarth, 1993). Although important in the nitrogen cycle for marshes, proportionally little carbon is consumed by denitrifiers, accounting for only a small fraction of total carbon oxidation. Several studies have shown that denitrification accounts for less than one percent of total carbon oxidation (Alongi, 1998; Howarth, 1989). Further research is necessary to determine the extent of coupled nitrification and denitrification occurring in the rhizosphere of *Spartina.* Nitrification is the oxidation of ammonium to nitrate by autotrophic bacteria. Since high concentrations of ammonium are found in the rhizosphere, it is possible that the oxygen injected into this zone by grass roots could chemically oxidize ammonium or allow for nitrification and provide a supply of nitrate for denitrifying bacteria. In addition, vegetation can directly take in ammonium as its nitrogen source (Sullivan and Daiber, 1974).

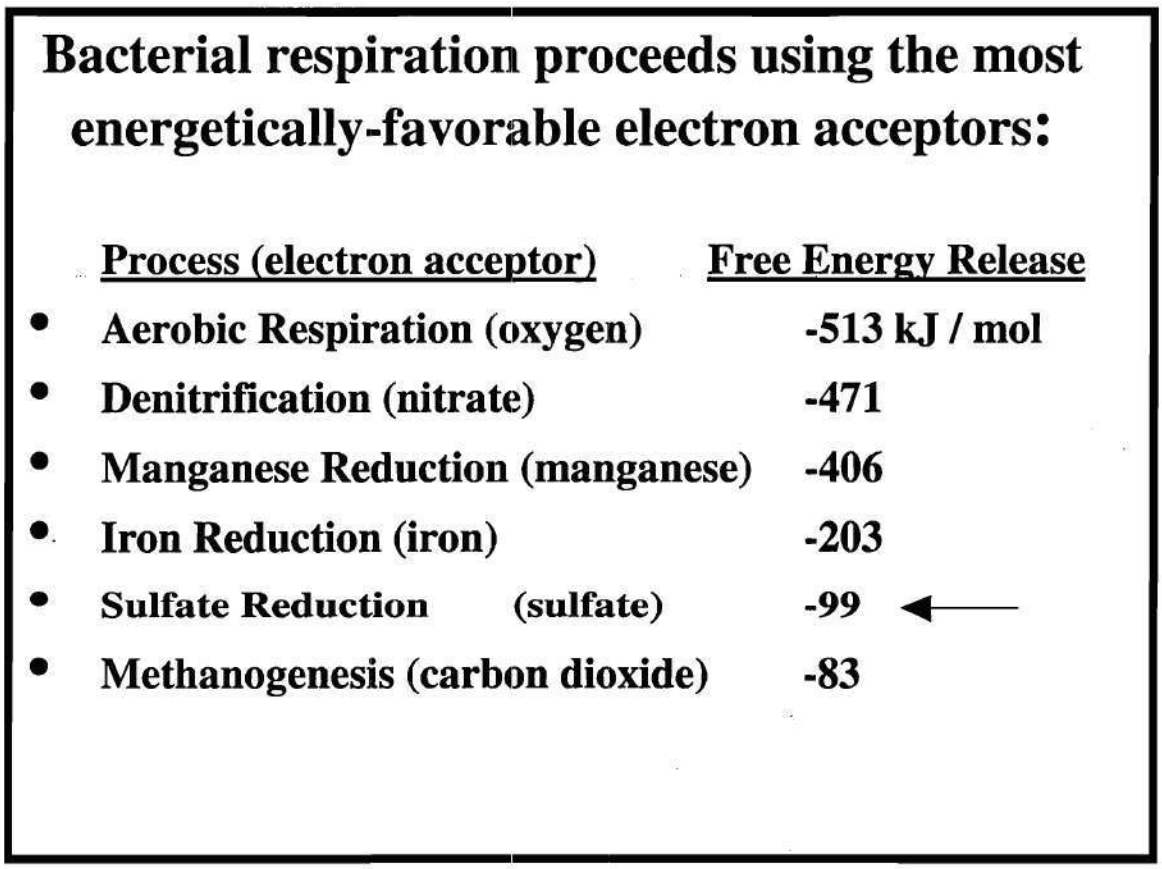

Figure 2.2 Bacterial respiration processes, indicating position of sulfate in electron tower (Atlas and Bartha, 1998).

Research has shown that metal reduction, e.g. iron and manganese, is negligible in total carbon oxidation (Howarth, 1993). Manganese is abiotically reduced before becoming available for bacteria in saltmarsh sediments. Further, manganese concentrations in marshes are two orders of magnitude less than iron concentrations (Howarth, 1993).

Iron is mostly supplied to saltmarsh systems in terrestrial runoff and sediments. Kostka and Luther (1995) observed that a majority of iron in saltmarsh sediments is stored in the solid phase and cycled rapidly between oxidized reactive iron and reduced iron as pyrite. Iron cycling is controlled by sulfate reduction and sediment oxidation in saltmarshes. Fe(III) can be reduced in saltmarsh sediments biotically by iron-reducing bacteria or abiotically by reaction with hydrogen sulfide (Kostka *et al.*, 2002). Common products of chemical oxidation are FeS and FeS_2 (pyrite). Due to abundance of sulfides from sulfate reduction in saltmarsh sediments, ferric iron will often react abiotically before becoming available for iron-reducing bacteria. However, recent studies have shown that biotic iron reduction may be more important in saltmarsh systems than originally believed (Kostka *et al.*, 2002). Lowe *et al.* (2000) found that propagation of sulfate-reducing bacteria (SRB) is stimulated by the disappearance of iron-reducing bacteria (FeRB), indicating that, in the presence of reducible Fe(III), FeRB may outcompete SRB for growth substrates.

Sulfate reduction is a major decomposition process for organic carbon in saltmarsh sediments (Howarth, 1993; Hines *et al.*, 1989; Kostka *et al.*, submitted). Studies have shown sulfate reduction responsible for up to 90 % of carbon oxidation in anoxic marine sediments (Howarth and Giblin, 1983). Fermenting bacteria in saltmarsh

sediments provide a steady supply of low-molecular-weight alcohols and fatty acids needed by SRB. Also, *Spartina* roots produce low-molecular-weight organic compounds, such as ethanol and malate, when roots metabolize anaerobically (Mendelssohn *et al.*, 1981). SRB utilize these compounds. Further, sulfate is regularly re-supplied to a saltmarsh by seawater infiltration at high tide, resulting in steady sulfate concentrations of 10-25 mM (Howarth and Teal, 1979).

Only a few studies have observed significant methane formation in saltmarshes. Available evidence suggests that methanogenesis is only a minor part (< 5 %) of carbon metabolism in saltmarsh sediments (Howarth, 1993; Alongi, 1998), especially for the top 10 cm.

Seasonal Cycle of Sulfate Reduction

As a microbially-mediated process, sulfate reduction responds to changes in temperature. Numerous studies have looked at seasonal changes in sulfate reduction rates. King (1988) found maximum sulfate reduction rates in a short *Spartina* marsh in South Carolina occurring in August, while minimum rates of sulfate reduction were measured in January. Hines *et al.* (1989) found that sulfate reduction maxima in a *Spartina* marsh in New England occurred from late June to early August, the time during which plants were actively growing above ground. Upon the onset of flowering in September, sulfate reduction rates decreased dramatically. Hines *et al.* (1989) observed minimum sulfate reduction rates in January.

Sulfate reduction rates (SRR) are intimately linked to both temperature and growth cycle of *Spartina*. During vegetative growth, sulfate reduction is stimulated as sediments are supplied with organic matter and oxidants from *Spartina* roots (Hines *et al.*, 1989). Oxygen is introduced into the sediment during the vegetative growth cycle by active O_2 infusion through *Spartina* roots (Lord and Church, 1983). This oxygen can re-oxidize sulfide to sulfate, which further supplies sulfate reducers.

As shown in Equation 2.1 (Richards, 1965), sulfate reduction releases ions of carbonate, ammonium, phosphate, and sulfide into sediment porewaters, resulting in changes in geochemistry:

Equation 2.1:

$$53SO_4^{2-} + \overset{\text{(organic matter)}}{C_{106}H_{263}O_{110}N_{16}P_{39}} \rightarrow CO_2 + 67HCO_3^- + 16NH_4^+ + 53HS^- + 39H_2O + HPO_3^{2-}$$

The resulting depth-vs.-concentration profile of these ions is affected by the rate of sulfate reduction, specific stoichiometry of each ion, diffusion rates of each ion, and rates of any subsequent consumption processes, biotic or abiotic, for each ion within the sediment (Lord and Church, 1983). As mentioned before, Figure 2.3 offers a hypothetical concentration-depth profile.

Both King (1988) and Hines *et al.* (1989) found maximum SRR in the top few centimeters of sediment with a marked decrease with depth to about 10 cm. This is largely explained by the greatest supply of sulfate from tidal inundation at the sediment

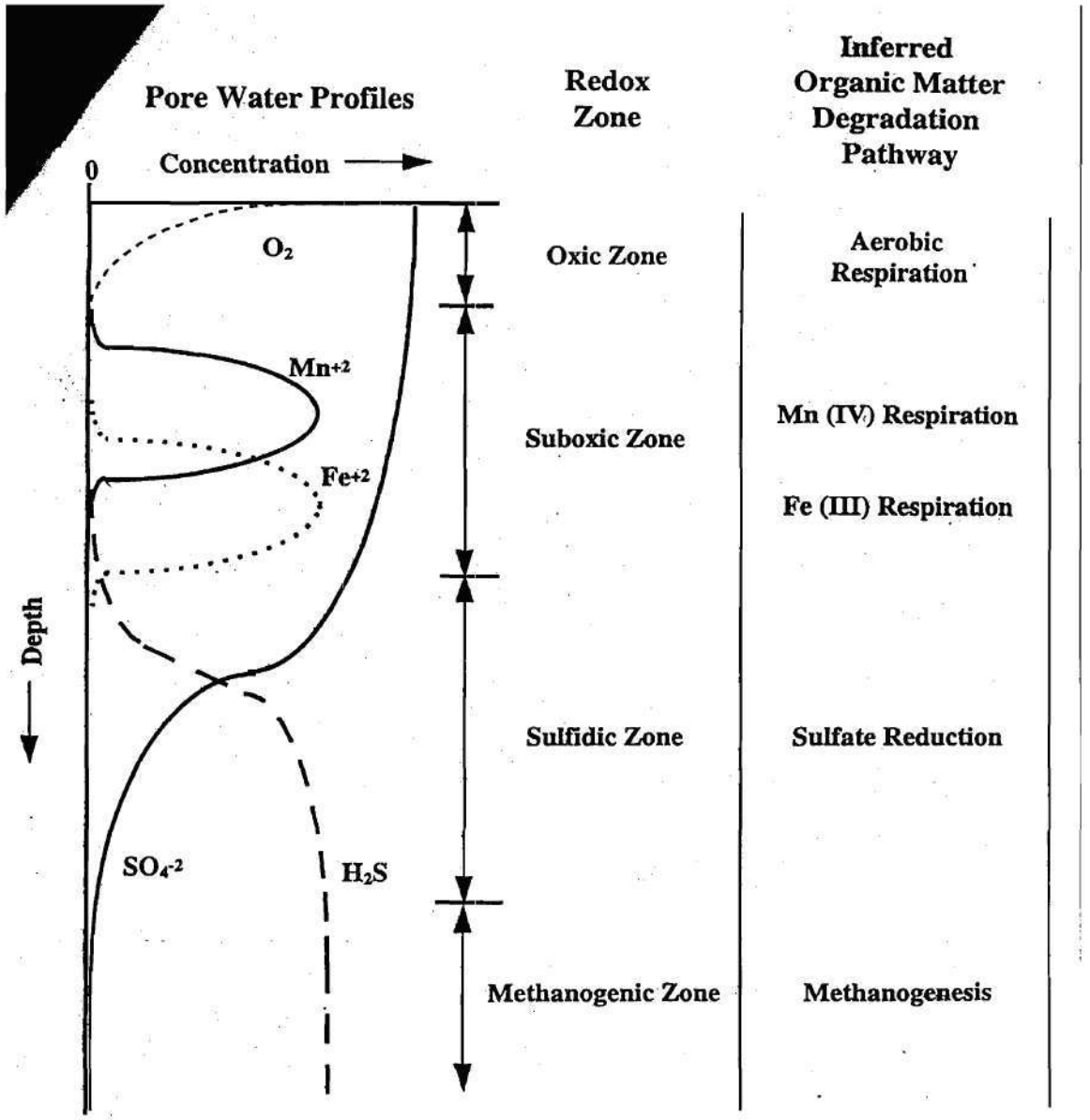

Figure 2.3 Hypothetical profile of chemical constituents in porewater. These constituents are the reactants and products of bacterial respiration (Koretsky *et al.*, 2000).

surface. Below 10 cm, sulfate reduction is usually no longer dominant. Thus, sulfate reduction research often focuses on the 0-10 cm interval.

In saltmarsh systems, it is believed that pyrite is the major short-term end product of sulfate reduction. Pyrite (FeS_2, sulfur valence of -1) and elemental sulfur (S^0, sulfur valence of zero) are often referred to as "residual sulfur" or chromium-reducible sulfur (CRS) since they can be extracted from sediment through a distillation procedure with Cr^{2+}. Pyrite can form rapidly by precipitation after reaction of Fe(III) with dissolved sulfide. Howarth and Teal (1979) observed that 70-90 % of the short-term end products of sulfate reduction were present as a fraction not volatilized by acid and were primarily pyrite. Kostka and Luther (1995) corroborated Howarth and Teal (1979) when they found in a Delaware saltmarsh that AVS concentrations were small relative to pyrite in vegetated marshes. In contrast, King *et al.* (1985) found that pyrite accounted for no more than 15 % of the short-term end products, with acid-volatile sulfides (AVS) and elemental sulfur accounting for the remainder.

Mercury in the Environment

Mercury is one of the oldest known elements. The Greeks and Romans used Hg in gold mining and termed it "hydrargyrum," from where the chemical symbol "Hg" comes. Mercury was a curiosity to them because it is the only metal which is liquid at room temperature. In liquid form, mercury has the ability to dissolve gold in a solution

called an amalgam. The gold can then be recovered by heating the solution, causing the mercury to evaporate.

The world production of mercury today is about 9,000 metric tons a year (Zumdahl, 1993). Much of the use over the past century has been in the chlor-alkali industry. Equations 2.2a and 2.2b show how mercury is used in chemical production at chlor-alkali plants.

Equation 2.2:

a) $2Cl^- \rightarrow Cl_2(g) + 2e^-$ at carbon anode ↑

b) $2e^- + 2Na^+ + 2H_2O \rightarrow 2NaOH + H_2(g)$ at mercury anode ↑

The element has also been widely used in thermometers, electrical devices, and batteries, in metals refining, as a fungicide in paint products and seeds, and in dental preparations and pharmaceuticals (Rood, 1996).

As part of the natural global flux of mercury, it is estimated that 5,900 to 16,000 metric tons are naturally released each year, mostly through weathering. In addition, 2,300 metric tons are believed to come from man-made sources.

Mercury use and discharges into the environment are now of vital concern because non-hazardous forms can be transformed through natural processes into toxic monomethylmercury, CH_3Hg^+ (Compeau and Bartha, 1984). Monomethylmercury (also called methyl mercury) has been reported as being the most bioavailable and

biologically-persistent form of mercury; it is known to bioaccumulate and can cause serious illness and death in humans, as described later in this chapter.

Exposure to mercury can result in health disorders, mainly those associated with central nervous and renal systems (Wheatley and Paradis, 1996). An infamous use of mercury during the early days of the Industrial Revolution was for the softening of fur in hat making. This practice gave rise to perhaps the first suspicions of mercury's neurological effects - the phrase "mad as a hatter" and the "Mad Hatter" character in Lewis Carroll's *Alice in Wonderland* were both derived from hat makers' seemingly common mental problems.

The toxicity of mercury, methyl mercury to be more precise, stems from its solubility in lipids and consequently its susceptibility to biomagnification within muscle and fat tissue. Of all mercury species, methyl mercury makes up only 1-10 % of species found in sediments, but greater than 95 % of mercury found in biota is in the methylated form (Bloom, 1992).

In the 1950s, at Minamata Bay, Japan, over 2,000 people contracted serious central nervous system disorders and over 900 eventually died as a result of mercury contamination (Hosokawa, 1995). The mercury had naturally methylated and bioaccumulated in commercial seafood in the bay and consumption of contaminated seafood by humans led to the tragedy.

Other mercury contamination episodes that affected human health were reported in Iraq (1961, 1972), Pakistan (1963), Guatemala (1966), New Mexico, U.S.A. (1961), Ontario, Canada (1970), and Indonesia (2000).

There are numerous sites known to be contaminated with mercury around the world. Two of the worst in the U.S. are the LCP site in Brunswick, Georgia and the ALCOA site at Lavaca Bay, Texas. LCP as well as Berry's Creek, a lesser known site in New Jersey, are discussed below.

Case Study: LCP Superfund Site - Brunswick, Georgia

One of the most contaminated sites in the U.S. is near the coastal city of Brunswick, Georgia. This area is shown in Figure 2.4. Since 1919, a 550-acre tidal marshland along the Turtle River has been occupied by industrial ventures, including an oil refinery, a paint manufacturing company, a power plant, and a chlor-alkali plant. Linden Chemicals and Plastics (LCP) was perhaps the worst polluter of the group, ultimately failing to account for as many as 172 metric tons of mercury. In the 1970s, restrictions on fishing and hunting were initiated (Winger *et al.*, 1993).

LCP used mercury in cathodes for the production of chlorine and caustic soda, two chemicals needed in chlor-alkali processes. Equations 2.2a and 2.2b describe the process, in which aqueous NaCl undergoes electrolysis. Mercury does not necessarily have to be used in the cathodes, but it was the economical choice at LCP for many years. Water used in cleaning and cooling the cathodes and other equipment carried particles of corroded and dissolved mercury away as wastewater.

LCP generated more wastewater than its treatment facility could handle. Excess waters were stored illegally in railroad cars or dumped into a sewer system which discharged into Purvis Creek or Turtle River. Also, contaminated mud was stored in

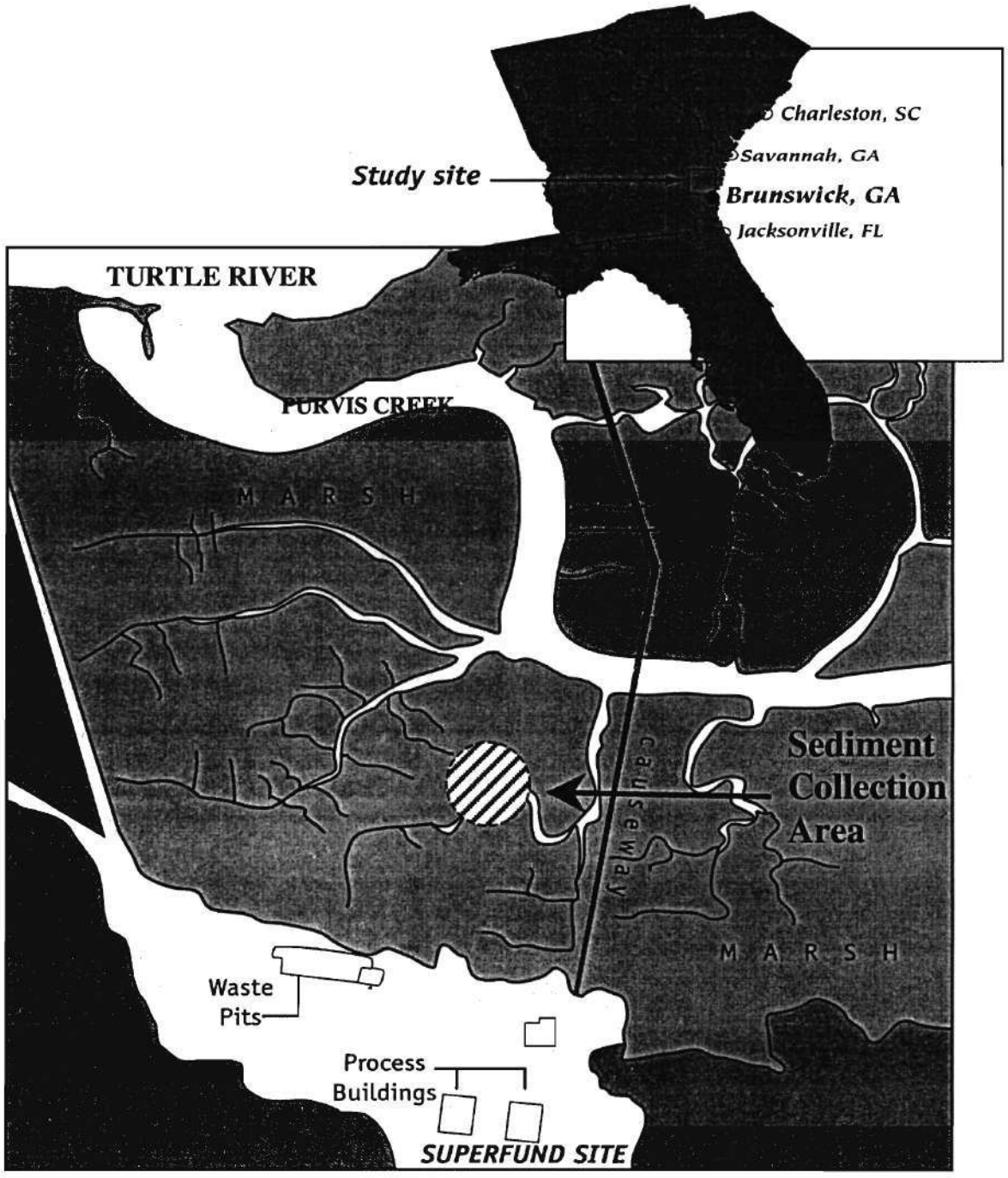

Figure 2.4 Contaminated sediment collection area, located at LCP Superfund site, just north of Brunswick, Georgia. *Inset*: LCP's location in the southeastern United States.

drums inside buildings. Further, the company failed to do routine maintenance, which resulted in caustic wastewater leaking beneath the foundation of the production building. The building eventually began to shift and break apart.

Mercury concentrations as high as 12,500 $\mu g/g_{dry}$ were detected at the site, as were pockets of pure mercury. In fact, a pool of mercury still exists in the subsurface near a production building. Since mercury is 13.5 times denser than water, the contaminant has sunk down to bedrock 12 m below.

In 1992, mercury was detected again in seafood samples taken near the plant. State officials warned people not to eat crabs and oysters from the area and fined LCP for violating mercury discharge permits. In 1994, the plant was closed. Due to the severity of the situation, LCP was deemed worthy of EPA's "silver bullet" and immediately placed under the Superfund program. After more than 80 years of industry, the federal government had finally heeded to complaints from site workers, local residents, and seafood interests. As part of clean-up efforts, approximately 13 acres of marsh had been excavated by the EPA by 1999.

The Turtle River - Brunswick estuary system, where LCP is located, is considered environmentally-sensitive in that it provides important habitat for endangered species and supports an important sport and commercial fishery (Winger *et al.*, 1993). The area is dominated by cord grasses (*Spartina alterniflora*) and provides habitat for endangered manatees, threatened brown pelicans, and wood storks. Recent research into the site was conducted by Winger *et al.* (1993). Sediment toxicity attributed to Hg was confirmed in studies with crustaceans and levels up to 27 $\mu g/g_{dry}$ were found along the Turtle River.

Highest concentrations were consistently in the top 8 cm. In addition to mercury, high levels of PCBs were also detected.

LCP data obtained by research at the Skidaway Institute of Oceanography are shown later; some of these researchers were also involved in this thesis.

Berry's Creek – Hackensack Meadowlands, New Jersey

Another site noted for mercury contamination and associated problems is Berry's Creek. Located in northern New Jersey's Bergen County, the creek is best known for running underneath a thoroughfare to New York City, the New Jersey Turnpike, and the Meadowlands Sports Complex. New York City is 13 miles to the east.

Berry's Creek, part of the Hackensack River watershed, is a combination of marshland and tidal estuary where salinity reaches 12 ppt (Weis *et al.*, 1986). Reed grass (*Phragmites australis*) dominates the vegetation and migratory waterfowl are the chief wildlife.

The Berry's Creek area was the location of Ventron mercury processing plant from 1930 to 1974 (Turner and Southworth, 1999). Industrial discharges, such as dumping of untreated waste material onto the property, resulted in mercury-laden effluent draining into the land and adjacent creek. The New Jersey Department of Environmental Protection (DEP) and the EPA determined that, during the years of Ventron, mercury was being loaded into Berry's Creek on a daily basis. It is estimated that as many as 300 metric tons of mercury were released into the environment.

Ventron at one time attempted to deter pollution through installation of a wastewater treatment system, but that was not enough to contain the problem. In the 1970s, Ventron sold its interests, and the ensuing owner sought to demolish the plant. Mercury-contaminated water from the site was used in the demolition process and this water was allowed to run into the creek. DEP finally took action at this point, ordering containment of the site and filing suit in March, 1976.

Mercury levels in sediment were soon found to reach 10,000 $\mu g/g_{dry}$ at the refinery and 1,000 $\mu g/g_{dry}$ in the creek (Berman and Bartha, 1986). Several researchers examined conditions at the site in the 1980s. Weis *et al.* (1986) brought contaminated sediments into the laboratory and set-up aquaria where conditions of pH, salinity, aeration, and mixing were manipulated. Mercury uptake into killifish (*Fundulus heteroclitus*) was measured and trends were assessed. Mercury concentrations in sediments were determined to be 39-183 $\mu g/g_{dry}$ with a mean of 109 $\pm$ 47 $\mu g/g_{dry}$. Particulate analysis estimated organic matter at 8.7 $\pm$ 2.1%. Mercury levels in the filtered water column samples were consistently below detection (< 3 $\mu g/L$).

The researchers found that low oxygen (i.e., low aeration) correlated with higher mercury levels in, and poorer health of, fish. However, no relationship was found between Hg in sediments and Hg accumulation in fish. More importantly, minimal Hg in the sediments was in methylated form, while nearly all Hg in fish was methylated. It was inferred from this that methylation occurred in the water column and in fish tissue, but not in sediments. Experimental chemical variables in aquaria, rather than the relative amounts of Hg in the sediments, were determining factors in making Hg available to the

killifish. Further, Hg levels in the sediments varied considerably over short distances; samples taken just 25 cm apart varied by as much as nine-fold.

To investigate the lack of methylation in Berry's Creek sediments, Berman and Bartha (1986) spiked sediment samples with $HgCl_2$ and CH_3HgCl to assess methylation and demethylation, respectively. When compared to pristine control samples, the contaminated sediments exhibited similar pH, redox potential, microbial counts, and methylating potential. The main difference was sulfide levels, which were relatively high in contaminated samples. Total sulfide was 7.06 ± 0.59 mg/g_{dry} in contaminated sediments and 2.8 ± 0.60 mg/g_{dry} in pristine. The mercury plant refined mercury from base ore, predominantly cinnabar (HgS); these sulfides likely were discharged into Berry's Creek.

To more closely examine effects of sulfide, researchers amended samples with Na_2S, then continued with methylation studies. Sulfide appeared to inhibit methylation. A causal connection was established between high sulfide levels in Berry's Creek and its inability to methylate mercury. Berman and Bartha (1986) concluded that, as long as sulfide was concentrated in Berry's Creek sediments, mercury was immobile as HgS and harmless to present biota. In other words, the researchers believed that sulfide-rich sediments would limit the bioavailability of mercury.

Now more than a decade later, current understanding of Hg processes shows that the availability of Hg at Berry's Creek is more a concern than the researchers concluded. First, stormwater flooding of the creek can carry mercury loadings to other areas. Second, better water quality or clean-up activities can lower sulfide concentrations and,

paradoxically, increase dangerous methylation activity. For example, remediation by dredging would expose oxygen to creek sediments and therefore oxidize sulfide and liberate mercury. It would be imperative to minimize oxygen exposure and immediately bury or cap dredged sediments in order to keep them sulfidic.

Further, technological advances have vastly enhanced detection limits of Hg, especially in water. Berman and Bartha (1986) reported a detection limit of 3 μg/L in their water column analysis. Also note that they failed to look at porewaters. Current researchers are able to detect Hg in ng/L-range, more than three orders of magnitude more sensitive than technology fifteen years ago. Additionally, ecological research concerning Hg over the past two decades has established the importance of available (dissolved) Hg in sediment. Hg near the sediment-water interface is susceptible to microbial action and transformation as well as movement into the food chain.

Mercury Speciation and Processes

Mercury levels in surface waters, porewaters, and sediments and sludges have been reported at various sites. Tables 2.1 includes many examples, including some values just mentioned above. Table 2.2 shows mercury levels used in regulations and other thresholds.

Mercury is found in several forms. Methyl mercury (MeHg) and total mercury (THg; this represents the sum of all Hg species) are the most studied forms. Elemental

Table 2.1 Mercury levels reported in various environments.

Mercury Levels of Surface Waters

Location	Environment	Total, Unfiltered [ng/L]	Total, Dissolved [ng/L]	MeHg, Dissolved [ng/L]	Reference
Gironde Estuary, France	estuarine	4.4 - 20.7	—	—	Cossa *et al.* 1998
St. Lawrence Estuary, Canada	estuarine	—	1.8 - 3.0	—	Cossa *et al.*, 1998
Pacific Ocean	saltwater	0.9 - 1.9	—	—	Fitzgerald and Watras, 1989
Pacific Ocean	saltwater	—	—	0.0 - 0.1	Gill and Fitzgerald, 1988
East North Atlantic Ocean	saltwater	0.1 - 2.0	—	—	Cossa *et al.*, 1998
West North Atlantic Ocean	saltwater	0.65 - 0.94	—	—	Gill and Fitzgerald, 1987
Patuxent River, Maryland	estuarine	0.4 - 2.1	—	0.02 - 0.13	Benoit *et al.*, 1998
Port Phillip Bay, Australia	estuarine	—	1.7	—	Fabris *et al.*, 1999
Rhine Estuary, France	estuarine	0.4 - 3.7	—	—	Tseng *et al.*, 1998
Elko County, Nevada	freshwater	14 - 320	—	—	Engle *et al.*, 2001
Lake Superior	freshwater	—	0.4 - 4.2	—	Hurley *et al.*, 1998
Lake Michigan	freshwater	—	0.8 - 5.8	—	Hurley *et al.*, 1998
Ria de Aviero, Portugal	freshwater	—	3 - 85	—	Pereira *et al.*, 1998

Mercury Levels of Porewaters

Location	THg [ng/L]	MeHg [ng/L]	Reference
Everglades	1.5 - 13.0	0.00 - 0.10	Gilmour *et al.*, 1998
Patuxent River, Maryland	1.2 - 7.7	0.03 - 0.18	Benoit *et al.*, 1998
Lavaca Bay, Texas mud flat	262	243	Bloom *et al.*, 1999
Lavaca Bay, Texas grass flat	53.1	39.6	Mason *et al.*, 1998
Pallette Lake, Wisconsin	4.0 - 20.0	0.1 - 4.6	Krabbenhoft *et al.*, 1998
Little Rock Lake, Wisconsin	5.0	—	Gilmour and Riedel, 1995

Mercury Levels of Sediments and Sludges

Location	Total [mg/kg]	MeHg [µg/kg]		Reference
Little Rock Lake, Wisconsin	0.14	10.4	dry	Gilmour and Riedel, 1995
Canadian peat	0.06	—	wet	Fitzgerald and Watras, 1989
Okefenokee Swamp, Georgia peat	0.40	—	wet	Fitzgerald and Watras, 1989
Everglades	0.22 - 1.86	—	wet	Cossa and Martin, 1991
Everglades	0.05 - 0.45	0.1 - 6.0	dry	Gilmour *et al.*, 1998
Municipal wastewater sludge	1.24	—	wet	Cossa and Fileman, 1991
Pristine activated sludge	0.03	—	wet	Dalziel, 1992
Chlor-alkali lagoon	420	—	wet	Dalziel, 1992
Patuxent River, Maryland	0.06 - 0.16	0.12 - 0.78	dry	Benoit *et al.*, 1998
Lavaca Bay, Texas open water	32.1	—	dry	Santschi *et al.*, 1999
Lavaca Bay, Texas mud flat	11.5	12.7	dry	Bloom *et al.*, 1999
Lavaca Bay, Texas grass flat	0.748	—	dry	Mason *et al.*, 1998
Berry's Creek, New Jersey	39 - 183	—	dry	Weis, 1996
Port Phillip Bay, Australia	0.5	—	wet	Fabris *et al.*, 1999
Pallette Lake, Wisconsin	0.001	0.06	dry	Gilmour and Riedel, 1995
Portugal	10 - 60	—	dry	Pereira *et al.*, 1998
Scheldt Estuary, Portugal	0.02 - 1.30	0.0 - 3.5	dry	Tseng *et al.*, 1998

Table 2.2 Current mercury contamination thresholds.

Matrix	Level	Reference
Total Hg in human blood	28 μg/L	New Jersey State Department of Health
Total Hg in drinking water	2 μg/L	EPA
Methyl Hg in seafood	1 μg/g	FDA
Total Hg in workplace air	0.1 mg/m^3	OSHA

mercury [Hg(0)], ionic mercury [Hg(II)], cinnabar (HgS), and ligand-complexed (Hg-L) are also fairly common in literature.

Figure 2.5 illustrates a conceptual mercury model. Mercury exists in crystalline solid form as HgS (cinnabar) or ligand. The solid form is in chemical equilibrium with dissolved ionic mercury. Biological reduction of Hg(II) produces elemental Hg, a very volatile species that readily enters the atmosphere, where it can subsequently be chemically oxidized back to ionic form. Hg(II) can also undergo biotic transformation into methyl mercury both in sedimentary and aquatic environments. Methyl mercury, more toxic and much less volatile than elemental mercury, presents a problem in that it naturally occurs and readily enters the food chain, as described previously. MeHg also can biotically be converted back to Hg(II).

Mercury Methylation

Studies over the past two decades have shown that methyl mercury production in marine sediments is intimately linked to sulfate reduction by sulfate-reducing bacteria (Compeau and Bartha, 1985). The researchers tied over 95 percent of methylation in anoxic sediments to the activities of SRB. As discussed previously, sulfate is the dominant terminal electron acceptor in marine sediments and is coupled to metabolism of sediment carbon. The co-metabolism of MeHg in sulfate reduction is the result of secondary metabolism by SRB in which Hg is taken as an analog to carbon substrate.

Research has been carried out to determine the quantitative relationship between mercury methylation rates (MMR) and sulfate reduction rates (SRR) in saltmarsh

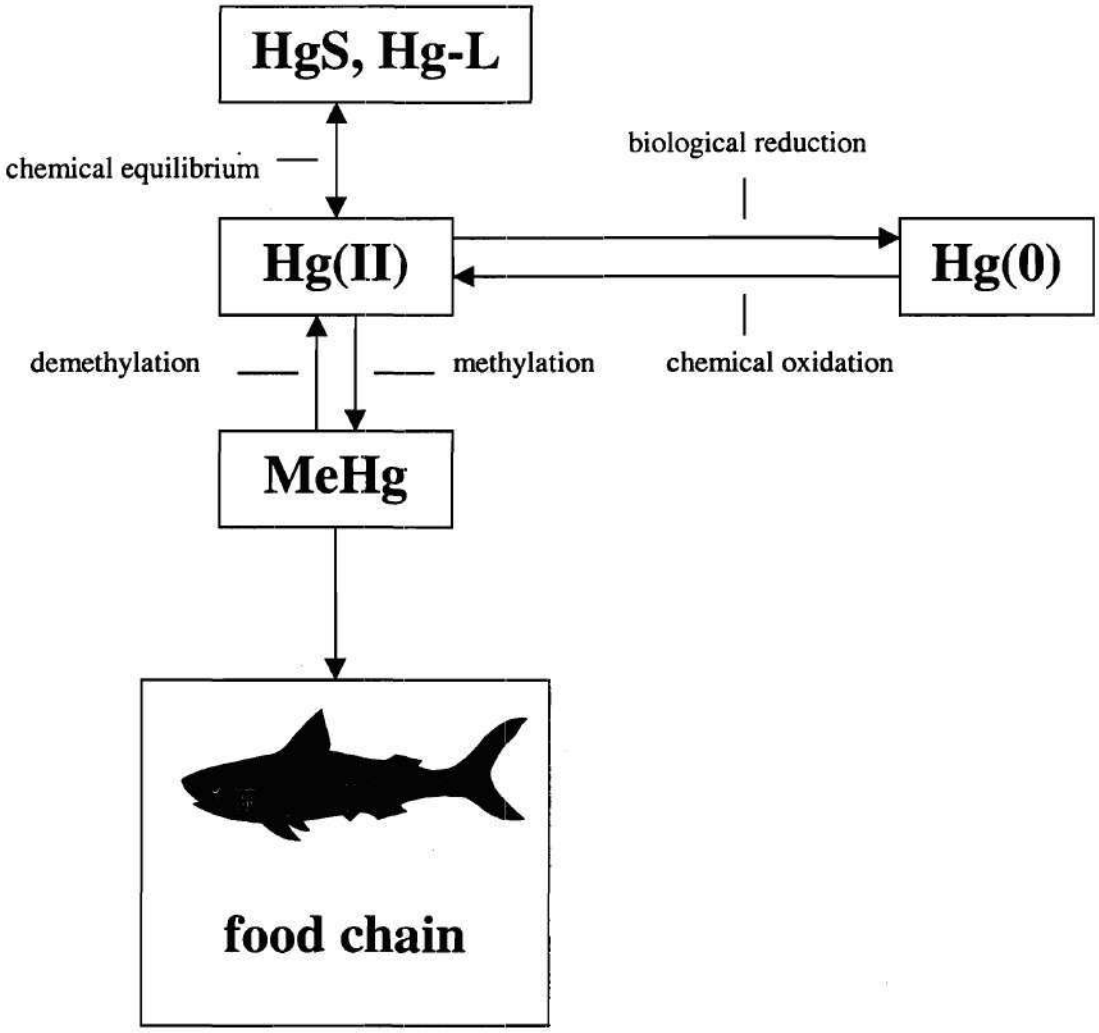

Figure 2.5 Conceptual model of mercury speciation.

sediments. King *et al.* (1999) attempted to predict MMRs based on sulfate and mercury levels in sediments. King (1999) confirmed in laboratory studies with sediment slurries that a direct proportion between MMR and SRR exists and the relationship is dependent on mercury availability, growth substrate, temperature, and oxygen. However, the same study showed that the relationship between MMR and SRR becomes more complicated in whole-core sediment studies. It appears that additional parameters are critical for defining the relationship between MMR and SRR occurring naturally in the environment.

Since sediment slurry experiments like the one just described have generally not included plants, limited data are available on effects of seasonal plant inputs on mercury methylation. The physiology of *Spartina alterniflora* heavily influences microbial processes and redox reactions, including sulfate reduction, occurring in saltmarsh sediments (Hines *et al.*, 1989). Therefore, it has been hypothesized that the *Spartina* growth cycle may have an important role in the rates of mercury methylation and demethylation.

This concept has been shown to have some merit in a recent study. Weber *et al.* (1998) demonstrated that production of methyl mercury in saltmarsh sediment slurries varied seasonally with *Spartina* growth. Decreases in methyl mercury production coincided with the active growing season of *Spartina*. Data indicated that in small-scale experiments, while mercury methylation occurred throughout most of the year, net demethylation prevailed during the *Spartina* active growing season.

As mentioned previously, growth of *Spartina* has a direct effect on sediment geochemistry. Dissolved oxygen and organic matter are introduced into the rhizosphere

during the vegetative growth cycle from late spring through summer (Howes *et al.*, 1981; Hines *et al.*, 1989). Also linked to the *Spartina* growth cycle are concentrations of sulfate and sulfide in saltmarsh sediments. Because of rapid consumption of oxygen and abundance of sulfate in seawater, sulfate reduction is the dominant microbial respiration process in saltmarsh sediments. Sulfate reduction is at a maximum during *Spartina* vegetative phase in spring and summer, and decreases with onset of reproductive phase in the fall (Hines *et al.*, 1989; King, 1988). Further, in a study of estuarine sediments, Choi and Bartha (1994) established a positive linear correlation between methylation and organic matter in sediments. All of the factors described here affect competition between various microbial populations that may have the ability to transform mercury.

Phylogeny of Mercury-Methylating Sulfate-Reducing Bacteria

The phylogeny of SRB capable of mercury methylation has been studied by several investigators. King (1999, 2000) demonstrated that in pure-culture and marine sediment research, certain genera of SRB methylated soluble inorganic mercury to a much larger extent than other genera, even when normalized to sulfate reduction rates.

King (2000) used cultures of five genera of SRB, i.e., *Desulfovibrio desulfuricans*, *Desulfobulbus propionicus*, *Desulfococcus multivorans*, *Desulfobacter* sp. strain BG-5, and *Desulfobacterium* sp. strain BG-33, to be representative of five phylogenetic groups. Previous work had used only a single SRB, *Desulfovibrio desulfuricans*, to generally assess the Hg methylation potential of the entire SRB population (Choi *et al.*, 1994; Compeau and Bartha, 1985; Gilmour and Henry, 1991; Pak

and Bartha, 1998; Pak and Bartha, 1998). The problem with these previous studies was that each phylogenetically distinct group could have a different potential to methylate Hg.

King (2000) made two major findings. First, Hg methylation activities varied by nearly two orders of magnitude for phylogenetically-distinct SRB groups, as depicted in Figure 2.6. Activities were based on Hg methylation rate normalized to sulfate reduction rate, referred to as *f*. This ratio reflects the direct and co-metabolism of methyl mercury in sulfate reduction, where SRB produce CH_3Hg^+ in parallel with respiration measured as SO_4^{2-} reduced. The incidence rate is low, but the two-orders-of-magnitude variation in methylation rates could have significant impacts. Second, *Desulfobacterium* exhibited a pronounced ability to methylate Hg, especially under acetate oxidation. Rooney-Varga *et al.* (1997) previously showed that acetate-utilizing SRB, similar to those used by King (2000), are prevalent and active in marine sediments. Specifically, when compared to other groups, *Desulfobacterium* methylated mercury at a rate of 2.58×10^{-5} nmol CH_3Hg^+ per nmol SO_4^{2-} produced, an incidence rate that was 92-fold higher than the lowest mercury methylator studied, *Desulfobulbus* (King, 2000). Therefore, if this organism is present in higher numbers than other SRB, methyl mercury could be an even greater contaminant of concern in the overlying water column.

In summary, King *et al.* (1999, 2000) used two independent experimental approaches to relate Hg methylation to both phylogeny and carbon metabolism. In relation to marine sediments, bacteria capable of such Hg methylation are present in marine sediments, even more than other SRB families (Rooney-Varga *et al.*, 1997).

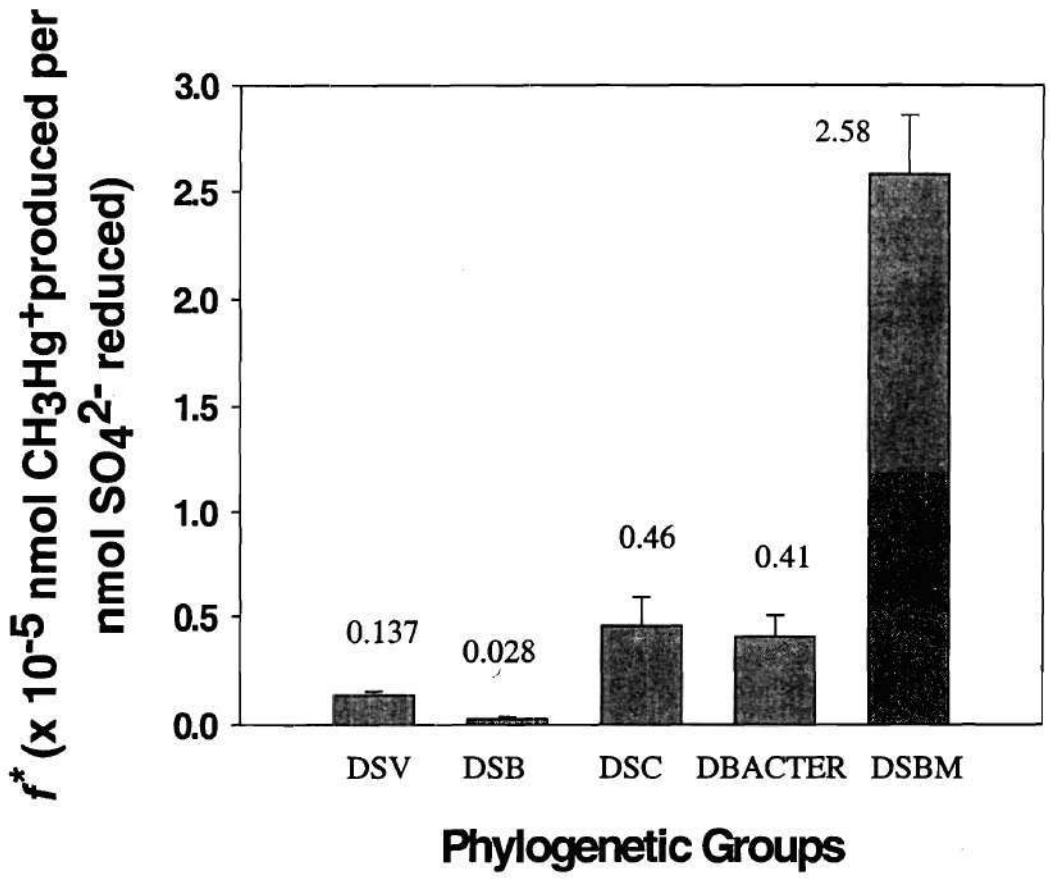

Figure 2.6 Values of f* for pure-culture representatives of SRB phylogenetic groups (King, 1999).

Mercury Demethylation

Since *net* formation of MeHg is realistically that which accumulates in the environment, the process of mercury demethylation requires attention as well. The demethylation of mercury and subsequent reduction of Hg(II) to Hg(0) occur through microbial processes (Summers and Silver, 1978). Further, demethylation rates have been found to nearly equal methylation rates in sediments with high redox potentials (Compeau and Bartha, 1984). Overall, the net availability of MeHg is regulated by the rates of production (methylation) and decomposition (demethylation). Thus, the bacterial mechanisms of demethylation have been of interest.

Demethylation has been shown to follow two pathways: organomercurial-lyase (OML) and oxidative demethylation (OD). In OML, the organomercurial lyase gene of the mer A operon cleaves the carbon-mercury bond of MeHg to produce methane and Hg(II). Bacteria possessing *mer* B further reduce Hg(II) to Hg(0) (Summers, 1986). However, when demethylation experiments began detecting CO_2, and not methane, as a product, a second mechanism was suspected.

Oremland *et al.* (1991) observed CO_2 production in freshwater and estuarine environments where demethylation occurred anaerobically. This finding supported an oxidative demethylation mediated by SRB in which MeHg served as an analog of carbon substrate. In a later study, Oremland *et al.* (1995) reproduced these results in Hg-contaminated and pristine environments and further concluded that oxidative demethylation was most extensive in the surficial (0-4 cm) layer and occurred regardless of the degree of mercury contamination.

Pak and Bartha (1998) confirmed for the first time that, in pure culture, SRB participated in demethylation in anoxic sediments. The researchers also measured methylation and demethylation activities in lake sediments. The activities appeared to correlate positively with level of organic matter in sediment, sulfate in porewater, and mercury in fish. The sediments used in their study had organic levels of 24-31% (based on loss-on-ignition) and porewater sulfate concentrations of 0.31-0.70 mM, while fish contained mercury levels of 0.7-8.9 μg/g.

Impetus for Mercury Research

Mercury levels in fish are a chief indicator of biomagnification of methyl mercury and have been the recent impetus in the Hg-research community. Estuaries, a haven for fish, represent the key area where anthropogenic sources of mercury are exposed to fish and other life. Saltmarshes often accompany and dominate shorelines of estuaries. Thus, studying mercury processes in these saltmarshes is vital in understanding the mercury problem. The balance of microbial mercury methylation and demethylation activities is critical since MeHg accumulates in fish to levels that require toxicological and regulatory attention. Since practically all of the mercury found in fish is in the form of methyl mercury, methylation and demethylation is expected to correlate with elevated mercury levels in fish (Pak and Bartha, 1998).

Looking more closely, mercury may enter the food chain at the saltmarsh sediment-water interface, where fish, macrofauna, and micoorganisms feed and graze and where mercury dissolves or partitions from sediment into the overlying water. Either

way, sediment surfaces are where mercury likely becomes bioavailable and exposed to the food chain. To assess Hg exposure, geochemical parameters, plant growth, and microbial process rates in these sediments can be compared to Hg levels in the same sediments, especially near the surface.

CHAPTER III

MATERIALS

Mesocosms and BERM Facility

Mesocosms were constructed at the Bioremediation and Environmental Research Mesocosm, or BERM (plan view shown in Figure 3.1), located on the campus of the Skidaway Institute of Oceanography near Savannah, Georgia, USA. The mesocosm design was a result of a collaborative effort by Dr. F. Michael Saunders, Georgia Institute of Technology; Dr. Joel E. Kostka, Florida State University (and formerly of Skidaway Institute of Oceanography); and Dr. Marc E. Frischer, Skidaway Institute of Oceanography.

Three mesocosms within the BERM facility were used in this research (Figure 3.2). Two of the mesocosms contained contaminated sediments from the LCP Superfund site in Brunswick, Georgia. One of these contaminated mesocosms was vegetated with *Spartina alterniflora*. The third mesocosm, which served as a control, contained pristine sediment from a nearby saltmarsh on Skidaway Island, Savannah, Georgia and was also planted with *Spartina*.

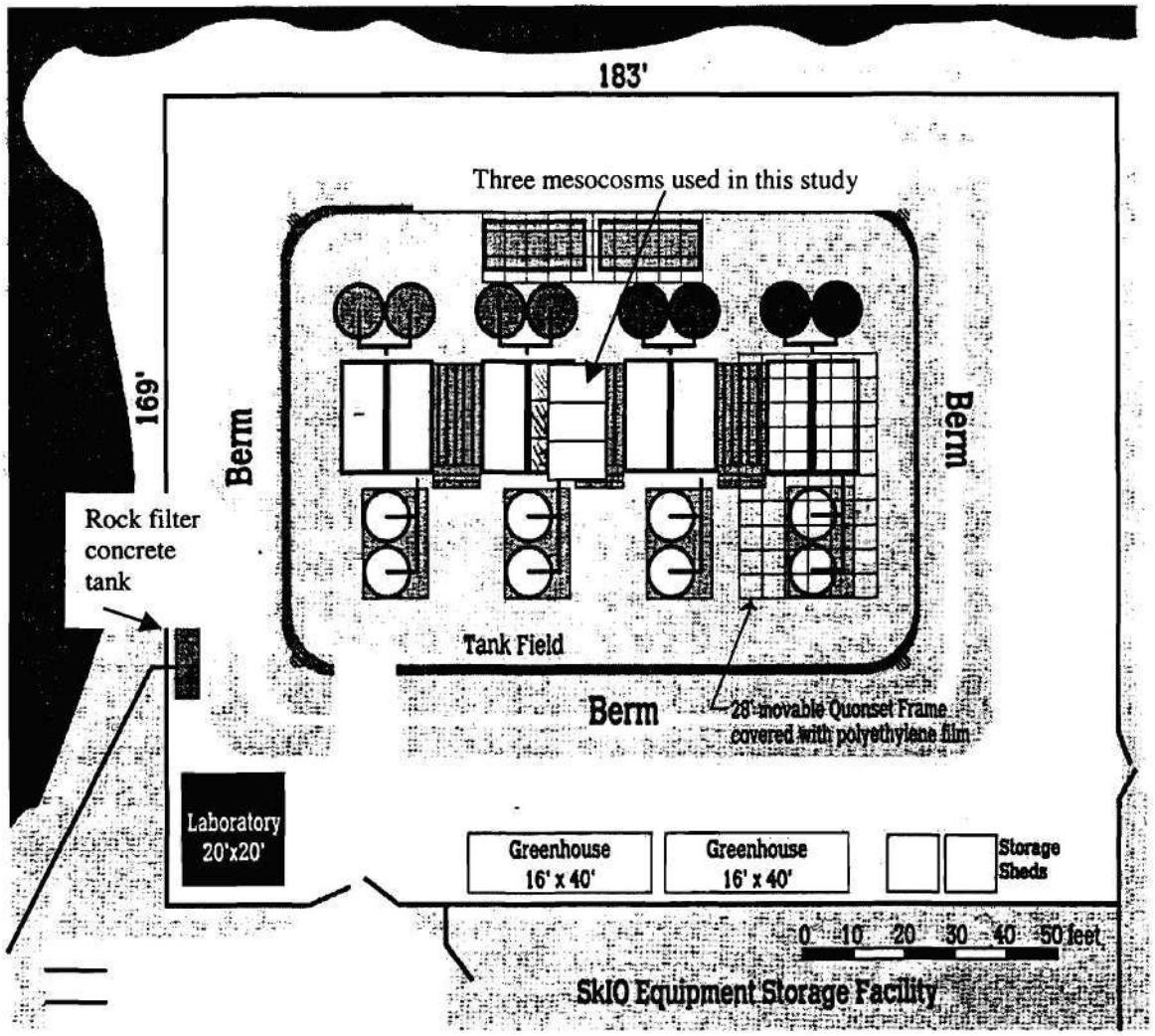

Figure 3.1 Site plan of BERM facility, showing mesocosms used in this study.

BERM Mesocosms

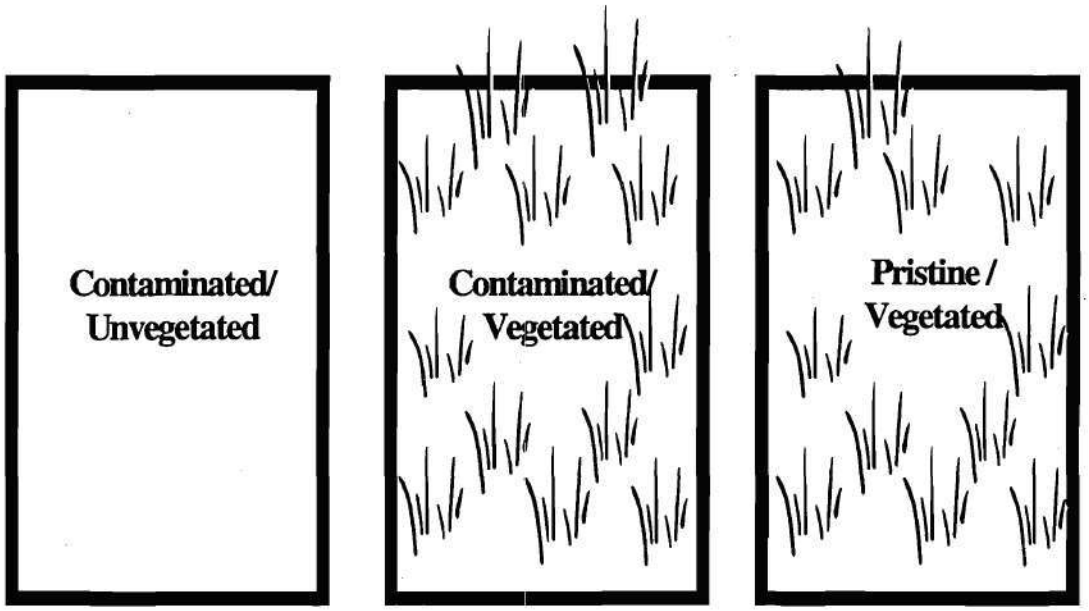

Figure 3.2 General schematic of BERM mesocosms. Contaminated sediments were collected at the LCP Superfund site. Pristine sediment was collected at Grove's Creek on Skidaway Island, Georgia.

Physical Design and Construction

The design shown in Figure 3.3 was used for all three mesocosms. Each mesocosm spanned 3.05 m (10 ft.) in length, 1.52 m (5 ft.) in width, and 1.52 m (5 ft.) in depth. Each mesocosm contained approximately 97 cm (38 in.) of sediment and 15.2 cm (6 in.) of drainage stone underneath the sediment. Two liners, a 0.15-mm (6-mil) –thick erosion-control cloth and a 0.15-mm (6-mil) –thick string-reinforced polyethylene sheeting, were used between the sediment matrix and the mesocosm structure. The erosion-control cloth was in direct contact with the sediment matrix.

The piping system for the mesocosms was designed to control and monitor system influent and effluent. Piping and other components of the mesocosm system are further described in the following paragraphs and can be seen in Figure 3.3.

The source of water for the mesocosms was the Skidaway River, located approximately 250 m from the BERM facility. River water was pumped continuously to the BERM facility. The water flowed through parallel vertical rock filters before it went to another concrete-encased rock filter (approximately 3,500-L total volume, porosity = 40%) at the BERM, from where it was pumped continuously to the various BERM areas. For the mesocosms of this study, the water was pumped to an elevated reservoir (5,000-L capacity), situated 2.1 m above the mesocosms. This reservoir maintained a constant head via an overflow orifice with the return flow going back to the BERM rock filter for continuous filtering and recycle.

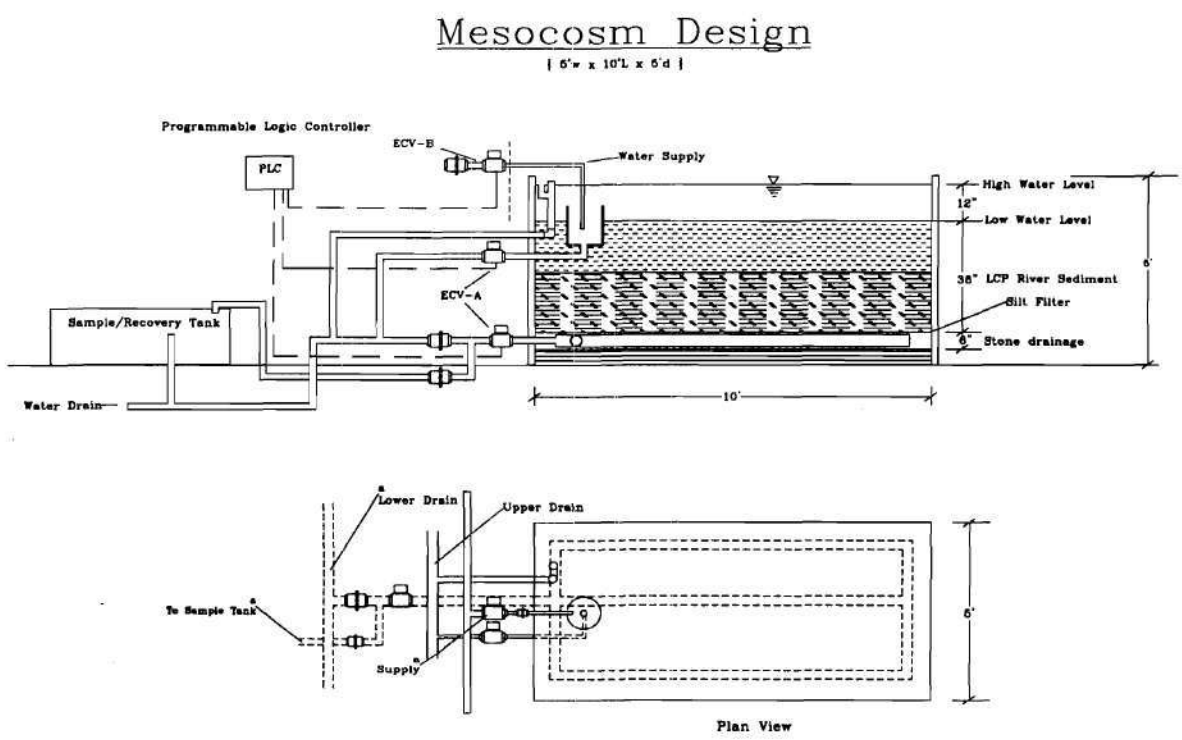

Figure 3.3 Physical design of an individual mesocosm. ECVs refer to PLC valves.

The supply line from the reservoir to the three mesocosms was controlled by several manual gate valves and three electronic gate valves. The electronic valves were controlled by programmable logic controllers (PLCs); thus, the electronically-controlled valves (ECVs) were also referred to as PLC valves. Each mesocosm had its own PLC (#1, #2, #3), each of which controlled the influent and the underdrain PLC valves. When the influent PLC valves were opened, influent water traveled by gravity from the elevated reservoir into the mesocosms.

Influent flow rates were controlled by both a manual gate valve and a 0.64-cm -diameter orifice drilled in a pipe slip cap attached to the end of the influent line. This orifice size was designed to obtain the desired flow rate and tidal flooding period. Influent water streamed down into a 30.5-cm -diameter plastic bucket embedded in the mesocosm sediment; this bucket allowed for energy dissipation. The bucket was approximately 0.6 m deep, with half of this depth below the sediment elevation. As the bucket filled, water flowed out through a series of 2.5-cm -diameter orifices at the sediment surface, which allowed for simulation of a smooth incoming tide along the surface of the marsh.

Each mesocosm had two independent drainage systems. Surface drainage occurred through the same bucket previously discussed. In surface drainage, water re-entered the bucket through the orifices at sediment elevation. Once in the bucket, water exited the mesocosm through a 10.2-cm -diameter hole at the bottom; a manual gate valve and a PLC valve controlled the flow through this orifice. This mechanism let the

mesocosm drain without any significant drainage through the sediment or through any potential cracks developing between the mesocosm sides and the sediment.

The PLC valve for surface drainage of all three mesocosms was controlled by a single PLC (#4), different from the other PLCs (#1, #2, #3). Once the PLC valve was opened for surface drainage, the effluent flow rate from each mesocosm was controlled not by the diameter of the drainage pipe, but rather by partially closing the manual gate valve at each mesocosm in order to restrict outflow. The manual gate valve in each of the three mesocosms, located beneath the surface drain, was manipulated to achieve the desired surface drainage period.

Effluent from the surface drainage system could be directed back to the river or to an effluent holding tank (6,000-L capacity) for evaluation and treatment. A T-section in the effluent piping system and a gate valve allowed for selection of outflow destination; for this study, surface drainage was directed back to the river.

Each mesocosm also had a bottom drainage system, also known as the underdrain, which included a grid of perforated PVC pipe located within the drainage stone at the bottom of each mesocosm. This system in effect flushed porewater from the sediments and drainage stone. Water that had drained through the marsh sediment could be collected for study. A material balance of pertinent sediment and porewater parameters could be conducted with samples from this bottom drainage. Three PLCs (#1, #2, #3) and PLC valves governed flow through the underdrain.

Just as with the surface drainage mechanism, effluent from the underdrain could be directed back to the river or to an effluent holding tank for evaluation and treatment.

A T-section in the effluent piping system with a gate valve allowed for the selection of outflow destination; for this study, bottom drainage was directed to the effluent holding tank.

An overflow weir system allowed for drainage when the mesocosm water depth reached the maximum tidal depth. This system consisted of a 7.62-cm -diameter vertical primary overflow pipe at the maximum tidal depth (approximately 30.5 cm above sediment elevation). An additional 7.62-cm -diameter emergency overflow pipe was located adjacent to, and 2.5 cm above, the primary discharge pipe. This emergency pipe was used in the event that the primary overflow became clogged.

Overflow water could be directed back to the river or to an effluent holding tank for evaluation and treatment. A T-section in the effluent piping system with a gate valve allowed for the selection of outflow destination. For this study, overflow was directed back to the river.

The surface drain and two overflow pipes were protected from foreign materials and clogging by a retrofit system. This consisted of an oversized-diameter perforated bucket or pipe collared around each unit. Any material that could potentially obstruct the outlets was impeded by the perforated retrofit pipe.

It should also be noted that PLC valves, although electronically-controlled, could also be opened or closed manually, if necessary.

Simulated Tidal Cycle

Field research was conducted to monitor tidal depths and flooding periods in the native marsh. Data were collected for incorporation into the simulated tidal cycle to be used in the mesocosms. The research was conducted on Skidaway Island, Georgia in a saltmarsh near the BERM facility. Tidal depths and flooding observations were recorded hourly over several tidal cycles in an area of the saltmarsh where *Spartina* biomass and hydrologic regime were similar to that at the LCP site.

The mesocosm simulated tidal cycle is shown in detail in Figure 3.4. Corresponding status of the PLCs is displayed in Figure 3.5. In the tidal cycle, incoming tide (Time A) was initiated by the opening of the influent PLC valves. The influent water from the reservoir flowed through the inlet orifice, filling the mesocosms to a depth of approximately 30.5 cm over a programmed time period of 3.0 hours.

Incoming tide was followed by stagnant high tide (Time B), in which all valves were closed and the water level stayed constant at 30.5 cm. This stagnant high tide lasted 45 minutes. The midpoint of Time B marked the actual high tide point.

Upon completion of stagnant high tide, the outgoing tide (Time C) was initiated by the opening of the surface drain PLC valve. Surface drainage rate was controlled by partially closing a manual gate valve beneath the surface drain. Tidal waters drained over a period of 3.0 hours and the depth of water receded to the sediment surface. Thus, surface drainage rate was equal to influent rate (i.e. the slopes of Time A and Time C in Figure 3.4 are the same).

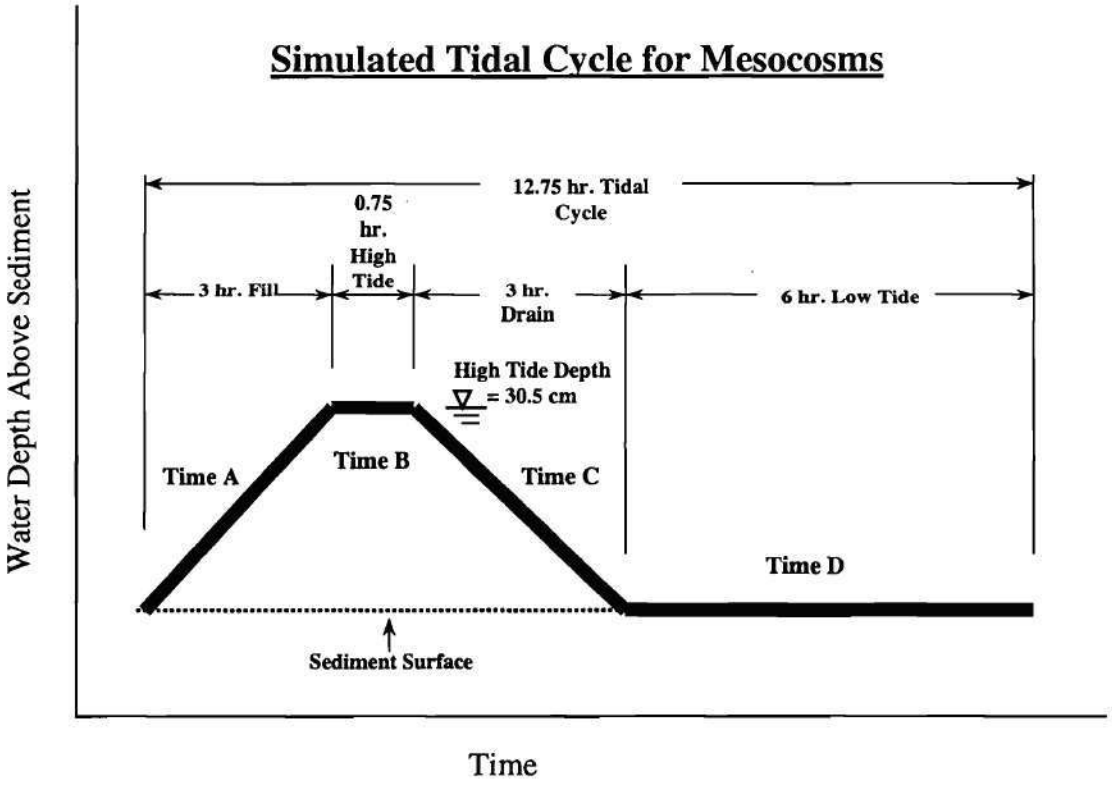

Figure 3.4 Simulated tidal cycle for BERM mesocosms, showing fill, high-tide, drain, and low-tide periods and relative water depths above sediment surface.

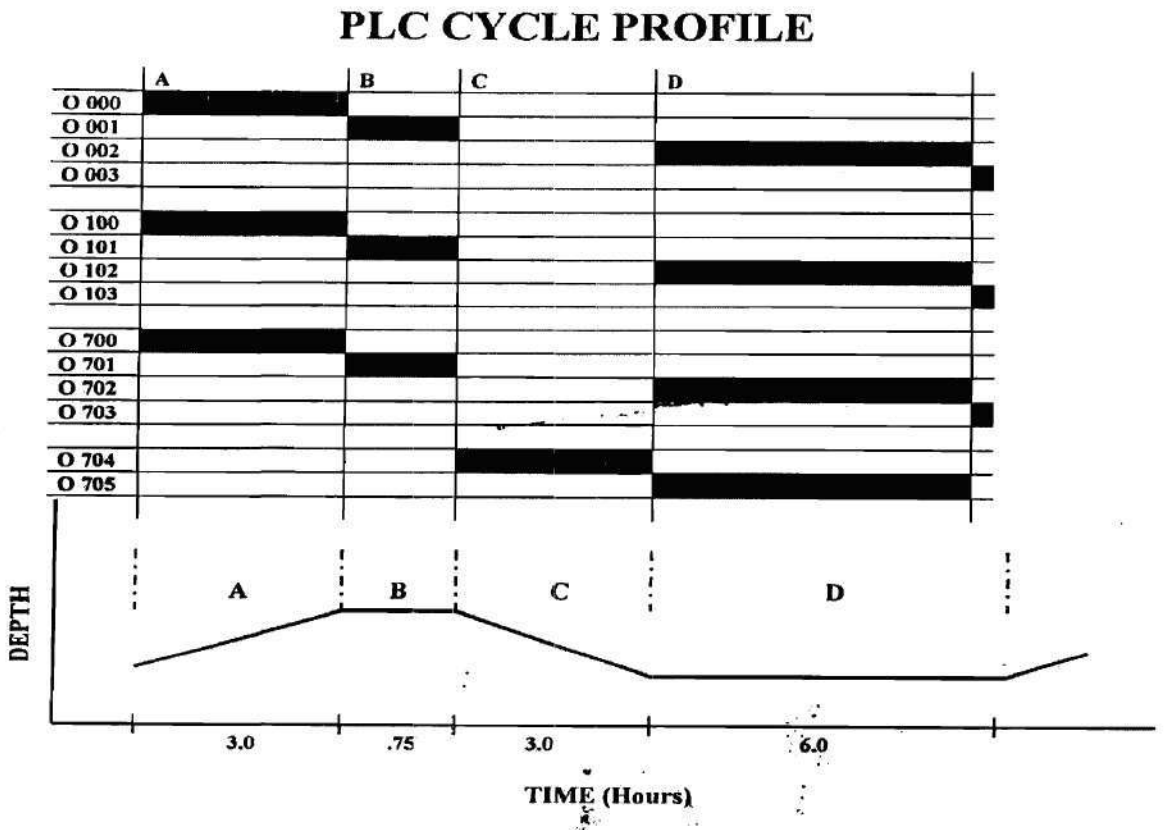

Switch		Time A	Time B	Time C	Time D	Transition	
						(5 seconds)	
000		Influent valve open.					
001			Influent valve closed.	Influent valve remains closed.	Influent valve remains closed.		
002					Underdrain open.		
003						Underdrain closed.	
100		Influent valve open.					
101			Influent valve closed.	Influent valve remains closed.	Influent valve remains closed.		
102					Underdrain open.		
103						Underdrain closed.	
700		Influent valve open.					
701			Influent valve closed.	Influent valve remains closed.	Influent valve remains closed.		
702					Underdrain open.		
703						Underdrain closed.	
704				Surface drain open.			
705					Surface drain closed.		

Reset to Time A — Reset to Time A — Reset to Time A

Figure 3.5 Programmed time cycle and profile for mesocosm PLCs. Valve status is also defined. Switches 000-003, 100-103, and 700-703 corresponded to PLCs #1, #2, and #3, respectively. Each of these PLCs controlled influent water supply and underdrainage for one of the three mesocosms. Switch 704-705 corresponded to PLC #4, which controlled surface drainage for all three mesocosms.

After the surface waters drained, the low tide period (Time D) was achieved by the closing of the surface drain valve and the opening of the underdrain valves. Water drained from within the sediments with the underdrain open. Low tide lasted for 6.0 hours, during which the mesocosm sediment surfaces were exposed to the atmosphere and were no longer under water. Similar to Time B, the midpoint of Time D marked the actual low tide point. The end of low tide marked the completion and automatic "reset" of a tidal cycle. After a five-second transition period, the cycle returned to Time A.

The tidal cycle could also be manually reset at any time with a simple trip wire connection at the PLC box (where the 24-volt power supply and four PLCs were kept). Before the trip was performed, power to PLCs was first turned off. Second, all PLC valves had to be set (manually, if necessary) to closed positions. Third, the trip wire ends were connected. Fourth, the power was restored. Finally, after several seconds of restored power (enough time for the PLCs to turn on), the trip wire ends were disconnected from each other. The trip turned all valves to Time A positions.

The trip reset was used to start the tidal cycle at specific times. In particular, the tidal cycle was coordinated to replicate the tides of the surrounding Skidaway Island saltmarsh. Tides were published and known; one such resource for tidal data for the Savannah River, Georgia area was WTOC-TV via their web page www.wtoc.com/cgi-bin/tidemonth.pl. Marsh tides for the Skidaway area were estimated from these, typically by adding one hour to the "entrance of Savannah River" tides. Once a reset was accomplished, mesocosm tides could be calculated and projected with a computer spreadsheet.

This simulated tidal cycle comprised 12.75 hours and was chosen as the representative cycle to be used in the mesocosms. This cycle was similar to that of the native marsh, which has a cycle of 12.42 hours.

Sediment Collection Areas

Sediments for the three mesocosms were collected from two geographic locations. Contaminated sediment came from the LCP site in Brunswick, Georgia, located approximately 100 km south of Savannah. Pristine sediment in the third mesocosm was collected from a saltmarsh on Skidaway Island.

Pristine Sediment Collection

Pristine sediment was collected from a saltmarsh along Groves Creek, a tributary of Wilmington River, on Skidaway Island, Georgia (Figure 3.6). The collection area stretched from the creek bank to approximately 9 m inland to the mid-marsh. This sediment was considered representative of the Skidaway Island area.

Sediment was excavated using a backhoe and transported by truck approximately 1.6 km to the BERM facility on the campus of the Skidaway Institute of Oceanography. Collection took place at low tide and the sediment contained *Spartina* vegetation.

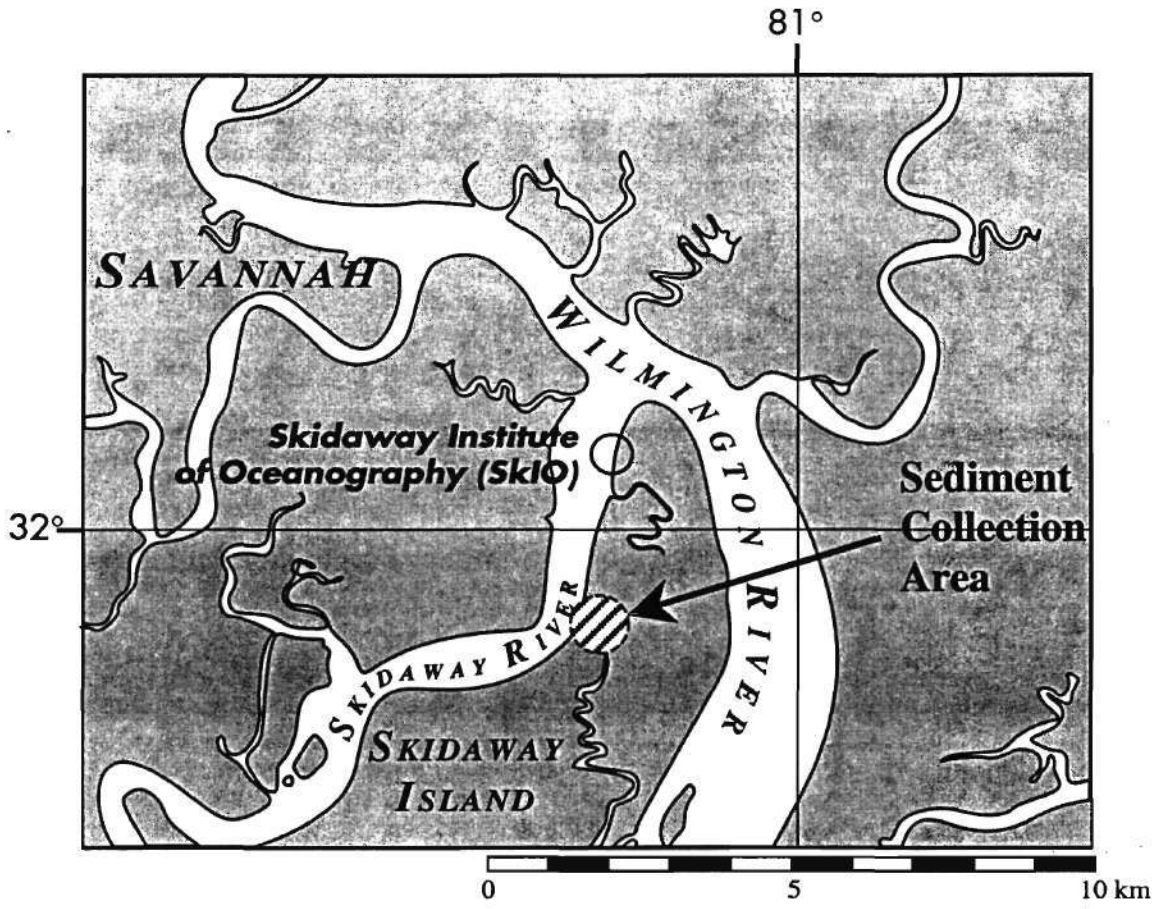

Figure 3.6 Pristine sediment collection area. The marked area was situated along Groves Creek, a creek east of Skidaway Island and a tributary of Wilmington River.

Contaminated Sediment Collection

Contaminated sediment was taken from the LCP Superfund site in Brunswick, Georgia (previously shown in Figure 2.4). The site bordered a brackish tidal marsh dominated by *Spartina alterniflora* and *Juncus romerianus* (black needle rush). The saltmarsh sediments were contaminated with mercury up to the g/kg (parts-per-thousand) range near the site buildings and up to the $\mu g/g_{dry}$ (parts-per-million) range in the surrounding area. The sediment collected for the mesocosms came from the surrounding area.

Due to federal safety regulations concerned with Superfund site access, the sediment (with *Spartina* vegetation) was loaded into barrels and sealed by on-site licensed personnel. The barrels were then transported by truck to the BERM facility on Skidaway Island, approximately 100 km away.

Overall, the time period between excavation of contaminated sediment and incorporation into the mesocosm spanned from two to seven days. There were two shipments of contaminated sediment. The first shipment arrived on October 30, 1998; this sediment was placed into the contaminated-unvegetated mesocosm on November 3, 1998. The second shipment of contaminated sediment arrived on November 4, 1998; this sediment was placed into the contaminated-vegetated mesocosm on November 10, 1998.

Hereafter, sediment from LCP will often be referred to as "LCP-vegetated" or "LCP-unvegetated," depending on the mesocosm. Also, pristine sediment from Groves Creek will be referred to as "GC."

Sediment Preparation

Sediments were emptied from barrels into the mesocosms with the help of a crane. The sediments were homogenized using shovels and rakes, care was taken not to damage the linings of the mesocosms. After mixing was complete, water from Skidaway River was pumped into each mesocosm to an approximate depth of 30.5 cm. The mesocosms remained flooded for approximately 24 hours. After draining, the mesocosm sediments were further homogenized using a shovel. The main purpose of the second mixing was to assure that no large air pockets existed in the sediments, especially along the walls of the mesocosm. Gaps and spaces such as these could present problems by allowing the tidal water to drain directly from the surface through the bottom drain, essentially short-circuiting the system.

Spartina alterniflora Collection and Planting

Spartina plants for all mesocosms were collected in the sediment collection area of Groves Creek. *Spartina* plants, including roots, were carefully removed from the marsh using a small shovel and by hand-digging. Care was taken to retain as much of the root system of each plant as possible. The plants were rinsed with saltwater to remove all sediment from the roots; this ensured that LCP sediment would not be diluted by GC sediment in the mesocosms and that all plants were treated equally.

After washing, *Spartina* was planted in the mesocosms by opening a 15-cm - diameter hole in the sediment and placing the entire root system into the hole. Due to the fluid nature of the sediment at the time of planting, the holes rapidly closed up around the newly-planted *Spartina*. All planting was completed by November 24, 1998.

A total of 35 plants were placed into the GC mesocosm and 36 into the LCP mesocosm. Before planting, each mesocosm was divided into a grid system of 15 equal 0.61 X 0.51 m (2.0 X 1.7 ft.) quadrants. At least two plants were placed into each quadrant. These plants were all similar in height and biomass when planted.

Mesocosm Timeline

The timeline below summarizes the sequence of significant events involved in Gentzler (1999) and this thesis. A "major sampling" refers to a comprehensive sampling. Starting with June 1999, duplicate cores for Hg solid phase analysis were taken; starting with January 2000, duplicate cores for Hg centrate analysis were collected. Gentzler (1999) sampled during the period of October 1998 to June 1999.

October - November, 1998	**Sediments placed in cells. Simulated tidal cycle begins.**
November 24, 1998	**Spartina from Groves Creek planted in mesocosms.**
December 3, 1998	**First major sampling.**
January 7, 1999	**Major sampling.**
March 10, 1999	**Major sampling.**
June 23, 1999	**Major sampling.**

August 31, 1999	**Major sampling.**
January 18, 2000	**Major sampling.**
March 31, 2000	**Major sampling.**

The methods used in these samplings are discussed next.

CHAPTER IV

METHODS

Sediment Sampling

Sediment cores were sampled for measurements of sediment density and porosity, sulfate reduction rates, porewater chemistry (pH, sulfate, sulfide, iron(II), dissolved inorganic carbon, and ammonium), mercury and methyl mercury analysis, and loss-on-ignition. Cores were collected using transparent Lexan core barrels (15-cm length, 2-cm I.D.) with a plunger. Plungers consisted of a steel shaft and a screw-on Teflon head. The plunger head was fitted with o-rings to maintain a gas-tight seal. A small amount of vacuum grease was used along the o-rings to lubricate the Teflon head as the plunger moved inside the core barrel.

Cores were taken by pushing the core barrel vertically into sediment while keeping the plunger head near the sediment surface. Cores were collected approximately 5-7 cm away from a *Spartina* plant in the vegetated mesocosms. When a core reached at least 10 cm in depth, it was slowly pulled out vertically. The open end was sealed immediately with a stopper and cores were inspected to ensure that the sediment was undisturbed and that no air pockets or voids were present. It was also important that sediments were not compressed during sampling. In addition, to keep the sediments in

their natural orientation and to minimize losses of porewater, all cores were maintained in a vertical position after sampling.

Cores were taken to the laboratory within minutes of sampling. Cores for porewater analysis were sectioned into sterile centrifuge tubes in an anaerobic glove bag. These sealed tubes preserved an anaerobic environment during further sample handling. Centrifuge tubes were then centrifuged for 10 minutes at 3000 x g. Centrate was poured into a plastic syringe and filtered in an anoxic environment through a 0.2-μm nylon filter.

Centrate aliquots for various analyses were conducted as follows:

a) Sulfate and Dissolved Fe(II) : 500 μL of porewater sample were acidified with 4 μL of concentrated hydrochloric acid (12 M) in a 2-mL gas-tight vial. Samples were shaken well and frozen at –15°C until analysis.

b) Dissolved Sulfide : In another 2-mL vial, 250 μL of porewater were added to 100 μL of 20 % (w/w) zinc acetate (ZnAc) solution. Samples were shaken well and frozen at –15°C until analysis.

c) Dissolved Inorganic Carbon and Ammonia : A 1.8-mL gas-tight vial was filled with porewater for dissolved inorganic carbon (DIC) and ammonium analysis. Care was taken with these samples to ensure no headspace was present in the vials since headspace affects dissolved concentrations of these two parameters (Hall and Aller, 1992). Samples were refrigerated at 4°C until analysis, which was completed within three days of sampling. It was imperative to not freeze these samples in that freezing affects concentration of DIC (Hall and Aller, 1992).

d) pH : 500 μL of porewater was placed into a small test tube and a pH electrode was placed into the test tube for pH determination.

In these analyses, smaller volumes were used for each partitioned porewater sample when necessary due to insufficient total porewater volume. Such variations were recorded.

Porewater Sipper Sampling

In addition to centrifugation, porewater was also obtained using an *in situ* sipper system. Similar devices have previously been used by Short *et al.* (1985) and Chambers and Odum (1990). Sipper samplers, shown in Figure 4.1, were constructed of high-density polyethylene (HDPE) stakes with a porous collar (100-μm pore size) located at the required sampling depth. The stakes were gas-tight except for a sampling tube (Teflon, 1.6 mm I.D.) entering the top and extending to the sampling depth and a gas tube (Teflon, 1.6 mm I.D.) entering the top and extending one cm into the stake.

To obtain porewater, suction was applied to the gas line using a vacuum hand pump. The sipper was allowed to fill and collect porewater for approximately fifteen minutes by vacuum from the sediment into the hollow stake. The volume of porewater was extracted by applying positive N_2 pressure. N_2-flushed 20-mL glass syringes were attached to the sample line for sample collection. N_2-filled 50-mL glass syringes were attached to the gas line in order to provide positive pressure to displace the porewater.

Figure 4.1 Sipper sampling device.

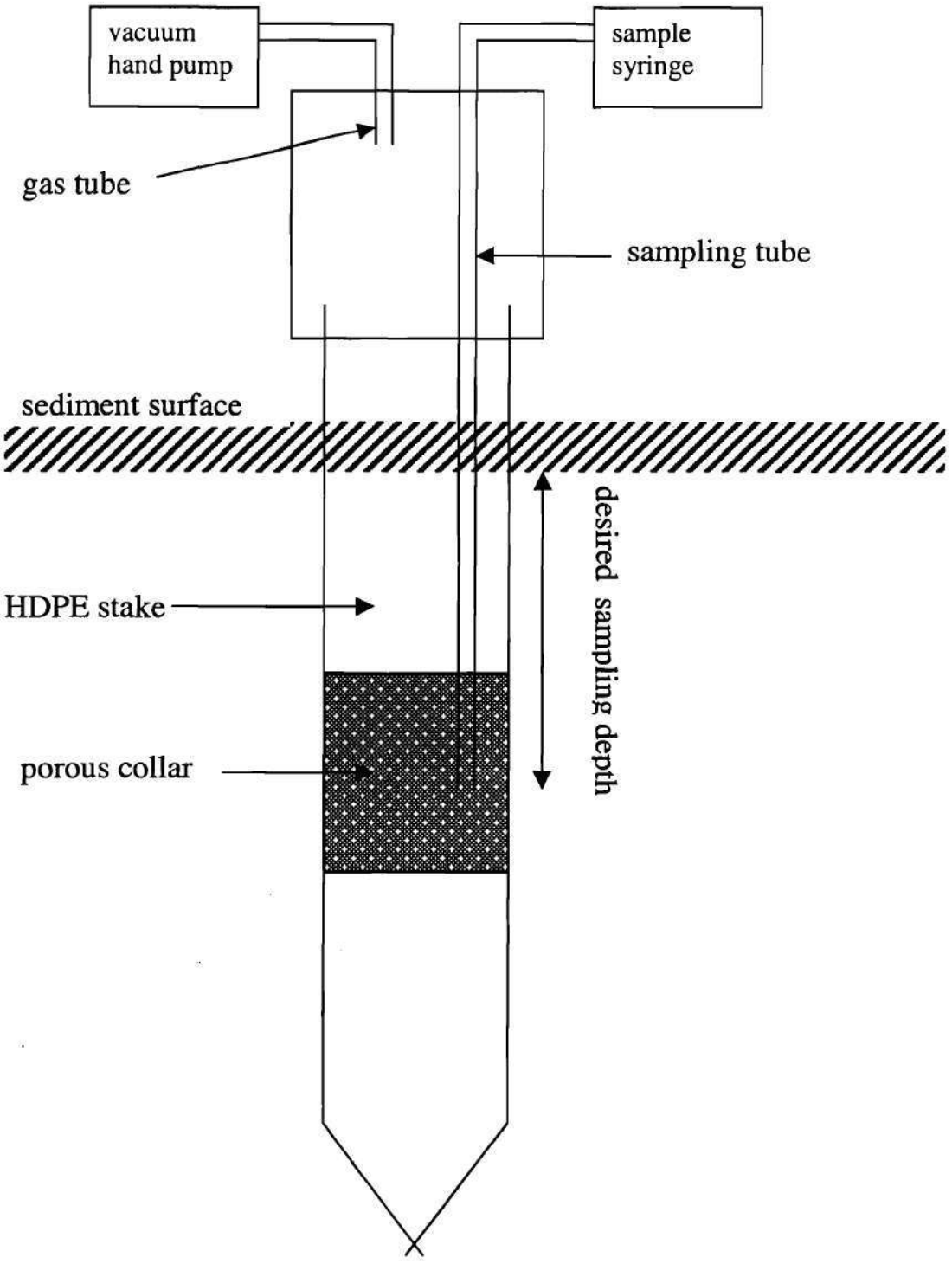

Sample syringes were kept cold and transported to the laboratory within minutes. Porewater in the syringes was filtered through a 0.2-μm nylon filter in an anoxic glove bag. The porewater samples were partitioned using the same procedure outlined in earlier this chapter.

Porewater sipper samples were taken in duplicate at depths of 3 cm, 6 cm, and 10 cm in each mesocosm.

After each sampling, sippers were taken apart and scrubbed and cleaned with tap water. Several days before the next sampling, tap water, 3M HCl, and tap water again were purged through all tubing. In the case of HCl, the sippers were left overnight in an 3M HCl bath with acid inside all tubing. In the final tap water purge, water was left in all tubing for several hours in order to assure removal of residual HCl. To confirm complete removal of HCl, water was run through tubing and checked with pH paper.

Temperature

Sediment temperatures were recorded in all mesocosms periodically, including each sampling date. At low tide, a glass thermometer was placed vertically down into the sediment and measurements were taken at the surface and at 5-cm and 10-cm depths.

pH Analysis

A pH electrode and meter were used to determine the pH of porewater samples. The electrode was calibrated each day of use with 4.0 and 7.0 pH buffer solutions. The electrode was placed into filtered porewater; the pH reading usually stabilized within 30 seconds.

Salinity

A refractometer was used to measure salinity of surface water and porewater samples. The refractometer was calibrated each day of use with DI (salinity = 0). Using a pipette, several drops of water were placed on the refractometer prism surface; the reading usually stabilized within 15 seconds. After each reading, the prism was cleaned with DI water and tissue.

Dissolved Inorganic Carbon and Ammonium Analysis

Dissolved inorganic carbon (DIC) and ammonium (NH_4^+) were measured by flow injection analysis (Hall and Aller, 1992). Using a 250-μL glass syringe, sample volumes of 50 μL were injected into a reagent stream in which the stable form of the solute of interest is the gas phase. For DIC, analysis required an influent acid stream to convert all dissolved inorganic carbon to gaseous CO_2. This reagent stream passed over a gas-

permeable hydrophobic membrane, in this case Teflon tape. On the other side of this membrane was another reagent stream in which the gas phase is not the stable species. This allowed the solute of interest to be separated from the sample solution and re-solubilized in the receiving stream. At this point, the receiving stream traveled into a conductance meter, which indirectly measured the quantity of the transferred solute. Solute concentrations were calculated from conductance standard curves.

For DIC, the injection stream ranged from 10-30 mM HCl and the receiving stream was 10 mM sodium hydroxide (NaOH). For ammonium, the injection stream was a combination of 0.2 M sodium citrate and 30 mM sodium hydroxide, and the receiving stream was 50 μM HCl. To adjust for sensitivity, the receiving streams were diluted further as needed.

Standards for DIC analysis were prepared using solid sodium bicarbonate ($NaHCO_3$) in deionized water (DI). A 100 mM $NaHCO_3$ working standard was prepared in a 100-mL volumetric flask. A typical standard curve consisted of 1.5, 3, 6, 12, 25, and 35 mM HCO_3^- concentrations, prepared using mass / mass dilutions of the stock solution or standards. Standards were refrigerated at 4°C until analysis.

Standards for ammonium analysis were prepared using solid ammonium chloride (NH_4Cl) in a 29 ppt NaCl solution (salinity adjusted to represent that of Skidaway River). Hall and Aller (1992) observed that conductivity response was partially dependent upon salinity. A working standard of 100 mM ammonium choride was prepared in a 100 mL volumetric flask. A typical standard consisted of 10, 25, 50, 100, 200, and 500 μM NH_4^+

concentrations and were prepared using mass / mass dilutions from the stock solution or standards.

During routine analysis of DIC and ammonium, it was necessary to clean the apparatus by changing the Teflon tape and running DI through all apparatus and tubing for approximately 10 minutes. Also, approximately every tenth sample was run through the instrument in duplicate to assure reproducibility. Further, to clean out the system, DI was injected after samples of relatively high concentration.

Detection limits for porewater analyses were obtained by analyzing seven replicates of the lowest point of the standard curve. Using a student's t value for a 99% confidence level (t = 3.14 for seven replicates) and standard deviation, S, of the replicate analyses, detection limit = (t) x (S). In this study, a detection limit of 0.27 mM, based on seven 0.99 mM replicates, was determined for DIC. A detection limit of 1.39 μM, based on seven 10 μM replicates, was determined for ammonium.

Dissolved Iron(II) Analysis

Dissolved Fe(II) was analyzed using a disodium salt reagent of 3-(2-pyridyl)-5, 6-bis(4-phenylsulfonic acid)-1,2,4-triazine, hereafter referred to as ferrozine. Ferrozine reacts with iron(II) to form a stable magenta-colored complex, which is very soluble in water and may be used for the direct determination of iron(II). The absorbance of the complex was measured at 562 nm (Stookey, 1970). A spectrophotometer and 1-cm cuvettes were used. All plastic and glassware used for this analysis were cleaned with 6

M HCl in order to avert iron contamination. Samples were acidified because dissolved Fe is unstable in water at neutral pH and would immediately precipitate out as Fe oxide. Under acid conditions, dissolved Fe is stable and maintains its oxidation state.

Ferrozine reagent was made by combining 23.83 g of solid hepes [4-(2-hydroxyethyl)-1-piperazineethanesulfonic acid] and 0.4 g of solid ferrozine in DI and diluting to 2.0 L. Hepes served as a buffer. The pH was then adjusted to 7.0 by adding solid NaOH.

Standards were prepared using solid ferrous ammonium sulfate [$Fe(NH_4)_2(SO_4)_2$] in DI. A $Fe(NH_4)_2(SO_4)_2$ stock solution was prepared in a 100-mL volumetric flask. This stock solution included 750 μL of 0.5 M HCl to prevent microbial growth. From this stock, a 1 mM working standard was made. From the working standard, typical standards of 1, 3, 10, 20, and 40 μM Fe(II) concentrations were prepared by dilution in 2 mL of ferrozine buffer. To ensure that acidity in samples and standards was approximately the same, 12 μL of 1 N HCl was added to each standard. After 30 minutes at room temperature, absorbance was measured at 562 nm.

For porewater analysis, 100 μL of sample was added to 2 mL of ferrozine in a test tube and measured after 30 minutes. For samples with iron(II) concentrations beyond the standard curve range, analysis was re-done with only 50 μL of sample or a dilution was performed.

In this study, a detection limit of 0.17 μM, based on 3.14 times the standard deviation of seven 0.99 μM replicates, was ascertained.

Sulfate Analysis

Sulfate was measured using the turbidometric method described by Tabatabai (1974). This method is based on the measurement of turbidity formed when a mixture of barium chloride and gelatin is added to an acidified water sample. The acid was used to drive off any hydrogen sulfide (H_2S) present in the sample. Without acid, the H_2S could oxidize to form sulfate and thus cause an inaccurate sulfate measurement.

To prepare the barium chloride gelatin reagent, 1.5 g of solid gelatin was dissolved in 500 mL of DI at 70°C. This gelatin solution was stored for a minimum of 16 hours at 4°C before use. Then, 1.5 g of solid barium chloride monohydrate was dissolved in gelatin solution to a volume of 150 mL and left for one hour at room temperature.

Standards for sulfate analysis were prepared using solid sodium sulfate at concentrations of approximately 10, 20, and 30 mM Na_2SO_4. These standards were refrigerated at 4°C when not in use.

For analysis, 500 µL of 1 N HCl was added to 10 mL of DI in a test tube. Then, 40 µL of acidified sample or standard was added and the test tube was mixed gently. In time increments of 30 seconds, 500 µL of barium chloride gelatin was added to each sample, followed by mixing. After 30 minutes, absorbance was read at 420 nm using 4-cm cells.

In this study, a detection limit of 0.50 mM, based on 3.14 times the standard deviation of seven 9.99 mM replicates, was ascertained.

Dissolved Sulfide Analysis

Dissolved sulfide was measured in porewater using the method of Cline (1969). The appropriate amount of diamine reagent, hereafter referred to as Cline reagent, was added to the ZnAc-amended sample. ZnAc was used to capture sulfide as zinc sulfide precipitate and prevent sulfide oxidation to sulfate. The absorbance was determined at 670 nm in a small-volume one-cm cuvette.

Cline reagent was prepared by dissolving 2.0 g of diamine and 3.0 g of ferric chloride ($FeCl_3$) in 6 N HCl for a total volume of 500 mL. The solution, yellow in color, was refrigerated at 4°C until use.

Standards were prepared anoxically using solid sodium sulfide (Na_2S) and DI purged with nitrogen gas. A small crystal of Na_2S was rinsed with DI, immediately weighed, added to purged DI, and sealed in a bottle. This stock solution was transferred to an anaerobic chamber where dilutions were completed. Standard Na_2S solutions of approximately 5, 15, 30, 50, and 100 μM were prepared and fixed with an appropriate amount of zinc acetate (e.g., 300 μL 20 % ZnAc per 4 mL standard solution).

The Cline reagent was added at a ratio of 80 μL per 1 mL of sample or standard. The reaction with dissolved sulfide produces a blue color. Absorbance was read after 20 minutes. Sample dilutions were made with DI when concentrations were beyond standard curve range.

In this study, a detection limit of 0.27 μM, based on 3.14 times the standard deviation of seven 0.87 μM replicates, was ascertained.

Sulfate Reduction Rate Measurement

Rates of sulfate reduction were determined in duplicate whole cores using the radiotracer ($^{35}SO_4^{2-}$) technique described by Jorgensen (1978). Cores (described earlier in this chapter) had 1-mm-diameter portals drilled into them at 1-cm intervals; these holes were sealed with silicone. Immediately after sampling, the sediment cores were injected with 6 μL (approximately 7.5 μCi) radiotracer (sulfuric acid, $^{35}SO_4^{2-}$) at 2-cm intervals to a 10-cm depth. Cores were then placed for approximately two hours in an incubator set at sediment temperature.

After incubation, cores were sectioned at 2-cm intervals into 10 mL of 20 % ZnAc in centrifuge tubes. These were mixed vigorously to ensure that the zinc acetate fixed any sulfide present and effectively stopped (a.k.a. "killed" or "sacrificed") any microbial processes, sulfate reduction in particular. The tubes were then sealed and frozen at –15°C for future analysis.

Prior to analysis, samples were thawed and centrifuged for 10 minutes at 4,200 x g to separate the porewater / ZnAc mixture from the sediment. Approximately 4 mL of the porewater / ZnAc was poured into a 7-mL polyethylene scintillation vial.

In addition to duplicate cores taken per mesocosm, a single core was taken from each mesocosm as the "background" core for a blank determination. This core was treated the same as the other cores except that injected cores were immediately fixed with ZnAc and frozen at –15°C without incubation.

A detailed explanation of the distillation method used for sulfate reduction rate measurement can be found in Fossing and Jorgensen (1989). A summary of the method employed follows here.

Sediment samples were treated and incubated with $^{35}SO_4^{2-}$ for approximately two hours. Sulfide was produced by microbiological respiration processes; the reduced form of sulfur was assumed to be present as solid sulfide minerals. The spun-down sediment sample was transferred to a distillation apparatus that consisted of a gas-tight reaction flask (three-way flask) that was supplied with a gas-bubbling tube, a condenser, and a zinc acetate trap. This set-up was continuously purged with nitrogen gas. The acid-volatile sulfide (AVS), predominantly H_2S and FeS, was volatilized by the addition of concentrated HCl and captured by a test tube trap containing 5 % ZnAc. The chromium-reducible sulfur, which includes pyrite (FeS_2) and elemental sulfur, was reduced to a valence of -2 by the addition of Cr^{2+} solution and collected in a second test tube trap, this one containing 20 % ZnAc.

Sulfide in the ZnAc traps was measured by the method of Cline (1969); radiolabelled sulfide was quantified using a scintillation counter.

The equation used in calculation of sulfate reduction rates for a particular sediment sample is as follows:

Equation 4.1:

$$SRR = [SO_4] * \frac{\text{TRS cpm}}{\text{g sediment distilled}} * \frac{\text{g sediment incubated}}{\text{time incubated}} * \frac{1.06}{\text{porewater cpm}} * \phi$$

where:

SRR	=	Sulfate Reduction Rate (nmol/cm^3_{bulk}-d)
$[SO_4]$	=	concentration SO_4 (nmol/mL)
cpm	=	radioactive counts per minute for ^{35}S
TRS	=	Total Reducible Sulfur (AVS + CRS)
1.06	=	isotope fractionation factor (constant) (Fossing and Jorgensen, 1989)
porewater	=	spun-down porewater / ZnAc mixture from sediment
ϕ	=	porosity of sediment (cm^3_{void} / cm^3_{bulk}) .

Fossing and Jorgensen (1989) found standard deviation values ranging from 0.39 to 2.85 % for sulfate reduction rates ranging from 33 to 833 nmol/cm^3-d. These rates are comparable to those found in this study.

Acid-Volatile Sulfide and Chromium-Reducible Sulfur Analysis

Acid-volatile sulfide and chromium-reducible sulfur levels were determined by a two-step distillation with 12 N HCl and 1.0 M Cr^{2+} solution (Fossing and Jorgensen, 1989).

To make the Cr^{2+} solution, 200 g solid chromium chloride ($CrCl_3$) were dissolved in 0.5 N HCl to a volume of 750 mL. A 2 L glass bottle with an outlet and stopcock at the bottom was filled to the 0.5 L mark with zinc granules. The zinc could be re-used several times, but it was imperative to first rinse them with approximately 50 mL of 6 N HCl. Once the zinc was acid-cleaned, the $CrCl_3$ solution was poured into the glass bottle under continuous flow of N_2. The zinc reduced Cr^{3+} to Cr^{2+} under the anoxic environment; complete reduction was verified by a color change from dark green (Cr^{3+}) to bright blue (Cr^{2+}). For 750 mL, this process required approximately three hours of bubbling with N_2. Once reduced, the blue solution was drawn from the bottom outlet into

50-mL plastic syringes and refrigerated. The solution was useful as long as it maintained its reduced state (bright blue color).

AVS was collected in a test tube trap containing 10 mL of 5 % ZnAc; distillation lasted for 30 minutes and began with the addition of 8 mL of 12 N HCl. CRS was collected in a test tube trap containing 20 mL of 20 % ZnAc; distillation lasted for 45 minutes and began with the addition of 15 mL of boiling 1.0 M $CrCl_3$ solution. AVS and CRS concentrations from the appropriate ZnAc trap were measured using the Cline (1969) method.

Fossing and Jorgensen (1989) found standard deviation values ranging from 2.8 to 6.7 % for AVS concentrations of 6.2 to 19.3 $\mu mol/cm^3$. Standard deviations ranging from 3.8 to 9.7 % were exhibited for CRS concentrations from 12.4 to 151.8 $\mu mol/cm^3$. These concentrations are comparable to those found in this study.

Density and Porosity Determination

Cores sampled for density and porosity measurements were sectioned in 2-cm lifts into a plastic syringe. Each subsample was homogenized using a small metal spatula. From this homogenized sediment, duplicate density / porosity samples were taken.

Wet sediment was inserted into a 5-mL plastic syringe. The syringe was cut to have a flat open end for insertion of sediment. This open end also allowed for a known volume of wet sediment to be measured and extracted from the syringe. One cubic

centimeter of wet sediment was extracted into a pre-weighed polyethylene scintillation vial. The wet weight of the sediment was determined by weighing the sediment-filled vial and subtracting the vial weight. Dry sediment fraction was determined by heating the known volume of sediment at 70°C for 48 hours in an oven. Saturated wet density was determined based on the known sediment volume and the wet weight of each sediment volume; since these sediments were obtained from the waterlogged mesocosms, saturation was assumed to be 100 percent. Porosity (void volume divided by total wet sediment; total wet sediment volume equals bulk volume) was determined based on mass and density of Skidaway River water (density = 1.02 g/cm^3) that occupied the void volume of sediment. Derived from the various physical parameters measured, the particle density of the sediment was calculated with the following equation:

Equation 4.2:

$$\rho_p = \frac{(X_p * \rho * \rho_w)}{(\rho_w - \rho * X_w)}$$

where:

X_p = mass fraction dry particle (g_p / cm^3_{bulk})
X_w = mass fraction water (g_w / cm^3_{bulk})
ρ = wet density (g_{bulk} / cm^3_{bulk})
ρ_p = particle density (g_p / cm^3_p)
ρ_w = density of Skidaway River water (g_w / cm^3_w) .

Loss On Ignition Measurement

To estimate the organic carbon content in the mesocosm sediments, loss on ignition (L.O.I.) was performed. Loss on ignition does not truly give organic content as related to sedimentary substrate for bacteria; components such as bound water (water of hydration), quality of organic material, and oxidation of solids are not accounted for in the technique. However, L.O.I. is an accepted proxy for sedimentary organic matter content and these data served as a relative comparison of the sediments from each of the three mesocosms used in this study. In similar fashion, Benoit *et al.* (1998) assumed that all L.O.I. was attributable to destruction of organic matter.

A sediment sample of several grams was placed into a pre-weighed crucible and then into an oven set at 105°C. After 12 hours, the crucible was taken out and weighed; minus the crucible, this is the dry weight. The sample was then placed in a muffle furnace set at 520°C. After another 12 hours, the crucible was taken out and weighed again; minus the crucible, this is the ash weight. The following equation was used for loss on ignition:

Equation 4.3:

$$\text{L.O.I.} = \frac{(dw - aw)}{dw} * 100$$

where:

L.O.I.	=	loss on ignition (%)
dw	=	dry weight of sediment (g)
aw	=	ash weight of sediment (g)

Determination of Total Mercury in Sediment

Total mercury levels in sediment samples were determined according to an adaptation of EPA Method 245.7, a new technique in draft form at the time of this study (EPA, February 1999 Draft). This method eliminated the use of gold traps, which are required in EPA Method 1631 (described earlier in this chapter). Samples were microwave-digested before being analyzed with a gas-liquid separator (Tekran) and cold vapor atomic fluorescence (CVAF) detector (Tekran, Model 2500).

Samples were collected as cores in duplicate and immediately sectioned into polyethylene scintillation vials. Samples were then promptly frozen at –15°C. Each sample was analyzed for both total mercury and methyl mercury.

All mercury analyses mentioned hereafter were performed in a trace metals clean room / laboratory and required scrupulously-cleaned polytetrafluoroethylene (more commonly known as PTFE or Teflon) ware. Cleaning was predominantly done by thorough washing with tap water, soaking overnight in a bath of heated concentrated nitric acid (60°C), more thorough rinsing with tap water, and drying in a fume hood. Gloves were worn during sampling, handling, and analyses. Ultra-high-purity argon carried sample streams and trace-metal-grade reagents were exclusively used. Tap water in this particular laboratory was used in all Total Mercury analyses because it had been found to contain less background mercury and thus produced lower blanks during analyses when compared to deionized (DI) water.

For microwave digestion, 0.2-0.5 g of thawed sediment (wet sediment) was combined with 5 mL tap water and 5 mL concentrated nitric acid (16 N HNO_3) in Teflon

microwave vessels. These solutions were digested in a microwave (CEM, Model MDS-2100) for 30 minutes at 120 psi and 60°C. When completed, the digests were poured into polyethylene scintillation vials.

To prepare samples for analysis, 1 mL of bromate / bromide 0.1 N solution was combined with 5 mL 6 N HCl in a 60-mL Teflon vial. The bromate / bromide solution formed bromine monochloride (BrCl) and oxidized all Hg compounds to Hg(II). An aliquot of digest sample, ranging from 0.005 to 1.0 mL and estimated to contain 0.2 – 5.0 ng of total mercury, was added to this mixture. The mixture was then diluted to 50 mL with tap water. After 30 minutes, 50 μL of hydroxylamine hydrochloride (NH_2OH-HCl, 1.7 M, purified with stannous chloride) were added to mainly reduce excess BrCl; the solution was allowed to stand for an additional five minutes.

The analytical train is illustrated in Figure 4.2. Prepared samples were pumped through a four-channel peristaltic pump set at 25 revolutions per minute. This setup simultaneously combined stannous chloride ($SnCl_2$) solution with the prepared sample; the $SnCl_2$ reduced all mercury species to Hg(0). After reacting with $SnCl_2$, the solution entered the gas-liquid separator. The separator featured a glass rod over which dripped a thin sheath of the sample solution. A counterflow of argon (200 mL/min) removed mercury vapor from solution and purged the vapor into a drying tube. The semi-permeable drying tube, composed of Nafion (a copolymer of Teflon), selectively removed water vapor from the sample stream. Nafion has a very high water-of-hydration; consequently, when gas containing water vapor passed through the drying tube, the water was absorbed by and passed through the walls of the tubing, evaporating

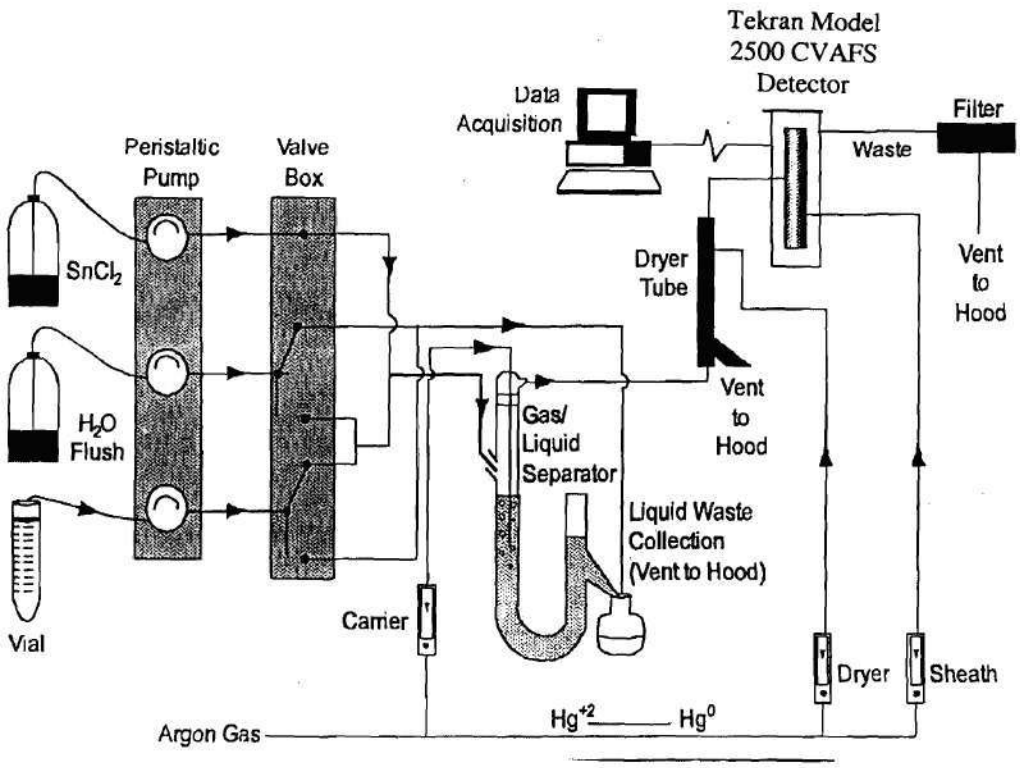

Figure 4.2 Analytical train including cold vapor atomic fluorescence spectrometer used in determination of total mercury, according to EPA Method 245.7 (EPA, 1999).

into the surrounding air. The remaining components of the gas, i.e. mercury vapor, were unaffected. The Nafion was enclosed by a shell, through which passed a countercurrent flow of argon (400 mL/min) that carried away the water vapor. The sample stream was directed to the CVAF detector. The detector measured the amount of total mercury in the stream; measurement was charted by an integrator in peak-height mode.

A standard curve was produced from a 10 ppb ($\mu g/L$) stock standard. Standards of 5.0, 2.5, 1.0, 0.5, 0.2, and 0 ng were made in 60-mL Teflon vials.

In this study, a detection limit of 0.028 ng, based on 3.14 times the standard deviation of seven 0.2 ng replicates, was ascertained. For a typical 0.25-g sample, this translated into a detection limit of 0.11 ng/g_{wet} (parts-per-billion).

For QA/QC considerations, continuing calibration verifications (CCVs) were regularly checked against the calibration curve. In addition to CCVs, reagent blanks, acid blanks, and distillation blanks were run concurrently with samples. Further, commercially-available certified reference materials (CRMs) or standard reference materials (SRMs) for mercury and methyl mercury were analyzed. MESS marine sediment is certified at 0.096 ($\pm$ 0.009) $\mu g/g$ (parts-per-million) for total mercury. IAEA (International Atomic Energy Agency) marine sediment is certified at 5.45 ($\pm$ 0.39) ng/g (parts-per-billion) for methyl mercury.

CCVs in total mercury analyses produced 105 ($\pm$ 9.9) % recovery, which fell within method quality control acceptance criteria of 76-111 % for ongoing precision and recovery, OPR (EPA, 1999). MESS showed 102 ($\pm$ 1.2) % recovery for total mercury.

To further assess the validity of data, a 95 % confidence interval was derived from a standard error of regression of calibration curves. This confidence interval was applied to measurements based on each curve and performed on the same day. Briefly, confidence interval was calculated as follows:

Equation 4.4:

$$X = \frac{(Y + 2\sigma) - b}{m} - \frac{(Y - b)}{m} = \frac{2\sigma}{m}$$

where:

X	=	95 % confidence interval (pg total mercury, x-axis)
Y	=	CVAF response factor (unitless, y-axis)
σ	=	standard error of regression (unitless)
b	=	Y-intercept (unitless)
m	=	slope of regression line (1/pg) .

Confidence interval was divided by sample mass or volume to arrive at a concentration.

Determination of Total Mercury in Porewater

Total mercury levels in porewater samples were determined according to a modified version of EPA Method 1631. Analysis was performed with a gas-liquid separator, gold-trap amalgamation, and CVAF.

Samples were obtained in two ways: sippers and centrifuged core sections. The two techniques are described earlier in this chapter. Sipper samples were filtered with a

0.2-μm nylon filter into 7-mL Teflon vials. For core sections, samples were collected as cores in duplicate and immediately sectioned aerobically into acid-cleaned centrifuge tubes. Supernatant water was then filtered with a 0.2-μm nylon filter into 7-mL Teflon vials. Samples then were acidified to 0.2 % with sulfuric acid (18 N H_2SO_4) and refrigerated in the dark.

To prepare samples for analysis, 1 mL of bromate / bromide 0.1 N solution was added to a 7-mL Teflon vial containing the sample. This mixture was combined with 2.5 mL of 6 N HCl in a 60-mL Teflon vial, then diluted to 25 mL with tap water. After 30 minutes, 50 μL of hydroxylamine hydrochloride was added; the solution was allowed to stand for an additional five minutes.

To begin analysis, a lime trap was connected to a gold trap (gold-coated sand in a quartz tube). The lime trap captured acid vapor in the sample stream and thus prevented acid decomposition of the gold trap. The upstream end of the lime trap was then connected to the gas-liquid separator. Prepared samples were pumped through a peristaltic pump set at 25 revolutions per minute. This setup simultaneously combined stannous chloride ($SnCl_2$) solution with the prepared samples, the same technique described previously for Total Mercury in Sediment. After reaction with $SnCl_2$, the solution entered the gas-liquid separator and was purged through the lime trap to the gold trap, where mercury vapor was adsorbed. The "loaded" gold trap was dried for five minutes by purging argon through it at 250 mL/min. The trap was then heated for three minutes (to approximately 350°C) to thermally desorb Hg into the CVAF detector. Argon flowed through the trap at 60 mL/min. The detector measured the amount of total

mercury in the sample stream; measurement was charted by an integrator in peak-area mode.

A standard curve was produced from a 5 ppb (μg/L) stock standard. Standards of 0.5, 0.25, 0.1, 0.05, and 0 ng were made in 60-mL Teflon vials.

In this study, a detection limit of 0.019 ng, based on 3.14 times the standard deviation of seven 0.05 ng replicates, was ascertained. For a typical 2-mL sample, this translated into a detection limit of 9.70 ng/L (parts-per-trillion).

Similar to that described for mercury in sediments, continuing calibration verifications (CCVs) were regularly checked against the calibration curve. In addition to CCVs, reagent blanks, acid blanks, and distillation blanks were run concurrently with samples. Unlike for sediments, SRMs for pollutants (such as mercury) are not commercially-available in seawater.

CCVs in total mercury analyses produced 100 ($\pm$ 16) % recovery, which fell within quality control acceptance criteria of 77-123 % for OPR (EPA, 1999).

To further assess the validity of data, a 95 % confidence interval was derived from a standard error of regression of calibration curves in the same manner (Equation 4.4) described previously for mercury in sediments. In the case of porewater measurements, this parameter varied greatly in that sample volumes varied by an order of magnitude.

Determination of Methyl Mercury in Sediment

Methyl mercury levels in sediment samples were determined according to a modified version of EPA Method 1630 as well as published work from Bloom (1989), Horvat *et al.* (1993), and Liang *et al.* (1994). Analysis was performed by distillation, aqueous phase ethylation, adsorption on a Tenax trap, chromatographic desorption, and CVAF.

Samples were collected as cores in duplicate and immediately sectioned into polyethylene scintillation vials. Samples were then promptly frozen at –15°C.

Distillation, which separated methyl mercury from other interfering species, was accomplished on a custom-built aluminum heating block and cold-water chiller, shown in Figure 4.3. In a 30-mL Teflon vial (the distillation vial), approximately 1 g of thawed sediment (wet sediment) was combined with 5 mL distilled DI water, 200 μL 20 % KCl (w/w), and 0.5 mL sulfuric acid (H_2SO_4, 16 N). Distilled DI was necessitated because tap water was chlorinated and would thus introduce excessive Cl^- interference. Distillation was accomplished with a quartz sub-boiling still. The KCl provided sufficient Cl^- ions later needed in the ethylation process. The H_2SO_4 released Hg compounds from binding sites on sulfides and organics. The mixture was then diluted with distilled DI to a weight of 15 g. A 60-mL Teflon vial with 7 mL of distilled DI served as the collection vial. The distillation vial was placed in the heating block, which was set to a temperature of 145°C. The collection vial was placed in the chiller (5°C) and connected to the distillation vial. Argon flowed through the distillation vial at 80 mL/min.

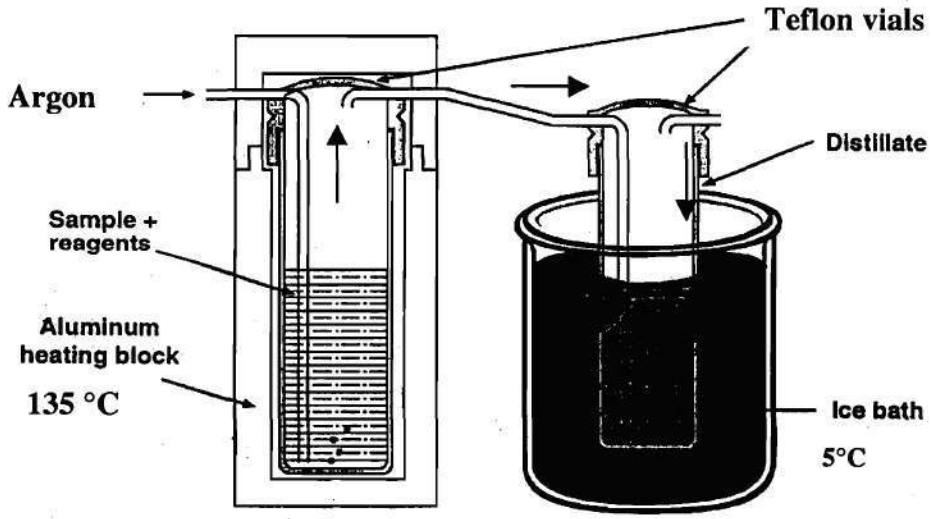

Figure 4.3 Distillation apparatus for determination of methyl mercury, according to EPA Method 1630 (EPA, 1999). Both the aluminum heating block and the ice bath were custom-built to hold 15 vials at-a-time.

Distillation continued until approximately 80 % of the sample volume was distilled. Thus, the collection vial was removed from the chiller once it contained 19 mL of distillate (7 mL water + 12 mL distillate). The sample was then diluted to 25 mL with distilled water. Finally, the sample solution was set to a pH of approximately 5.0 by μL-level additions of citrate and KOH. Prepared samples were kept refrigerated in the dark.

The ethylation set-up is illustrated in Figure 4.4. To begin ethylation, 60 mL of distilled water and 100 μL of citrate (for acidity) was added to an ethylation vessel. An aliquot of prepared sample estimated to contain 10–100 pg methyl mercury was added to the mixture. To incur ethylation of the mercury species, 50 μL of ice-cold 1 % sodium tetraethylborate [$NaB(Et)_4$] were added and the vessel was closed. A trap consisting of Tenax resin within a quartz tube was connected to the vessel; the set-up was allowed to equilibrate for 15 minutes. Bubbling of argon (250 mL/min) through the ethylation vessel for 12 minutes purged the highly-volatile ethylated mercury species into the trap. The trap was then dried with argon flow for seven minutes.

The trap was transferred to the analytical train, shown in Figure 4.5, and allowed to equilibrate for one minute under argon flow (40 mL/min). The trap was then heated for 30 seconds (to approximately 350°C) for thermal desorption. The sample stream was sent through a U-tube gas chromatograph, where separation of the species took place at 100°C. A pyrolysis tube located downstream decomposed the species to Hg(0) at 850°C. The resulting mercury vapor was input directly into the CVAF detector; measurement was charted by an integrator in peak-area mode.

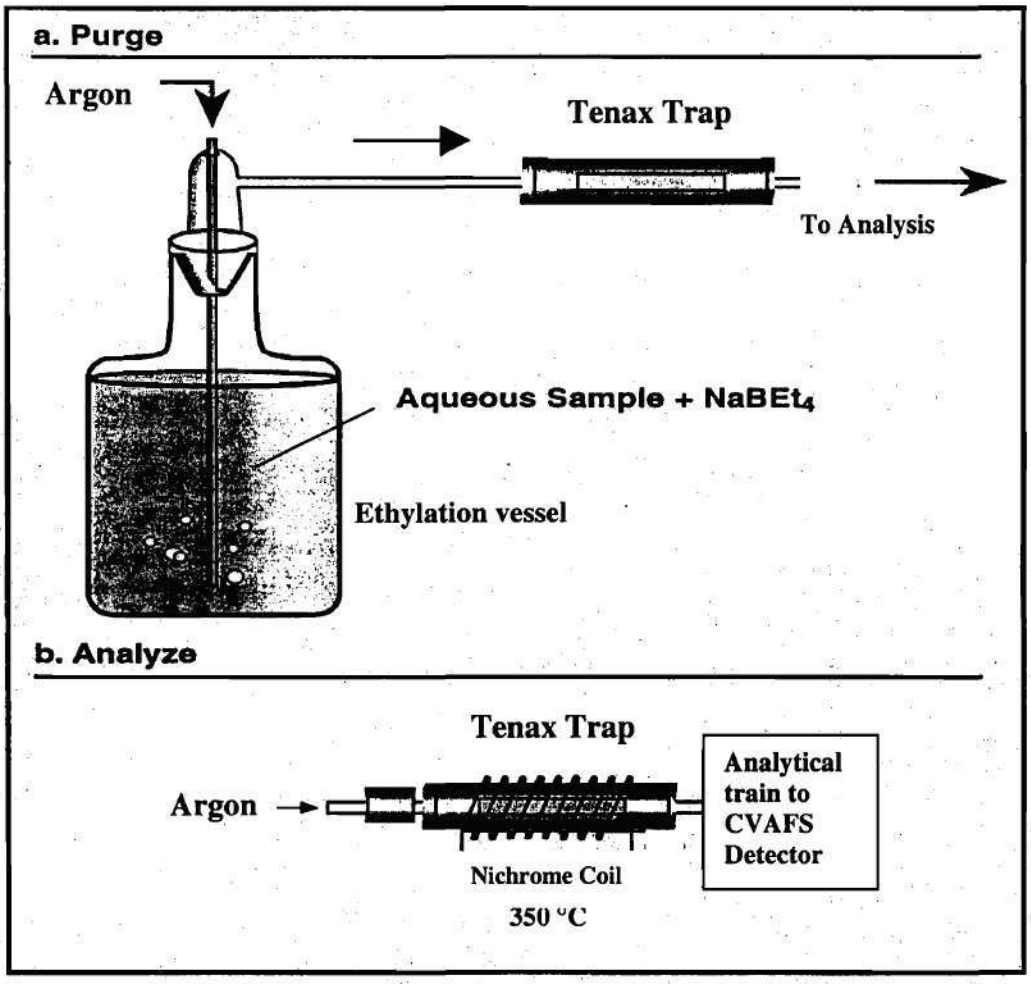

Figure 4.4 Ethylation and Tenax trap apparatus used in determination of methyl mercury, according to EPA Method 1630 (EPA, 1999).

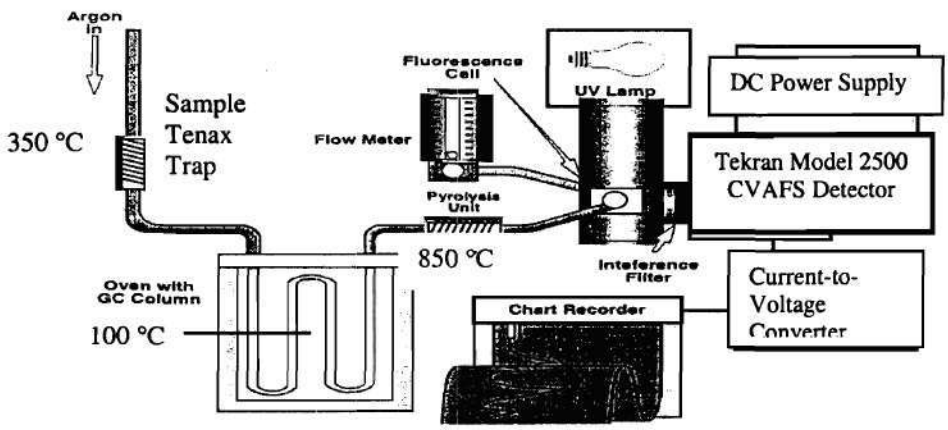

Figure 4.5 Analytical train including cold vapor atomic fluorescence spectrometer (CVAFS) used in determination of methyl mercury, according to EPA Method 1630 (EPA, 1999).

A standard curve was produced from a 100 ppb (μg/L) stock standard. One mL of stock standard was diluted to 100 mL with distilled DI to produce a 1000 ng/L working standard. This working standard also included 100 μL of concentrated HCl, which stabilized the standard. Aliquots of working standard of 100, 50, 20, 10, and 0 pg were added to the ethylation vessel.

In this study, a detection limit of 2.28 pg, based on 3.14 times the standard deviation of seven 10 pg replicates, was ascertained. For a typical 1-g sample, this translated into a detection limit of 2.28 pg/g (parts-per-trillion).

CCVs in methyl mercury analyses yielded 98 ($\pm$ 13) % recovery, which fell within method quality control acceptance criteria of 77-123 % for OPR (EPA, 1998). IAEA produced 116 ($\pm$ 14) % recovery.

Determination of Methyl Mercury in Porewater

Methyl mercury levels in porewater samples were determined according to a modified version of EPA Method 1630 as well as published work from Bloom (1989), Horvat *et al.* (1993), and Liang *et al.* (1994). The main difference with this technique was the sample volume; porewater sample volumes here were low (in the 0.25–5 mL range) and thus required dilutions with water for analysis. Analysis was performed by distillation, aqueous phase ethylation, adsorption on a Tenax trap, chromatographic desorption, and CVAF.

Samples were obtained in two ways: sippers and centrifuged core sections. With sippers, samples were filtered with a 0.2-μm nylon filter into 7-mL Teflon vials. With core sections, samples were collected as cores in duplicate and immediately sectioned aerobically into acid-cleaned centrifuge tubes. Supernatant water was filtered with a 0.2-μm nylon filter into 7-mL Teflon vials. Samples then were acidified to 0.2 % (v/v) with sulfuric acid (18 M H_2SO_4) and refrigerated in the dark.

Similar to the technique described for methyl mercury in sediment, distillation was accomplished on an aluminum heating block and cold-water chiller. In a 30-mL Teflon vial (the distillation vial), several mL of porewater were diluted to 10 mL with distilled DI. To maintain acidity, 50 μL of 12 M HCl were added. A 60-mL Teflon with 7 mL of distilled DI served as the collection vial. The distillation vial was placed in the heating block, which was set to a temperature of 145°C. The collection vial was placed in the chiller and connected to the distillation vial. Distillation continued until approximately 80 % of the sample was distilled. Thus, the collection vial was removed from the chiller once it contained 15 mL of distillate (7 mL water + 8 mL distillate). The sample was then diluted to 20 mL with distilled water. Finally, the sample solution was set to a pH of approximately 5.0 by μL-level additions of citrate and KOH. Prepared samples were kept refrigerated in the dark.

Ethylation, analysis, and standard curve preparation were conducted in the same manner as that described for methyl mercury in sediment.

In this study, a detection limit of 2.28 pg, based on 3.14 the standard deviation of seven 10 pg replicates, was ascertained. For a typical 1-mL sample, this translated into a detection limit of 2.28 ng/L (parts-per-trillion).

CCVs in methyl mercury analyses yielded 104 (± 13) % recovery, which fell within quality control acceptance criteria of 77-123 % for OPR (EPA, 1998).

Above-ground *Spartina* Biomass Measurement

Above-ground *Spartina* growth was assessed directly by measuring three indicators of plant growth: height of the tallest stalk, or culm, for each *Spartina* plant; the number of plants in each mesocosm; and the number of culms in each mesocosm. These parameters were measured with a ruler and by counting.

Also noted was the percent survival of plants from the initial planting over the first winter season. Percent survival was calculated by dividing the number of surviving plants by the number of plants initially planted.

In addition to monitoring of *Spartina*, the presence of algae on the sediment surface and macrofauna such as fiddler crabs and snails was observed. An effort was made to remove algal mats in summer months. Macrofaunal activity was assessed by counting crab burrows and viable snails.

Mesocosm Restoration and Maintenance

Sampling at the BERM caused a moderate amount of disturbance in the mesocosm sediments. Holes from core barrels and sippers remained after sampling events; these holes allowed oxygen to penetrate the sediments. Post-sampling mesocosm repair involved filling these holes, as well as removing any undesirable growth that may have occurred between sampling periods. Undesirable growth included algal mats in any of the mesocosms and any plant growth in the unvegetated mesocosm.

Sampling holes were filled by gently applying hand pressure around the hole until the sediment congealed together, pushing out any water that had accumulated in the open hole. This mesocosm repair was conducted the day after sampling in order to allow for maximum equilibration time before the next sampling.

To remove algal mats, which grew rapidly in the hot months of June - September, a jagged-edge paint scraper was applied lightly across the sediment surface. The scraper removed algae, which was placed in a bucket. When scraping was completed, the bucket of algae was weighed per mesocosm. For the unvegetated mesocosm, any floating materials were removed with a skimmer. Mesocosm maintenance was conducted soon after sampling in order to allow for maximum equilibration time before the next sampling.

Algae also accumulated in the reservoir tank and pipes. To combat this, the reservoir was skimmed regularly. When pipes became clogged and pressure loss was evident in the influent line, any two valves located between the reservoir and the mesocosms were removed and water pressure from a garden hose was applied inside the

pipes until the foreign materials were forced out. Also, the reservoir tank was drained, scraped, and pressure-cleaned.

Mesocosm Flow and Volume

To assess the flow of water through the mesocosm system, effluent waters from mesocosm underdrains were collected in graduated plastic drums. The total volume of water collected during low tide (Time D in Figure 3.4) represented how much water flowed through the respective mesocosm during one complete tidal cycle (12.75 hours). With this volume and time, flow velocities were calculated.

CHAPTER V

EXPERIMENTAL RESULTS

Data are presented in tables, depth profiles, histograms, and time series of data for three mesocosms over multiple sampling dates. All samplings and accompanying dates are summarized in Table 5.1. In general, sampling dates reflect the seasonal growth cycle of *Spartina*: June 23, 1999 – early summer, vegetative growth; August 31, 1999 – late summer, near end of vegetative growth; January 18, 2000 – winter, minimal growth, after reproduction; and March 31, 2000 – spring, just before vegetative growth.

Physical characteristics of sediments are presented first, followed by temperature, salinity, pH, mesocosm flows, DIC, ammonium, sulfate, dissolved sulfide, dissolved iron(II), sulfate reduction rate, acid-volatile sulfide, chromium-reducible sulfur, *Spartina* above-ground biomass, and mercury levels.

Data from both core (centrate) and sipper samples are included. Core and sipper data are distinguished by solid (core) and hollow (sipper) symbols in most figures.

Physical Characteristics of Sediments

Although sediments in this study all came from saltmarshes in Georgia with similar hydrologic regimes, it was important to measure basic sediment physical

Table 5.1 Sampling schedule.

	POREWATER				SOLID PHASE		MESOCOSM PARAMETERS					
SAMPLING	*chemistry cores*[2] *(centrate)*	*Hg cores*[3] *(centrate)*	*chemistry sippers*[4]	*Hg sippers*	*SRR cores*	*Hg cores*	*temperature*	*salinity*	*mesocosm flow*	*mesocosm volume*	***Spartina** biomass*	*sed. physical characteristics*
DATE												
11/98											24[1]	24
12/98												
1/99												
3/99												
5/99											17	17
6/99	23		23	23	23	23	23					
7/99							29				1	1
8/99	31		31	31	31	31	31					
12/99							15				3	3
1/00	18	18	18		20	18	20					
2/00							14, 16, 17	14				
3/00	31	31	31		31	31	10, 31		10			
4/00							12			18, 19		
6/00							22	22				

[1] Date of month, e.g. 24 = Nov. 24, 1998.
[2] Chemistry cores = centrate analyzed for sulfate, sulfide, Fe(II), DIC, NH4, and pH.
[3] Hg cores = centrate analyzed for THg and MeHg.
[4] Chemistry sippers = sipper sample analyzed for sulfate, sulfide, Fe(II), DIC, NH4, and pH.
[5] Hg sippers = sipper sample analyzed for THg and MeHg.

properties in order to effectively compare sediment chemistry and associated microbial activity.

Saturated wet density (or wet density), density of dry mass (or particle density), percent dry solids, porosity, and loss-on-ignition (L.O.I.) were measured and are tabulated in Table 5.2. No significant stratification with depth was observed for these physical characteristics and none varied significantly with time of year either.

Notable differences existed between GC and LCP sediments. The average wet density of GC sediment differed from that of LCP sediments, with a wet density of 1.46 g/cm^3 for GC and 1.21 g/cm^3 and 1.25 g/cm^3 for LCP–vegetated and LCP–unvegetated, respectively. Porosity exhibited similar results: average GC porosity of 0.681 (cm^3_{void}/cm^3_{bulk}) was significantly lower than that of LCP sediments, 0.836 and 0.850. L.O.I. followed the same trend in that GC had a combustible fraction of 7.03 % and LCP–vegetated and LCP–unvegetated had similar fractions of 15.59 % and 15.76 %, respectively. These data indicate that LCP had higher organic carbon fraction that GC. The physical differences are understandable in that GC sediment was obtained from one geographic location and LCP sediments from another.

These sediments are similar to sediments used in other saltmarsh studies. Giblin and Howarth (1984) worked with sediments with porosities of 0.83 and 0.84 for Massachusetts saltmarshes and 0.77 and 0.75 for Sapelo Island, Georgia saltmarshes. The same researchers found L.O.I. of 5-10 % for Sapelo Island. King (1999) measured porosities of 0.73-0.77 for Skidaway Island, Georgia saltmarsh sediments (a location very close to GC). Oremland *et al.* (1995) studied Carson River, Nevada sediments with

Table 5.2 Physical characteristics of BERM sediments. Each value represents the average of *n* samples. Standard deviations are shown in parentheses.

	GC	*LCP-veg.*	*LCP-unveg.*
Wet Density [g/cm^3] n=40	**1.46 (± 0.12)**	**1.21 (± 0.06)**	**1.25 (± 0.07)**
Particle Density [g/cm^3] n=40	**2.38 (± 0.43)**	**2.15 (± 0.50)**	**2.56 (± 0.82)**
Dry Solids [%] n=40	**52.9 (± 5.1)**	**30.6 (± 2.3)**	**31.7 (± 3.5)**
Porosity [cm^3/cm^3] n=40	**0.681 (± 0.056)**	**0.836 (± 0.040)**	**0.850 (± 0.045)**
L.O.I. [%] n=11	**7.03 (± 0.93)**	**15.59 (± 1.47)**	**15.76 (± 2.54)**

porosities of 0.63-0.82. Gilmour and Riedel (1995) investigated freshwater sediments with a L.O.I. of 29 %. Rood (1996) reported L.O.I. of 14.4 % in the Florida Everglades.

The only property in which GC and LCP are similar is particle density. Considering the large standard deviations, the particle densities of these three sediments overlap, suggesting that they are physically similar on a mineral basis. King (1999) measured similar particle densities of 2.25-2.38 g/cm^3 in Skidaway Island saltmarsh sediments. Values in this range are reasonable since mineral grains have a density of 2.65 g/cm^3 while organic materials have a density of 1.40 g/cm^3 (Brady and Weil, 1996). As L.O.I. results indicated, these saltmarsh sediments have a small organic fraction and thus would be slightly less dense than mineral grains.

Temperature

Temperature readings were periodically collected from mesocosms and other sites on Skidaway Island. In addition to these readings, archived air temperatures were obtained from the Chatham County Cooperative Weather Report at WTOC-TV Station ID # 09-7847-9 (displayed on the Internet at www.savannah-weather.com/weather/archive.htm).

Figure 5.1 shows temperature depth profiles of mesocosm sediments on four dates. Temperatures did not change significantly with depth, with the exception of the warmest time of the year, July. Trends with depth were nearly identical for all three

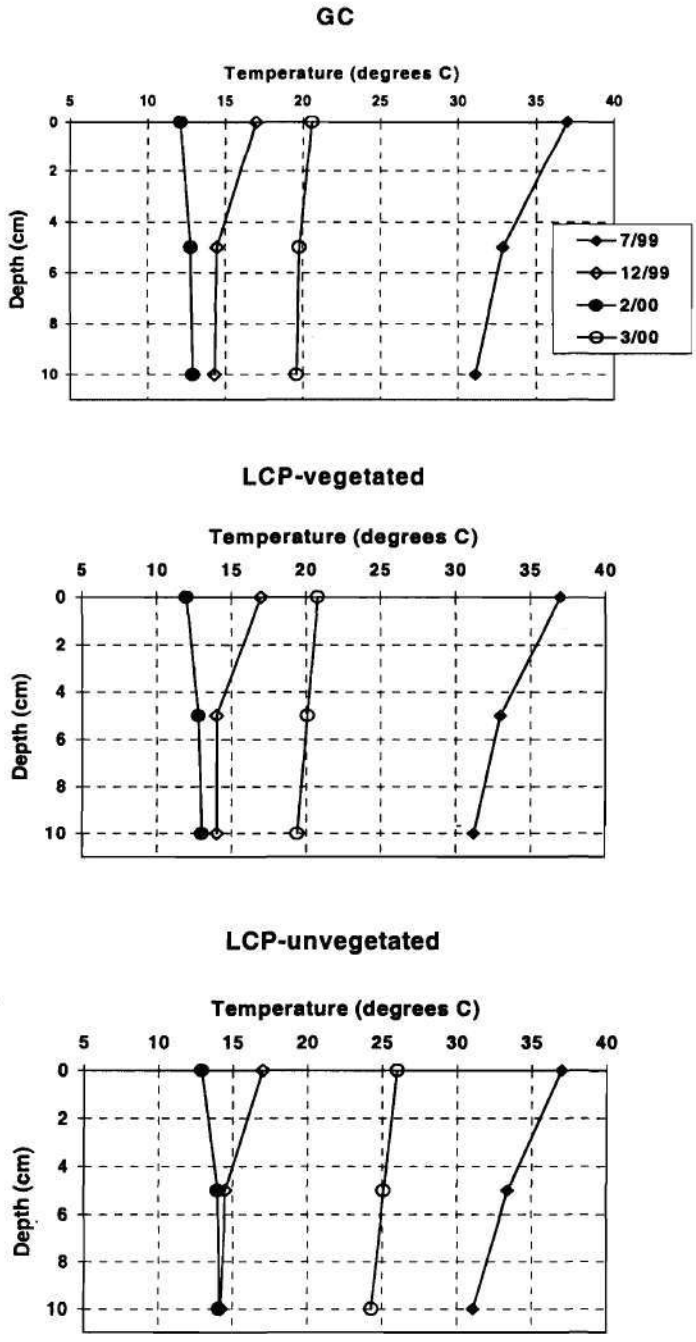

Figure 5.1 Temperature-depth profiles of mesocosm sediments. Each point is the average of duplicate measurements.

mesocosms; for July, December, and March, temperatures were several degrees cooler at depth, while in February, temperatures were slightly warmer at depth.

The most noteworthy findings of Figure 5.1 involve the July and March time periods. In July, temperatures dropped by 5.8-5.9° with depth for all three mesocosms, a significant cooling effect. March revealed a major difference between the mesocosms. In GC and LCP-vegetated, temperatures went from nearly 21° at the surface to less than 20° at depth. However, LCP-unvegetated showed much warmer temperatures, 26.0° at the surface to 24.3° at depth.

Natural solar input, controlled by the seasons, dictated sediment temperatures. Without plants casting a cooling shadow on the sediment surface, LCP-unveg. had the warmest temperatures, especially in March.

A similarity among mesocosms took place in February. Here, instead of a cooling effect, sediments were warmer with depth. The warming and cooling effects suggest that the sediment surface acted as an insulator, preventing extreme temperatures in the subsurface.

Figure 5.2 displays a temperature-time series reflecting nine separate dates. To serve as comparison, Savannah's daily high and low air temperatures are included for the length of a year. Sediment temperatures mostly followed the same trend as air temperature, falling between the high and low temperatures for a given day. In general, sediment temperatures remained approximately 3-7° cooler than the daily high air temperature. The only divergences occurred with LCP-unvegetated; its springtime March and April temperatures eclipsed GC and LCP-vegetated. The warmer temperature

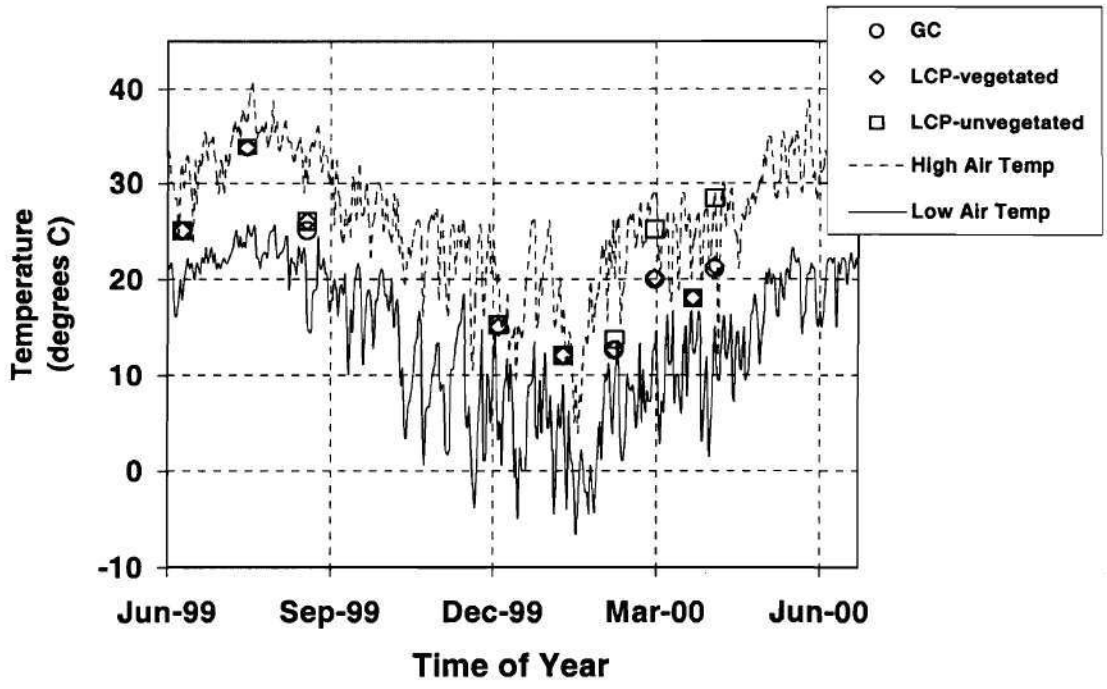

Figure 5.2 Temperature-time series of mesocosm sediments. Each temperature point represents the average of measurements taken from 0, 5, and 10 cm depths. The high and low daytime air temperatures were taken at a Savannah weather station.

for LCP-unveg. in March is also apparent in Figure 5.1. In April, LCP-unvegetated nearly matched the ambient air temperature. Again, the lack of plant shadows in LCP-unveg. allowed for these higher temperatures.

Salinity

Salinity was measured at several locations in the BERM system and at other sites on Skidaway Island. Table 5.3 compares salinities among the locations on two dates. Readings are quite consistent per date, differing by no more than 2 ppt. Between dates, there is a larger salinity difference of 3–4 ppt.

The BERM system itself was largely responsible for the uniformity in salinity on a given day. As later described, the recycle ratio and "integrator effect" of the system buffered changes in Skidaway River salinity and chemistry. Differences show up only on a gradual basis, e.g. seasonally. Salinity was 26 ppt for both the reservoir and Skidaway River in February and 29 ppt for both locations in June. Further, on each date, the salinities were nearly the same across the system.

pH Analysis

A summary of pH data for mesocosms is presented in Table 5.4. In June, average pH was nearly identical among the three mesocosms. In August, pH was higher in all three, with 7.59 in LCP-unveg. being the maximum value. This can be explained by an

Table 5.3 Salinity comparison throughout the BERM system. Salinity readings, given in parts-per-thousand, were taken on two dates; for the latter date, not all locations were included. Each point represents the average of duplicate measurements. Locations to the left are more "upstream" than locations to the right.

LOCATION	Skidaway River[1]	Concrete tank	Reservoir	Influent for GC	Influent for LCP-veg.	Influent for LCP-unveg.	GC	LCP-veg.	LCP-unveg.	Effluent for GC	Effluent for LCP-veg.	Effluent for LCP-unveg.	Skidaway marsh[2]
DATE													
2/00	26	26	26	26	26	25	26	26	26	27	27	26	25
6/00	29	30	29	N/A	N/A	N/A	29	29	29	N/A	N/A	N/A	29
	Upstream	>>>		>>>		>>>		>>>		*Downstream*			

[1] Skidaway River sample was taken at dock located approximately 200 m north of BERM water intake.
[2] Skidaway marsh sample was taken at marsh boardwalk located approximately one mile south of BERM.

Table 5.4 Average pH in mesocosm porewaters. Standard deviations are also given

	GC	*LCP-veg.*	*LCP-unveg.*
6/99	6.64 (± 0.81) *n=6*	6.59 (± 0.81) *n=5*	6.58 (± 0.81) *n=6*
8/99	7.13 (± 0.48) *n=11*	7.59 (± 0.71) *n=10*	7.05 (± 0.38) *N=8*
1/00	7.07 (± 0.51) *n=7*	6.99 (± 0.43) *n=8*	7.20 (± 0.58) *n=8*
3/00	6.64 (± 0.58) *n=11*	6.60 (± 0.40) *n=11*	7.05 (± 0.74) *n=11*

increase in microbial activity through summer, which pumped more bicarbonate (inorganic carbon) ions into sediment as sulfate was reduced to sulfide. Bicarbonate increases pH. As sulfate reduction lagged in the colder months, pH fell in January and March.

In general, both vegetated mesocosms exhibited increases of pH with depth over the four sampling dates. Such increases indicated accumulation of bicarbonate with depth. January, the coldest date, showed the greatest increases with depth among the four dates.

Mesocosm Flow and Volume

Water flushed through each mesocosm differently due to variations in sediment origin and physical properties as well as the presence or lack of vegetation. Using the technique described in Ch. V, volume of water collected from the GC underdrain averaged 114 L; for LCP-vegetated and LCP-unvegetated, the volumes were 174 and 257 L, respectively. Assuming that these volumes represented how much total water flowed through sediments during one complete tidal cycle of 12.75 hr, velocity of the water can be calculated. The volumes above correspond to velocities of 0.194, 0.297, and 0.438 cm^3/cm^2-hr, which are face velocities based on change of volume over time, normalized to cross-sectional area. More on velocity calculations is provided later.

Considering 30.5 cm of "high tide" in each mesocosm per tidal cycle, the effluent volumes mentioned above represented 8.1, 12.3, and 19.4 % of the volumes of water

contained above the sediment surface during high tide in GC, LCP-veg., and LCP-unveg., respectively. Also, accounting for sediment porosities, the effluent volumes represented 3.7, 4.6, and 6.7 %, respectively, of the total moisture contained in the saturated mesocosm sediments.

It was notable how similarly the mesocosms drained (from the underdrain). The majority of water exited immediately in a one-minute "gush" period. The flow then decreased to a trickle. Figure 5.3 serves as a graphical example of this underdrain flow. There were two causes for this. First, water that had accumulated in the grid of perforated pipe and drainage stone at the mesocosm bottom flowed out quickly. Water percolating out of the overlying sediment drained out more slowly. Second, the head of water in the mesocosm diminished, retarding the flow out.

Dissolved Inorganic Carbon

Dissolved inorganic carbon (DIC) results are shown in Figure 5.4. The three mesocosms showed similar results, with DIC accumulation at depth, especially during the summer months when sulfate reduction peaked. Sulfate reduction produces bicarbonate ions, i.e. DIC.

Levels of DIC were highest in June, attaining 13-17 mM in surface (0-2 cm) layers and then reaching 59.5 mM for GC and 73.2 and 66.6 mM for LCP-veg. and LCP-unveg., respectively, at 10-cm depth. Late summer (August) showed levels at 9-10-cm depth reduced more than four-fold in GC (to 11.8 mM), more than 2.5-fold in LCP-veg.

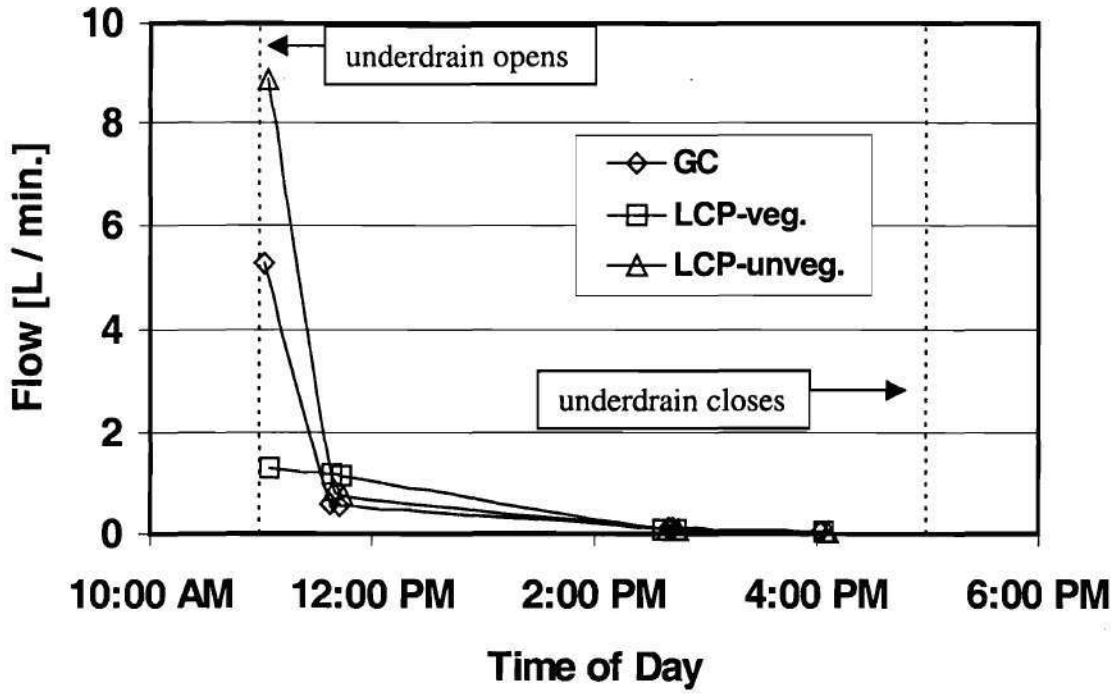

Figure 5.3 Underflow drain rate over one complete tidal cycle.

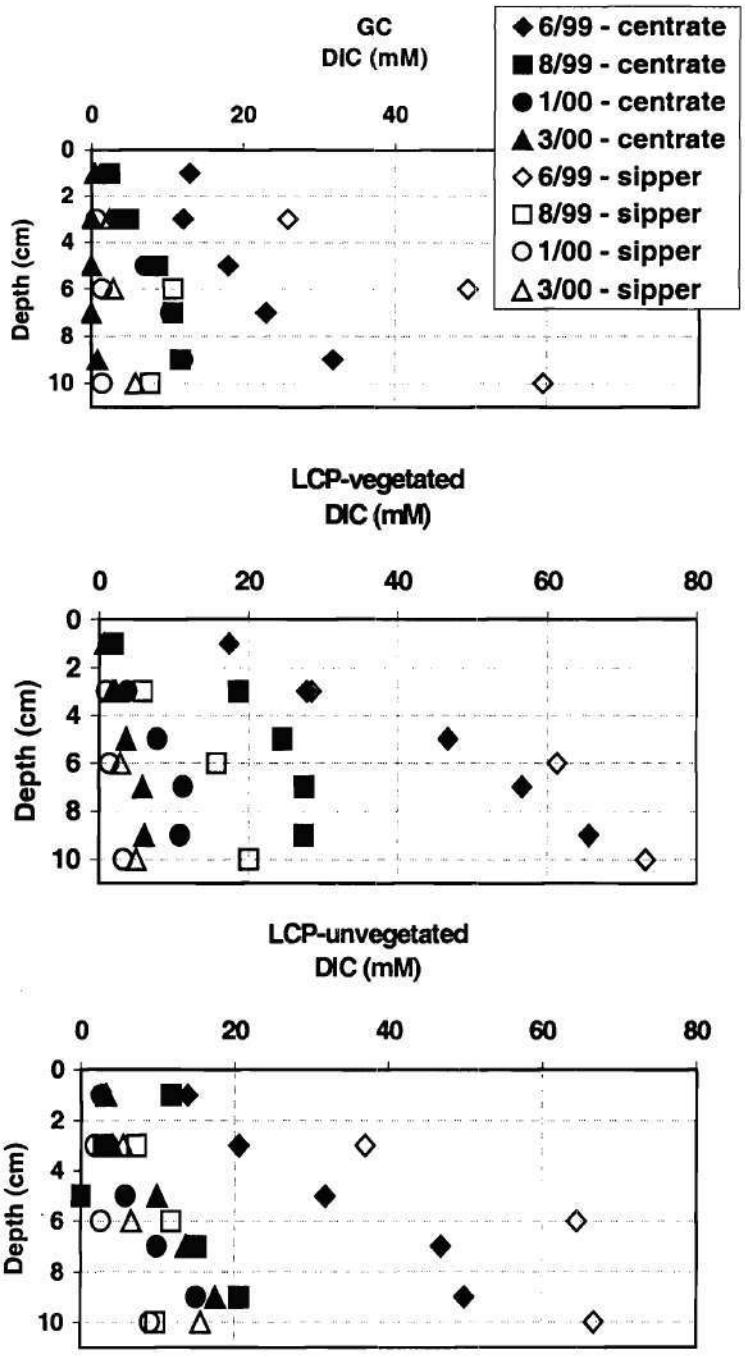

Figure 5.4 Dissolved inorganic carbon levels in mesocosm porewaters for four sampling dates. The standard deviation of replicate measurements was determined to be 0.08 mM.

(27.5 mM), and more than three-fold in LCP-unveg. (20.6 mM).

During the colder months of January and March, levels remained below 18 mM. Vegetated mesocosms seemed to be affected the most, with all levels dipping below 7 mM in March. The colder months also saw minimal surface concentrations, below 4 mM for all mesocosms.

DIC in porewater has a negligible impact on sediment carbon content, previously characterized by L.O.I. in Ch. V. Even if porewaters had a relatively high concentration of 50 mM, DIC made up less than one percent of carbon loss-on-ignition.

Ammonium

Ammonium concentrations are presented in Figure 5.5. Vegetated mesocosms differed drastically from the unvegetated mesocosm. The LCP-unvegetated mesocosm exhibited substantial accumulation with depth, especially during the summer months. *Spartina* utilizes ammonium as a nitrogen source and a lack of vegetation in LCP-unveg. obviously spurred the accumulation. In August, ammonium concentration peaked at 679 μM at 9 cm. This maximum level declined to 339 μM in March. Surface layers showed a similar trend, going to a low of 18.0 μM at 1 cm in March.

For GC, plants kept ammonium at low levels, rarely reaching 50 μM for any date or depth. Interestingly, LCP-veg. had August levels similar to that of LCP-unveg., exceeding 600 μM at 7-10 cm. Excepting August, LCP-vegetated resembled GC, staying below 50 μM, except for a 182 μM spike at 10 cm in June. Surface layers were low for

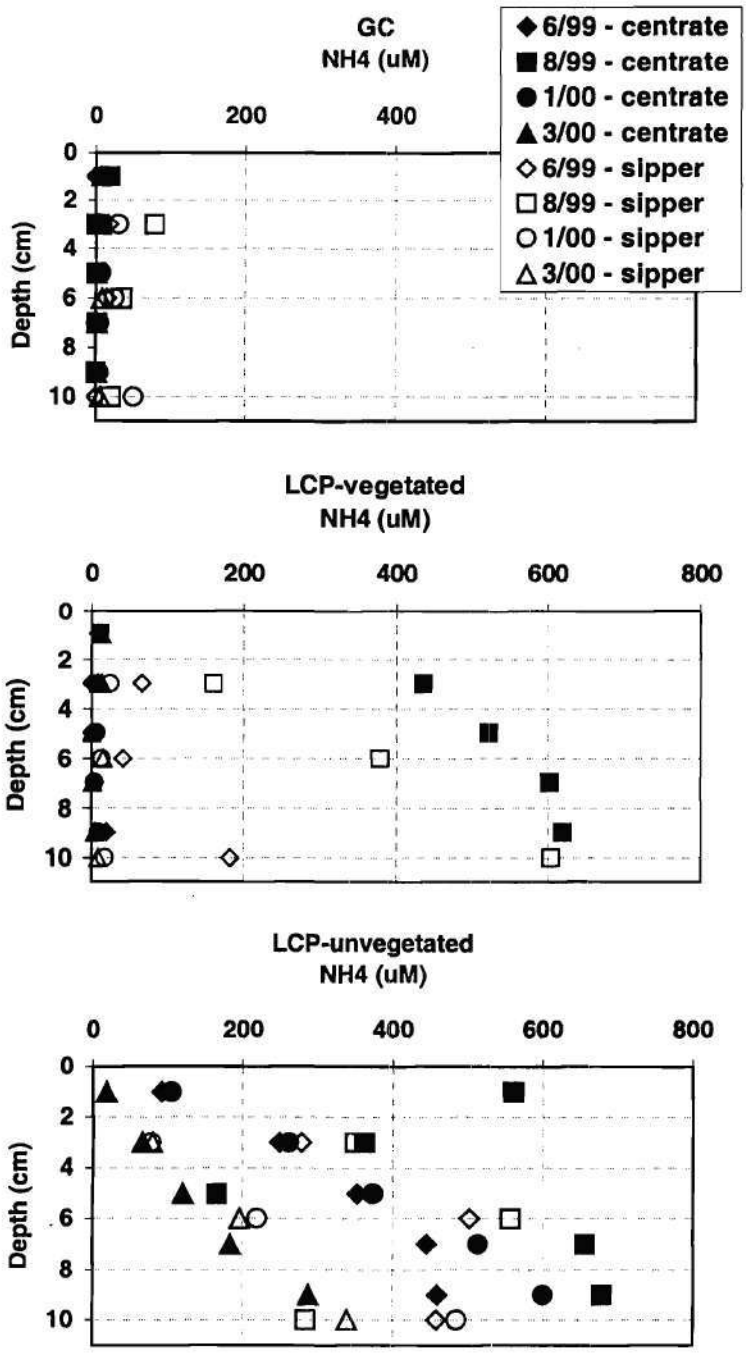

Figure 5.5 Ammonium levels in mesocosm porewaters for four sampling dates. The standard deviation of replicate measurements was determined to be 0.44 μM.

both vegetated mesocosms, less than 20 μM.

Sulfate

Figures 5.6a-d show porewater sulfate data for the four sampling dates. With the exception of several outlier data points in LCP-veg., mesocosms generally exhibited sulfate depletion with depth, an expected result of sulfate reduction. LCP mesocosms generally exhibited the greater gradients with depth as sulfate levels decreased by more than 20 mM in summer months. June levels (Figure 5.6a) went from 27.6 mM in the surface layer to 9.06 mM at 10 cm (change of 18.5 mM over 9 cm, a gradient of 2.1 mM/cm) in LCP-vegetated and from 26.0 mM to 7.47 mM (gradient of 2.1 mM/cm again) in LCP-unvegetated. August levels (Figure 5.6b) went from 25.9 mM in the surface layer to 1.61 mM at 10 cm (gradient of 2.7 mM/cm) in LCP-vegetated and from 25.1 mM (at 5 cm) to 0.20 mM (gradient of 5.0 mM/cm) in LCP-unvegetated.

Sulfate depletion was less during colder months. January levels (Figure 5.6c) went from 25.4 mM in the surface layer to 15.4 mM at 10 cm (gradient of 1.1 mM/cm) in LCP-vegetated and from 24.0 mM to 10.2 mM (gradient of 1.5 mM/cm) in LCP-unvegetated.

GC only showed minor depletion of sulfate at all times. June levels (Figure 5.6a) went from 29.1 mM in the surface layer to 22.9 mM at 10 cm (gradient of 0.7 mM/cm);

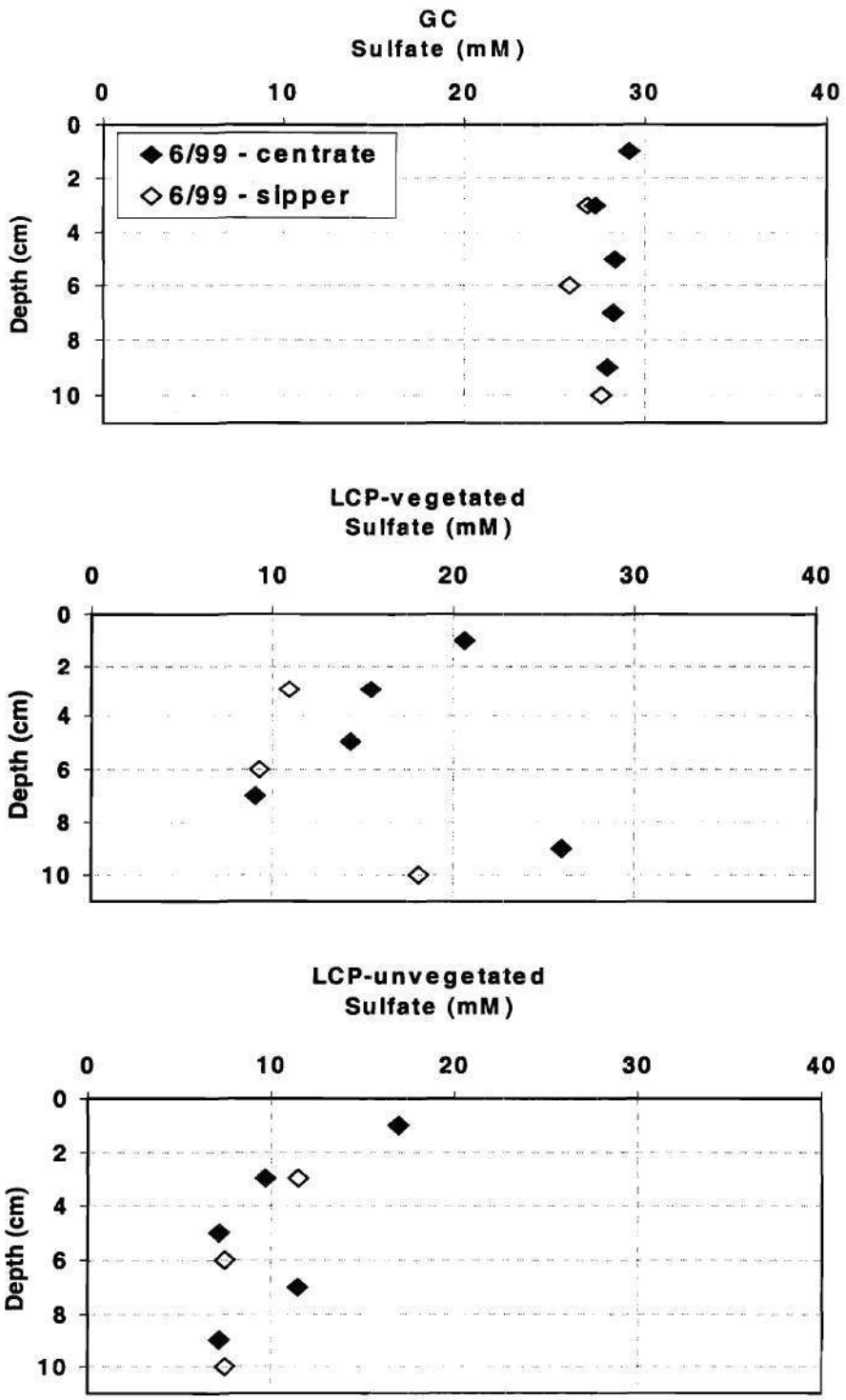

Figure 5.6a Sulfate levels in mesocosm porewaters for 6/99. The standard deviation of replicate measurements was found to be 0.16 mM.

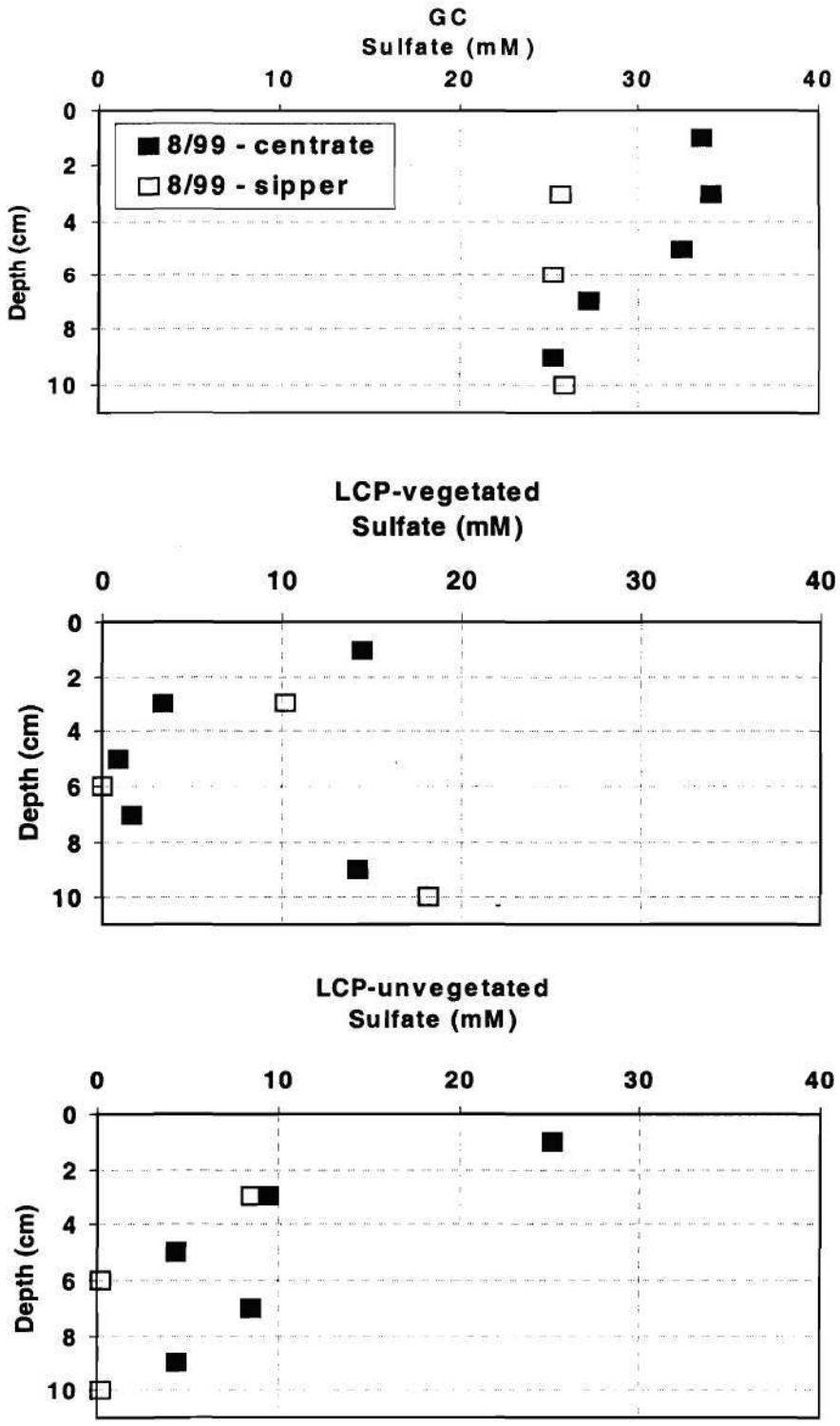

Figure 5.6b Sulfate levels in mesocosm porewaters for 8/99. The standard deviation of replicate measurements was found to be 0.16 mM.

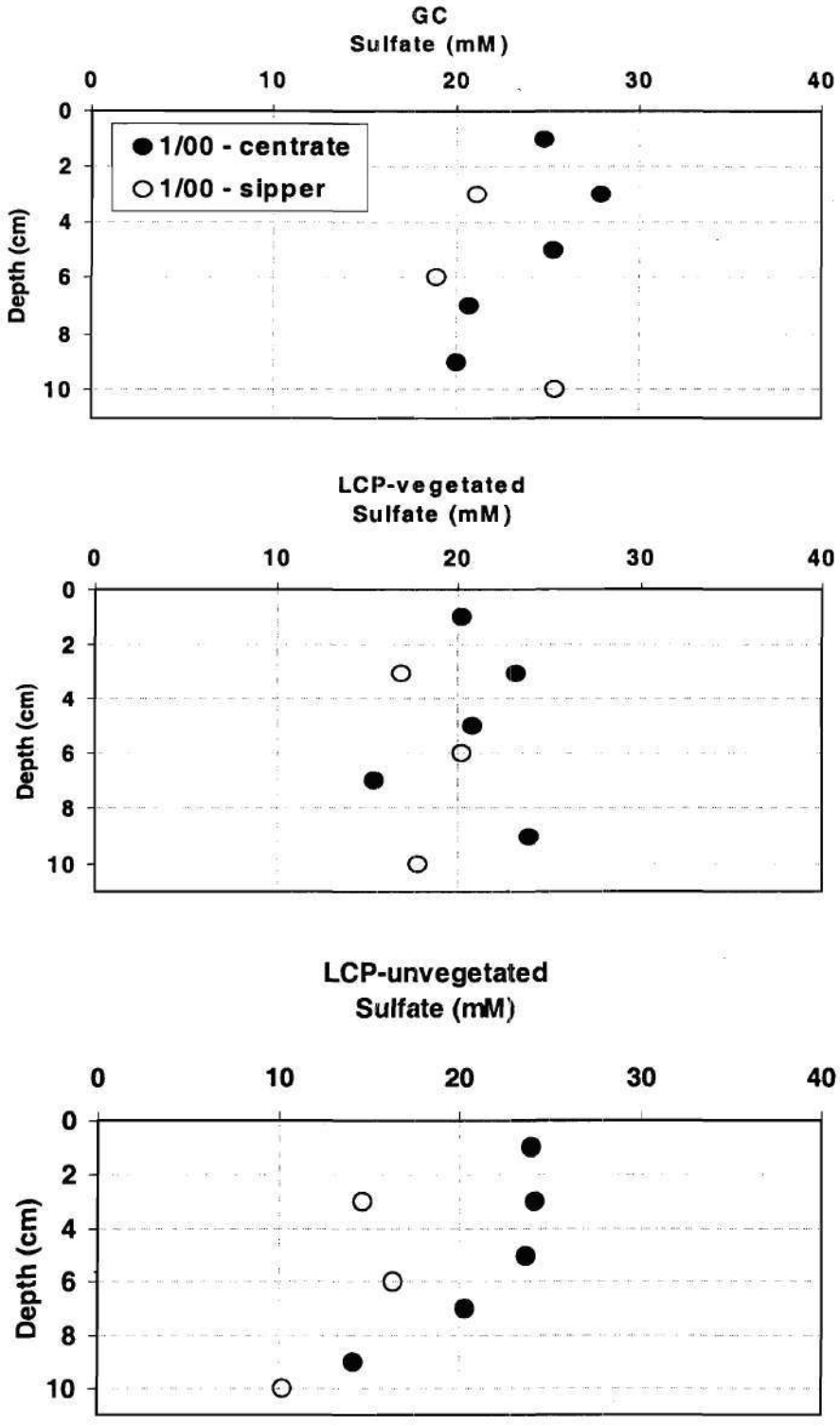

Figure 5.6c Sulfate levels in mesocosm porewaters for 1/00. The standard deviation of replicate measurements was found to be 0.16 mM.

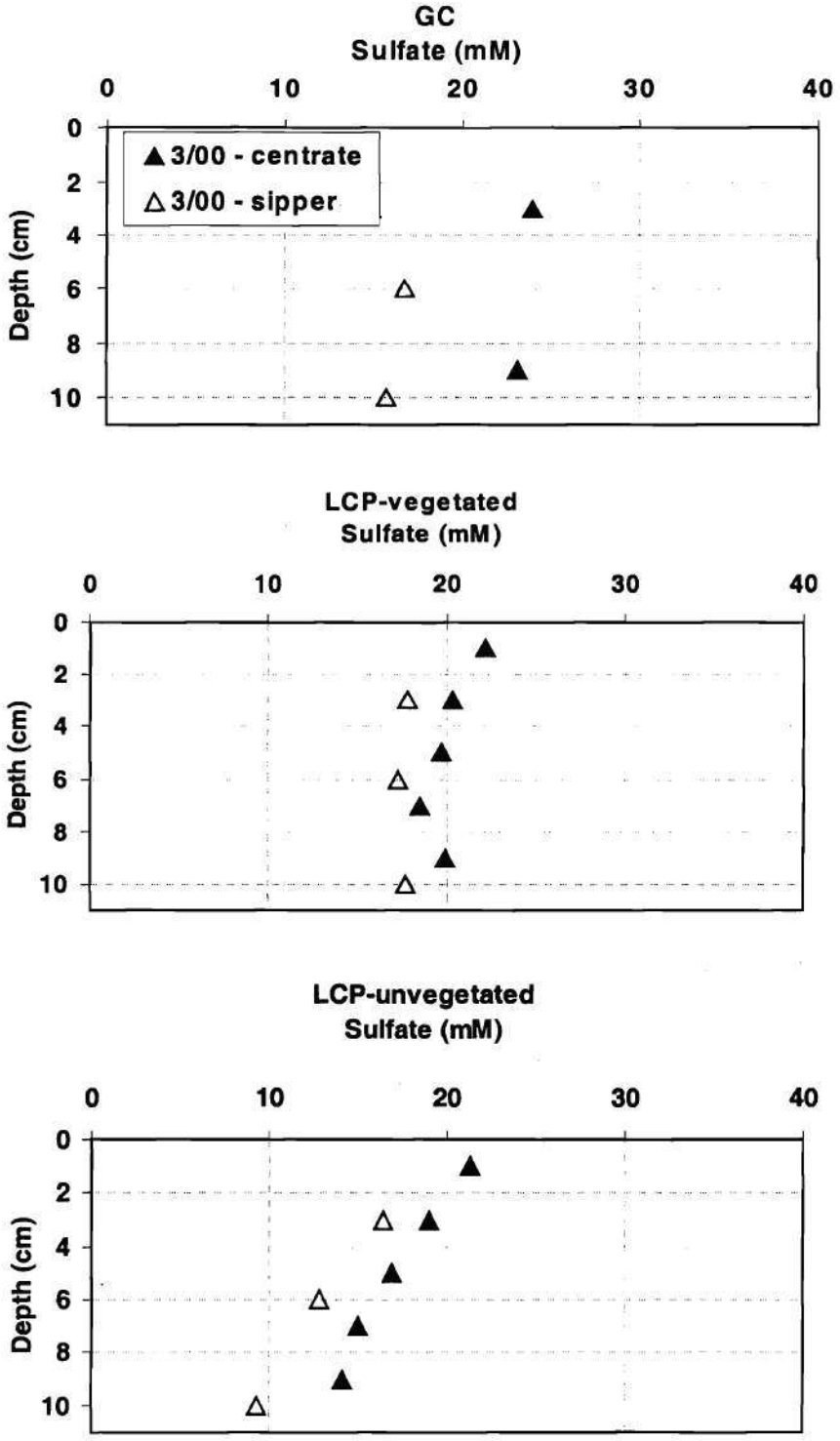

Figure 5.6d Sulfate levels in mesocosm porewaters for 3/00. The standard deviation of replicate measurements was found to be 0.16 mM.

March levels (Figure 5.6d) went from 24.0 mM at 3 cm to 15.8 mM at 10 cm (gradient of 1.2 mM/cm).

Dissolved Sulfide

Dissolved sulfide measurements for this study are shown in Figure 5.7. LCP mesocosms showed sulfide build-up during summer months, especially in LCP-unvegetated, where comparatively high sulfate reduction rates produced more sulfides.

LCP-vegetated levels exceeded 2000 μM at 7 cm in June and even reached 6320 μM at 5 cm in August. LCP-unvegetated levels ranged 1660-6480 μM at 5-10 cm in June, then reached 3400 μM at 10 cm in August. Sulfides were much lower during colder months. In January, LCP-unveg. peaked at 189 μM at 10 cm; in March, levels reached 400 μM at 9 cm.

GC showed quite low sulfide. The highest concentration recorded was 35.5 μM in August. In general, GC levels at all times were comparable to LCP colder month measurements.

Dissolved Iron(II)

Profiles of iron(II) concentrations for all mesocosms are shown in Figure 5.8. LCP mesocosms showed relatively low levels for all samplings, consistently below 200 μM. Such low levels of iron(II) may indicate that iron reduction was not a significant

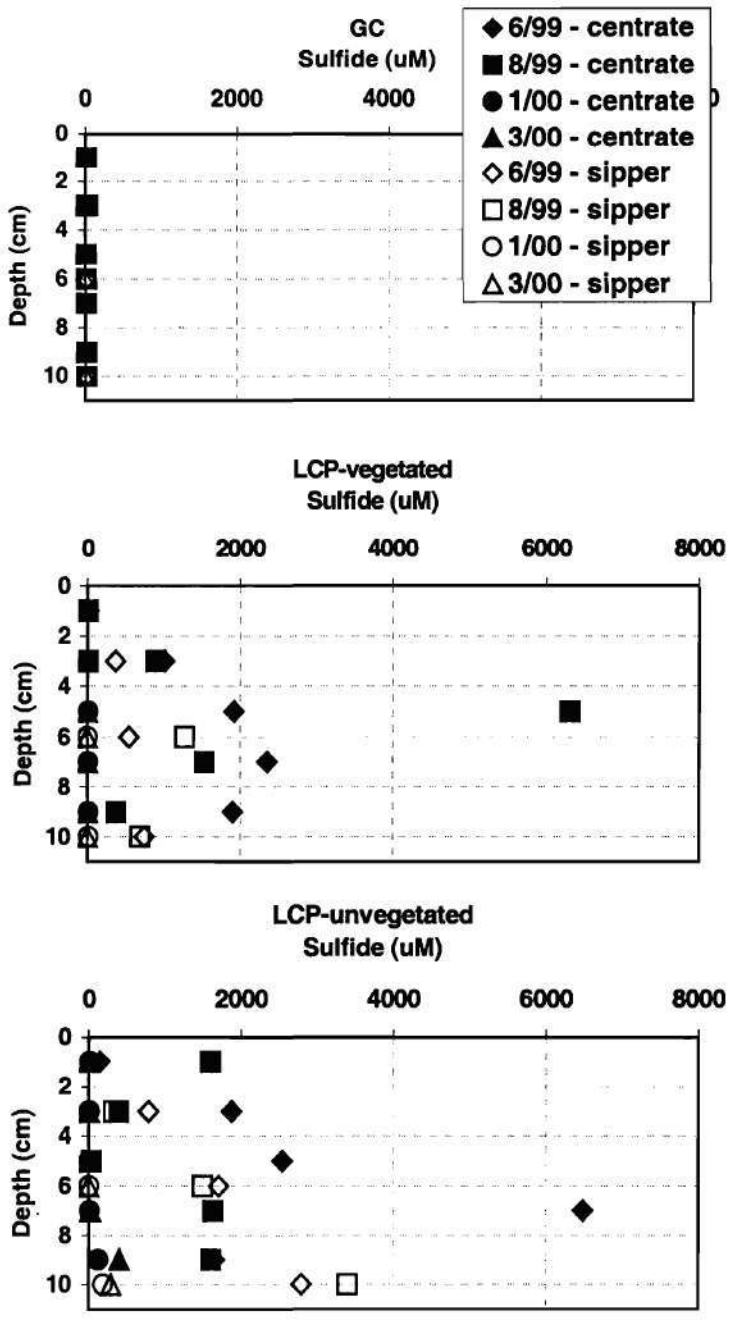

Figure 5.7 Dissolved sulfide levels in mesocosm porewaters for four sampling dates. The standard deviation of replicate measurements was determined to be 0.08 μM.

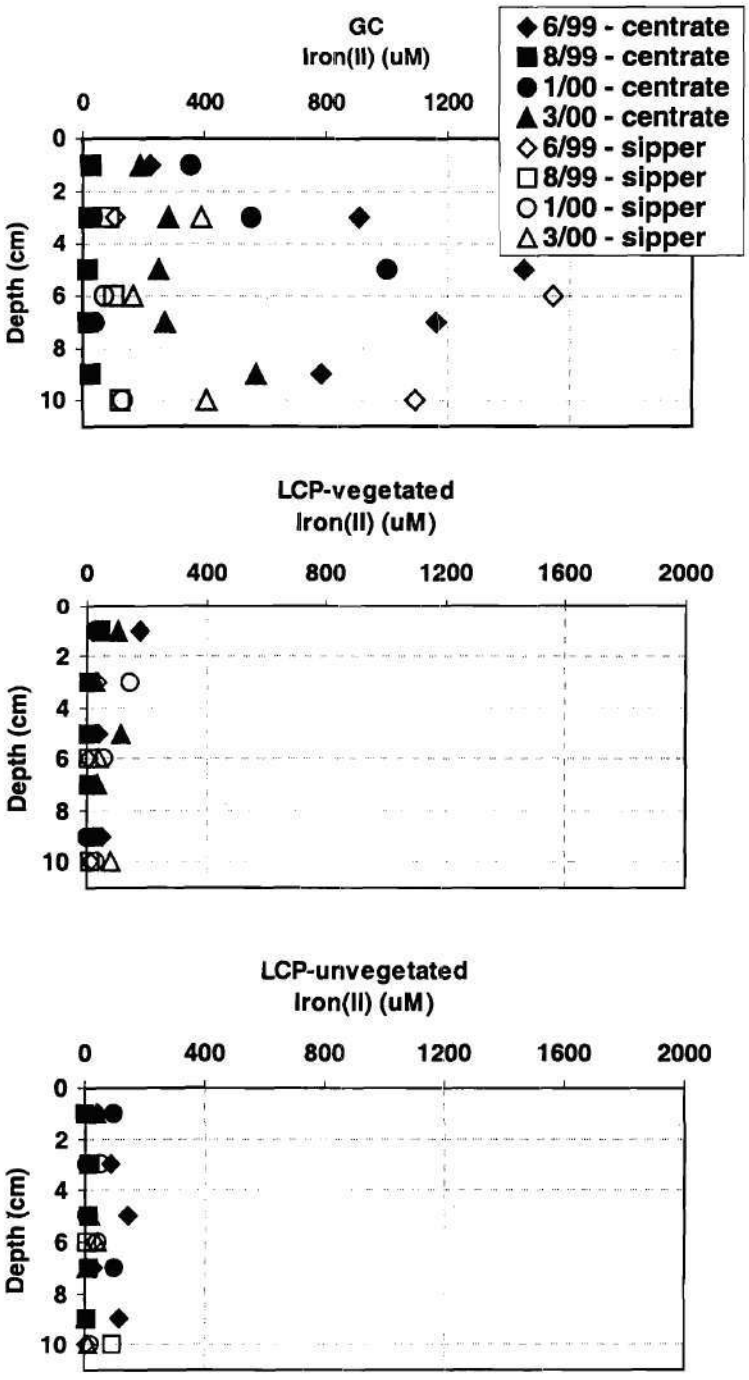

Figure 5.8 Dissolved iron(II) levels in mesocosm porewaters for four sampling dates. The standard deviation of replicate measurements was determined to be 0.06 μM.

anaerobic process in LCP sediments.

GC iron profiles contrasted greatly with those of LCP mesocosms. GC exhibited high concentrations at all times, especially at 5 cm and below. June levels went from 222 μM in the surface layer to nearly 1550 μM at 6 cm before tapering to 1090 μM at 10 cm. Iron remained in colder months as levels reached 1000 μM at 5 cm in January and 570 μM at 9 cm in March.

Sulfate Reduction Rate

Sulfate reduction rate (SRR) measurements were obtained from sediment core samples during four sampling periods. A summary of all depth profiles is shown in Figure 5.9 and profiles per sampling date are shown in Figures 5.10 through 5.13. Rates integrated to 10 cm are summarized in Figure 5.14 and a time series of these rates is presented in Figure 5.15.

Maximum rates in all mesocosms were found in the summer months of June and August, when microbial action was greatest. This was most evident in the LCP mesocosms, where rates exceeded 1500 nmol/cm^3-d at 1-cm depth in June. Also, LCP mesocosms exhibited highest rates consistently at 1 cm and rates decreased with depth. Comparatively, LCP sediments showed higher SRRs than GC. The maximum rate for LCP-vegetated for each sampling was two to five times greater than the corresponding maximum rate for GC. For example, in June, LCP-veg. peaked at 1638 nmol/cm^3-d,

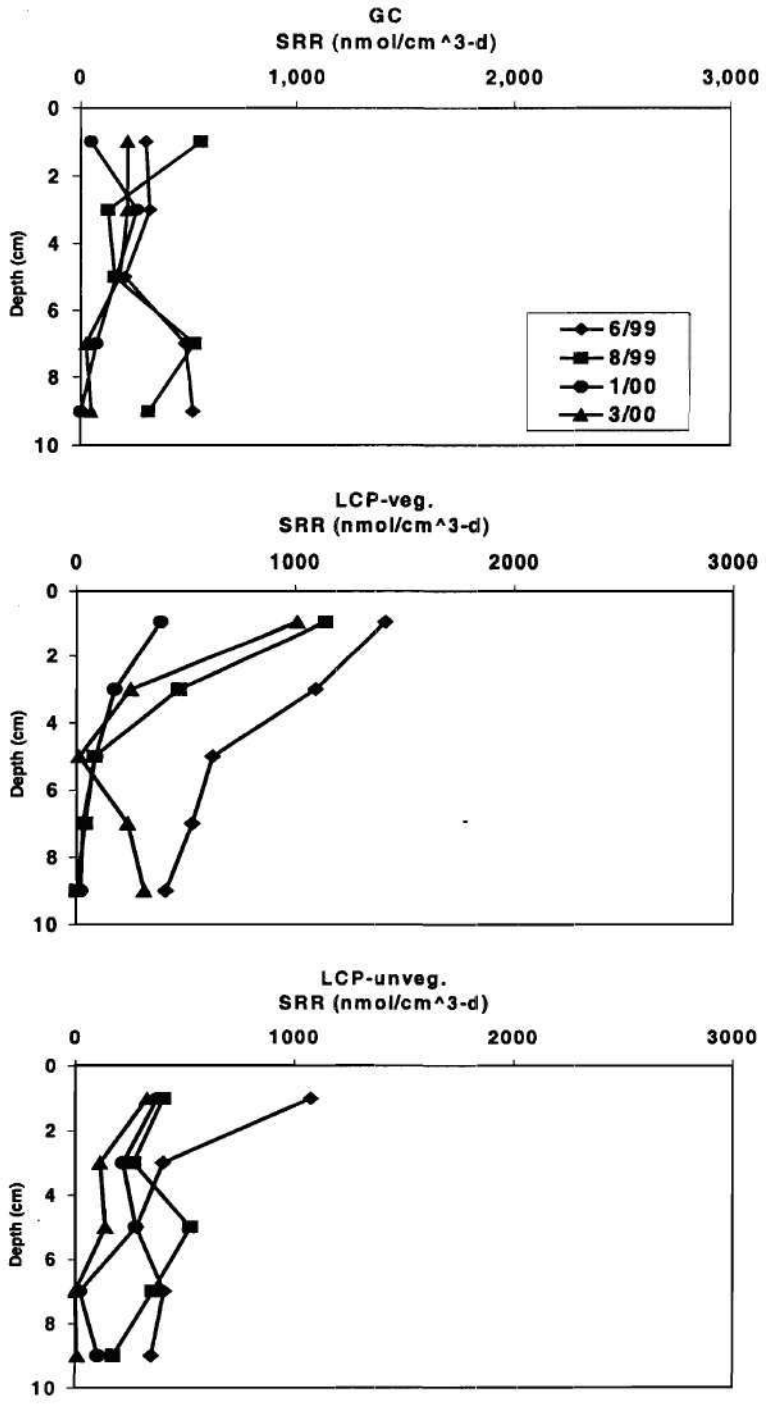

Figure 5.9 Summary of SRR-depth profiles. Each point is the average of duplicate measurements.

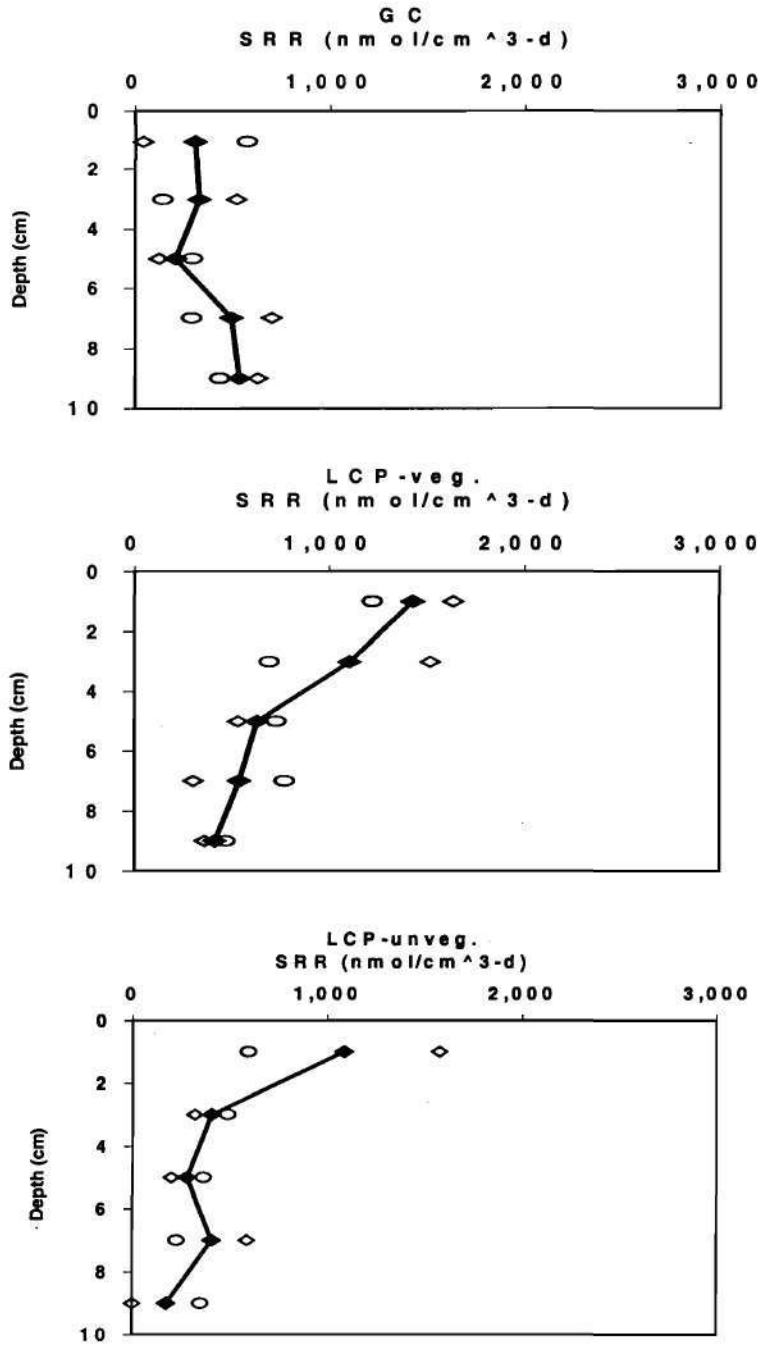

Figure 5.10 SRR-depth profiles for 6/99 sampling. Each solid point is the average of duplicate measurements, which are shown as hollow points on either side of solid points.

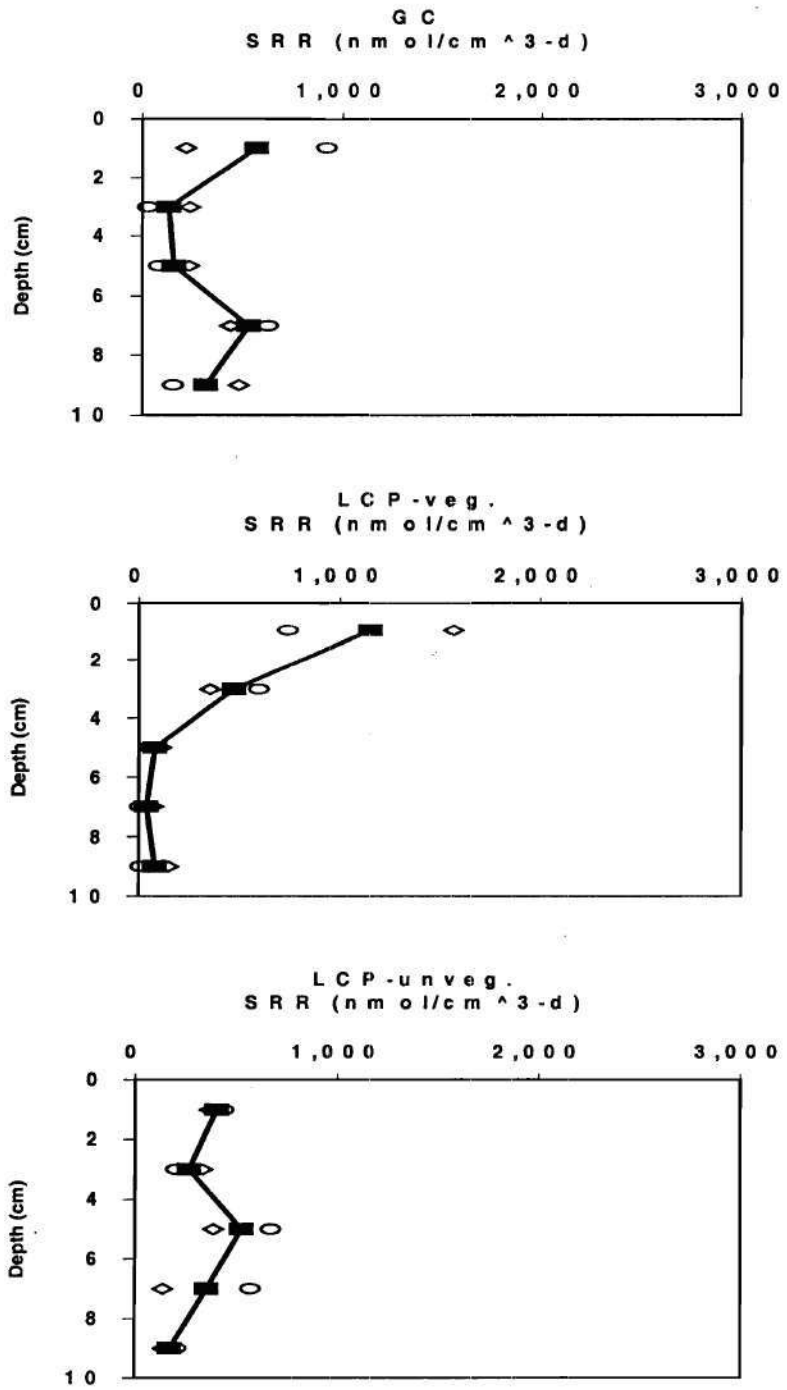

Figure 5.11 SRR-depth profiles for 8/99 sampling. Each solid point is the average of duplicate measurements, which are shown as hollow points on either side of solid points.

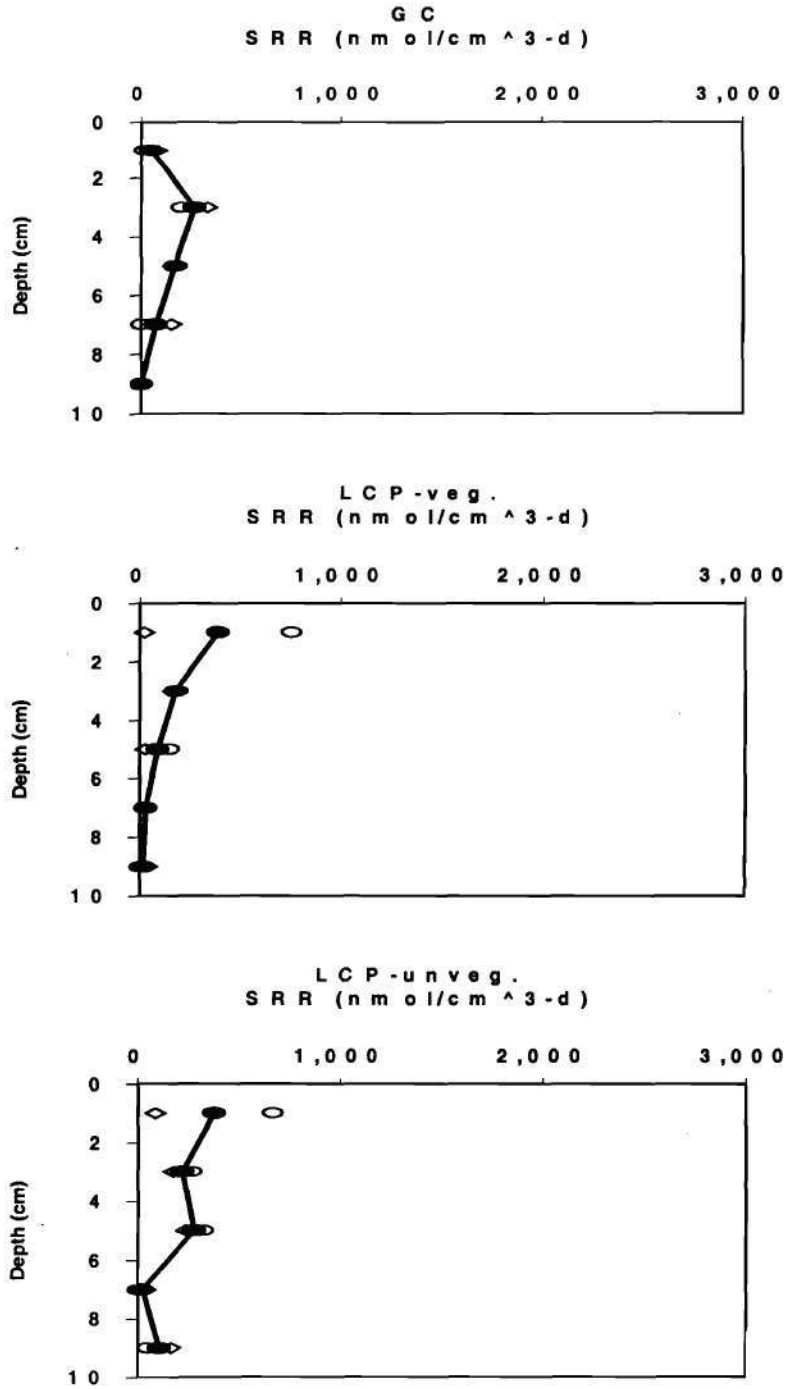

Figure 5.12 SRR-depth profiles for 1/00 sampling. Each solid point is the average of duplicate measurements, which are shown as hollow points on either side of solid points.

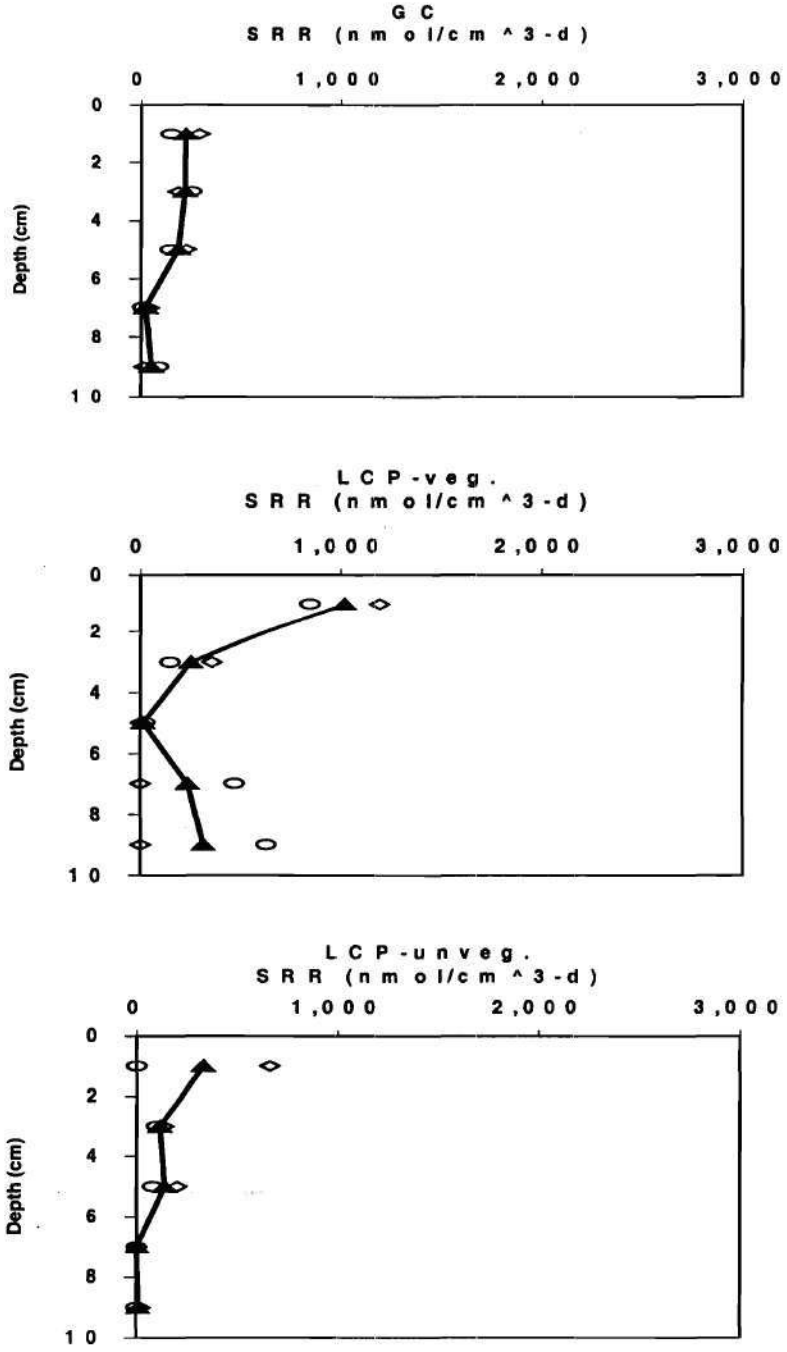

Figure 5.13 SRR-depth profiles for 3/00 sampling. Each solid point is the average of duplicate measurements, which are shown as hollow points on either side of solid points.

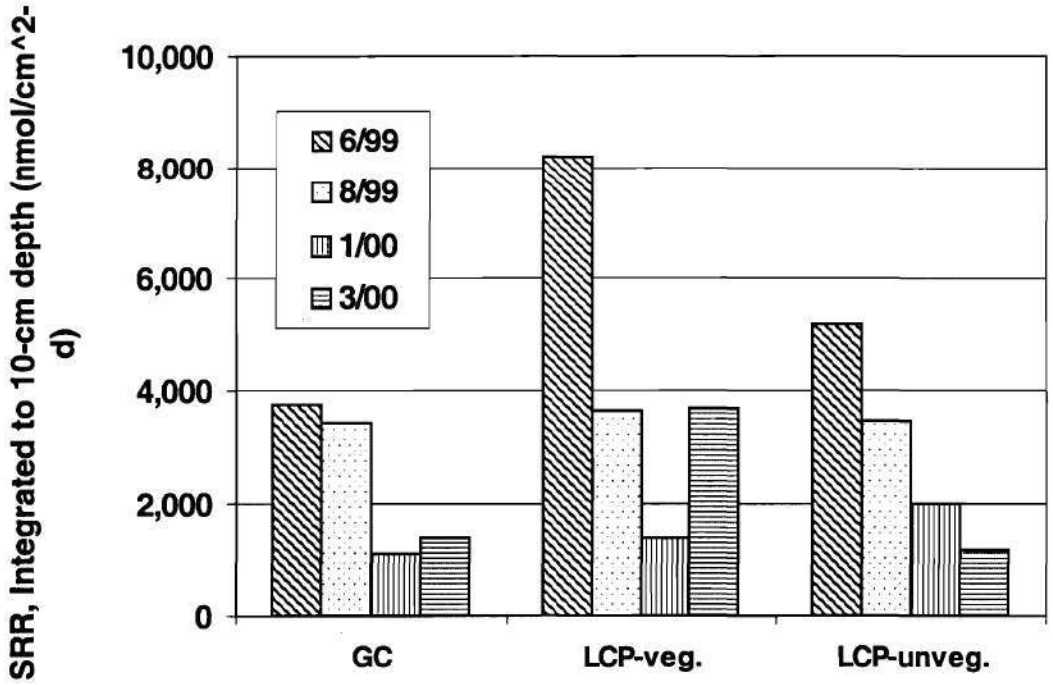

Figure 5.14 Summary of integrated SRRs in mesocosm sediments.

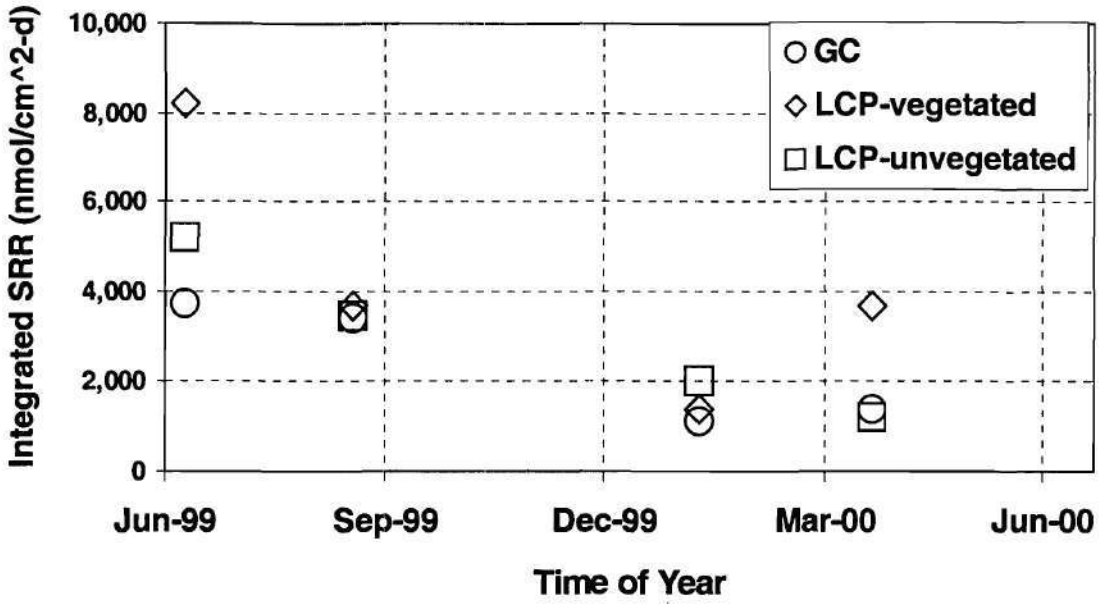

Figure 5.15 Time series of integrated SRRs in mesocosm sediments.

while GC reached 701 nmol/cm^3-d, a factor of 2.4 less. In March, LCP-veg. peaked at 1194 nmol/cm^3-d, while GC reached 292 nmol/cm^3-d, a factor of 4.1 less.

GC sediment showed the least variation in SRR with depth, regardless of sampling date. SRR ranges for GC samples were 39.9-701 nmol/cm^3-d in June, 26.1-921 nmol/cm^3-d in August, 0-331 nmol/cm^3-d in January, and 8.30-292 nmol/cm^3-d in March. Looking at averages of duplicate samples per depth interval, GC rates differed by no more than 450 nmol/cm^3-d per sampling date. Further, during the colder months of January and March, rates were quite low, all remaining below 300 nmol/cm^3-d.

The difference between the surface (1 cm) interval and the bottom (9 cm) interval was significant in LCP mesocosms. In LCP-vegetated, samples ranged 302-1638 nmol/cm^3-d in June, 5.74-1565 nmol/cm^3-d in August, 0-756 nmol/cm^3-d in January, and 0-1194 nmol/cm^3-d in March. In each instance, the maximum rate was found at 1 cm; for three of the four dates, the minimum was at 9 cm.

In LCP-unvegetated, a similar trend was found. Samples ranged 198-1577 nmol/cm^3-d in June, 141-673 nmol/cm^3-d in August, 0-669 nmol/cm^3-d in January, and 0-662 nmol/cm^3-d in March. For three of the four instances, the maximum rate was found at 1 cm; for three of the four instances, the minimum was at 7 or 9 cm.

Variability in SRR measurements, shown in Figures 5.10-5.13 as the difference between duplicate measurements, appeared to be greatest in the surface intervals and diminished with depth. Overall, GC sediment exhibited the least variability, especially in the colder months.

Integrating rates on an areal basis is another way to view and compare SRR. The units of nmol/cm^2-d indicate that SRRs over a profile were integrated to obtain an integrated SRR. In other words, average SRR per lift was multiplied by its representative 2-cm depth and summed together down to a depth of 10 cm. Figure 5.14 presents all SRR in such integrated fashion. For three out of four samplings, LCP-veg. featured the highest SRR and GC the lowest. Also note that the highest SRR for each mesocosm was found in the same sampling – June. Further, LCP-unveg. was the only mesocosm where SRR did not rebound with the onset of springtime and *Spartina* growth in March. This is especially evident in Figure 5.15, which shows integrated SRRs in a time series.

Acid-Volatile Sulfide and Chromium-Reducible Sulfur

Acid-volatile sulfide (AVS) and chromium-reducible sulfur (CRS) measurements obtained from sediment cores are shown in Tables 5.5 and 5.6, respectively. The abundance of sulfides from sulfate reduction in saltmarsh sediments facilitates the chemical reaction of ferric iron with sulfide to produce FeS (AVS) and FeS_2 (CRS).

In warmer months, average AVS levels were highest in LCP-vegetated, while in January+ and March, highest levels were found in GC.

LCP-unvegetated had the highest CRS concentrations among the three mesocosms in June and August; LCP-vegetated saw the highest in January and March. GC was lowest in every sampling. Further, for every mesocosm, average CRS levels were lowest in August.

Table 5.5 Acid-volatile sulfides in mesocosm sediments. Data are given in $\mu mol/cm^3_{wet}$. Standard deviations are also given.

	GC	*LCP-veg.*	*LCP-unveg.*
6/99	**1.68 (± 1.57)**	**3.48 (± 1.77)**	**2.11 (± 0.909)**
8/99	**0.254 (± 1.57)**	**1.43 (± 1.95)**	**0.486 (± 0.452)**
1/00	**1.52 (± 1.84)**	**0.313 (± 0.110)**	**0.283 (± 0.213)**
3/00	**1.41 (± 1.71)**	**0.131 (± 0.134)**	**0.173 (± 0.178)**

Table 5.6 Chromium-reducible sulfur in mesocosm sediments. Data are given in $\mu mol/cm^3_{wet}$. Standard deviations are also given.

	GC	*LCP-veg.*	*LCP-unveg.*
6/99	**209 (± 126)**	**271 (± 41.8)**	**441 (± 58.2)**
8/99	**85.3 (± 44.6)**	**238 (± 34.0)**	**299 (± 75.4)**
1/00	**267 (± 114)**	**587 (± 333)**	**474 (± 105)**
3/00	**241 (± 125)**	**443 (± 222)**	**325 (± 240)**

Radiolabel determinations of reduced sulfur were also performed. These determinations, since they were part of relatively rapid (< 24 hrs.) incubations, represented short-term end products of sulfate reduction. Data revealed predominance of CRS (Figure 5.16). All mesocosms showed that more than 80 percent of short-term solid sulfide end products were chromium-reducible.

Above-ground *Spartina* Biomass

Figure 5.17 summarizes *Spartina* above-ground biomass data for the two vegetated mesocosms. To get culm density, number of culms per mesocosm was divided by area of a mesocosm. *Spartina* plants experienced some die-off immediately after planting in the late fall. However, once the first growing season began in spring 1999, the plants rebounded.

Fewer *Spartina* plants died off in the first winter in GC than in LCP. GC had an initial plant count of 35 in December 1998 (right after planting) and two eventually died that winter. LCP had an initial count of 36, and nine died. However, in the first reproductive season, from July to December, there was a 78 % increase in GC culm density and 151 % increase in LCP.

GC plants grew in greater density and were taller than those in LCP. A culm density of 115 per m^2 and an average height of 141 cm were recorded in GC mesocosm in December 1999. From May to December, the average growth rate was approximately 0.26 cm/day. In the prime growth time of May to July, the growth rate was 0.58 cm/day.

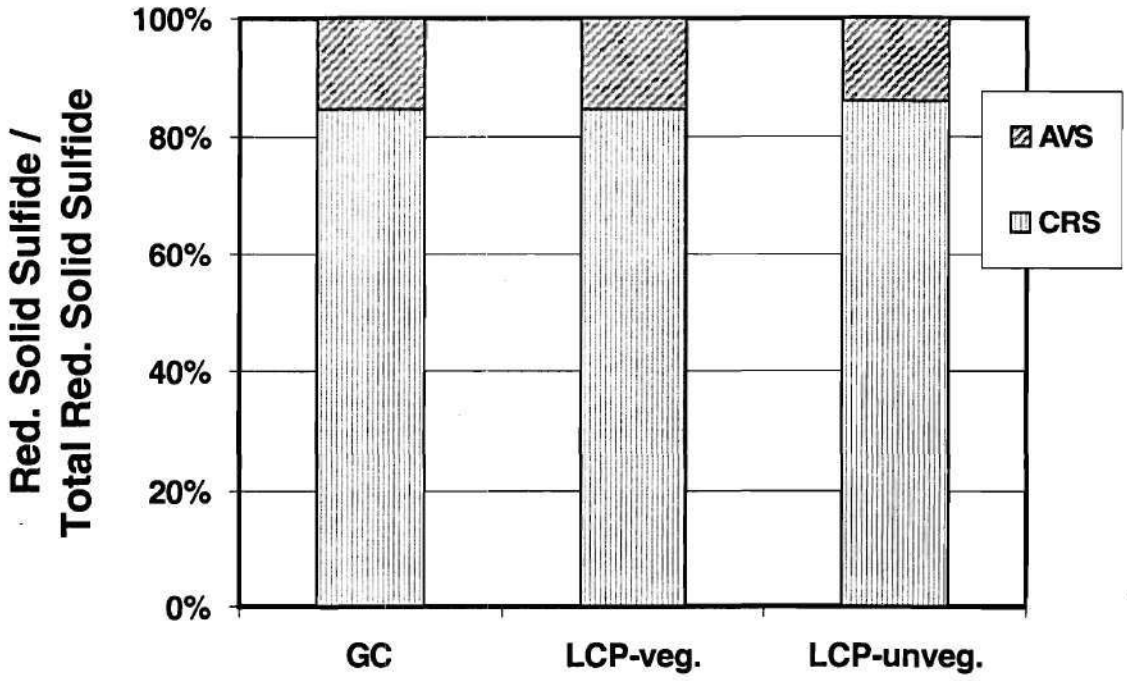

Figure 5.16 Radiolabel reduced solid sulfides, showing proportions of acid-volatile sulfide and chromium-reducible sulfur.

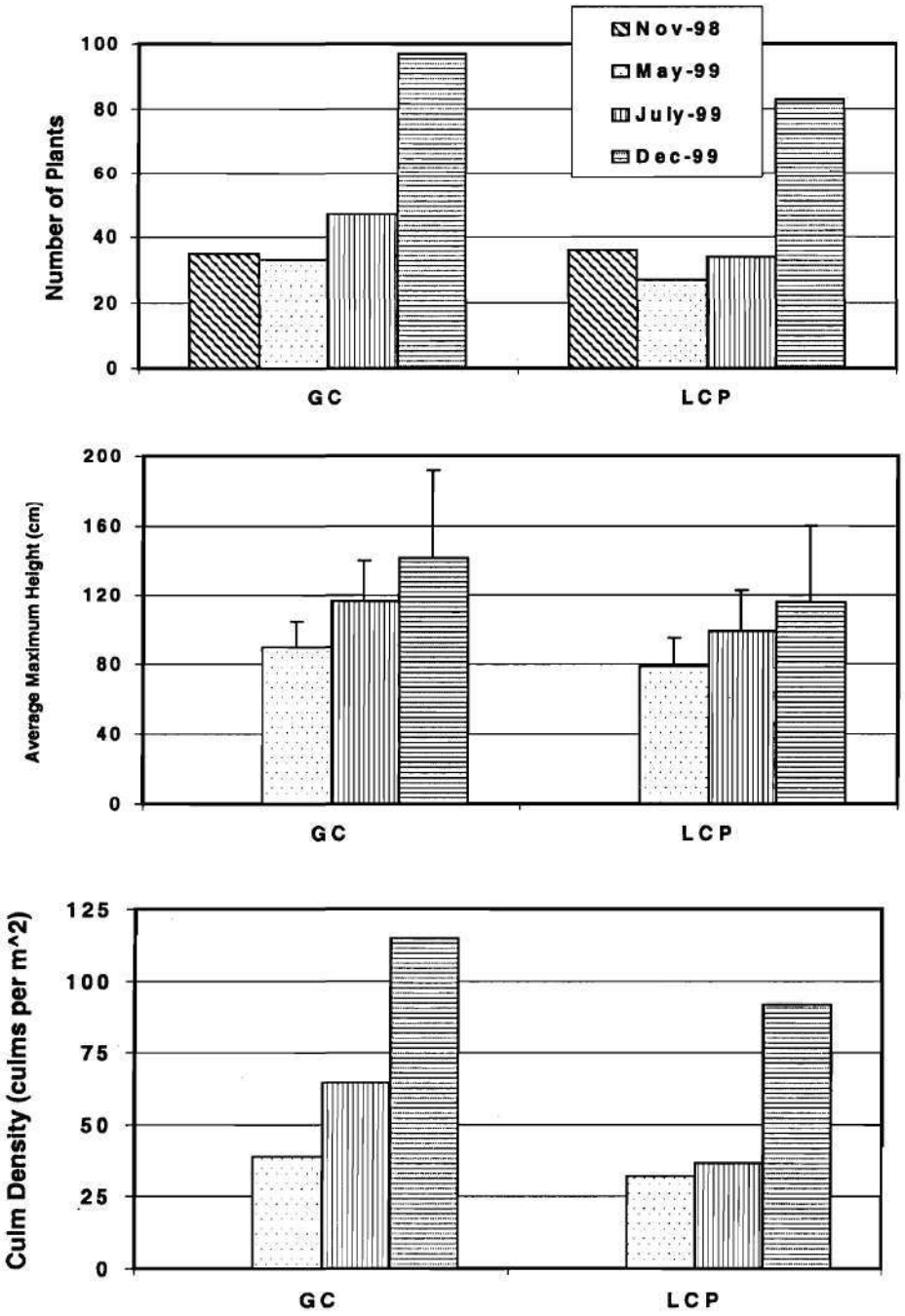

Figure 5.17 Above-ground *Spartina* biomass measurements for GC and LCP mesocosms over the first growing season. Error bars represent the standard deviation of all maximum height measurements on the particular date per mesocosm.

For LCP in December, culm density was 92 per m^2 and average maximum height was 116 cm. From May to December, the average growth rate was 0.18 cm/day. From May to July, the rate was 0.44 cm/day. Comparing the two mesocosms, GC was 25 % denser and 22 % taller than LCP. From May to December, GC grew 39 % faster.

These biomass measurements were comparable to other *Spartina*-inhabited salt marshes. *Spartina* along a transect of a Louisiana salt marsh reached 45-110 cm in height and 110-420 per m^2 in density (Mendelssohn *et al.*, 1981). A Georgia marsh reached a density of 140 per m^2 (Schubauer and Hopkinson, 1984).

Observations of Macrofauna

For the length of this study, macrofaunal abundance was unequal among the three mesocosms. During winter months, macrofaunal activity was very limited in GC and LCP-vegetated and non-existent in LCP-unvegetated. However, during the warmer months, mesocosms supported the activity of snails and crabs in GC and LCP-vegetated, i.e. both vegetated mesocosms. Macrofaunal activity was not observed in LCP-unvegetated.

In June 1999, macrofaunal activity in GC was assessed with a count of snails and crab burrows. A total of 29 crab burrows and 27 snails were found (6.2 burrows per square meter and 5.8 snails per square meter). It was estimated that LCP-vegetated possessed half this number of snails and burrows. Macrofaunal numbers increased

during the summer months for both mesocosms and approximately in the same 2:1 ratio. For the most part, no macrofauna was present in LCP-unveg.

Mercury in Sediments

Figure 5.18 summarizes, in histograms, total and methyl mercury levels found in sediments over the four sampling dates of this study. Data are discussed on both a wet and dry-mass basis. To convert to a dry-mass basis, i.e. from $\mu g/g_{wet}$ to $\mu g/g_{dry}$, wet concentrations were divided by the respective dry solids ratio of each sediment, shown previously in Table 5.2 (0.529 for GC, 0.306 for LCP-veg., and 0.317 for LCP-unveg.).

As expected, GC sediments showed only trace levels of mercury. Total mercury ranged overall from 0.023 to 0.249 $\mu g/g_{wet}$ (ppm), with an average of 0.043 ($\pm$ 0.007, n=10) $\mu g/g_{wet}$ in June, 0.043 ($\pm$ 0.004, n=10) $\mu g/g_{wet}$ in August, 0.099 ($\pm$ 0.103, n=5) $\mu g/g_{wet}$ in January, and 0.027 ($\pm$ 0.004, n=5) $\mu g/g_{wet}$ in March. These average concentrations are shown in Figure 5.18. Comparing dates, average THg concentration was highest in January. Methyl mercury ranged from 0.156 to 0.470 ng/g_{wet} (ppb), with an average of 0.358 ($\pm$ 0.081, n=10) ng/g_{wet} in June, 0.269 ($\pm$ 0.084, n=10) ng/g_{wet} in August, 0.243 ($\pm$ 0.033, n=5) ng/g_{wet} in January, and 0.212 ($\pm$ 0.066, n=5) ng/g_{wet} in March. Comparing dates, average MeHg concentration was highest in June.

LCP-veg. exhibited THg levels ranging from 3.10 to 21.3 $\mu g/g_{wet}$, with an average of 8.93 ($\pm$ 3.15, n=10) $\mu g/g_{wet}$ in June, 9.53 ($\pm$ 0.65, n=10) $\mu g/g_{wet}$ in August, 9.63 ($\pm$ 3.06, n=9) $\mu g/g_{wet}$ in January, and 8.90 ($\pm$ 5.12, n=10) $\mu g/g_{wet}$ in March. As with GC,

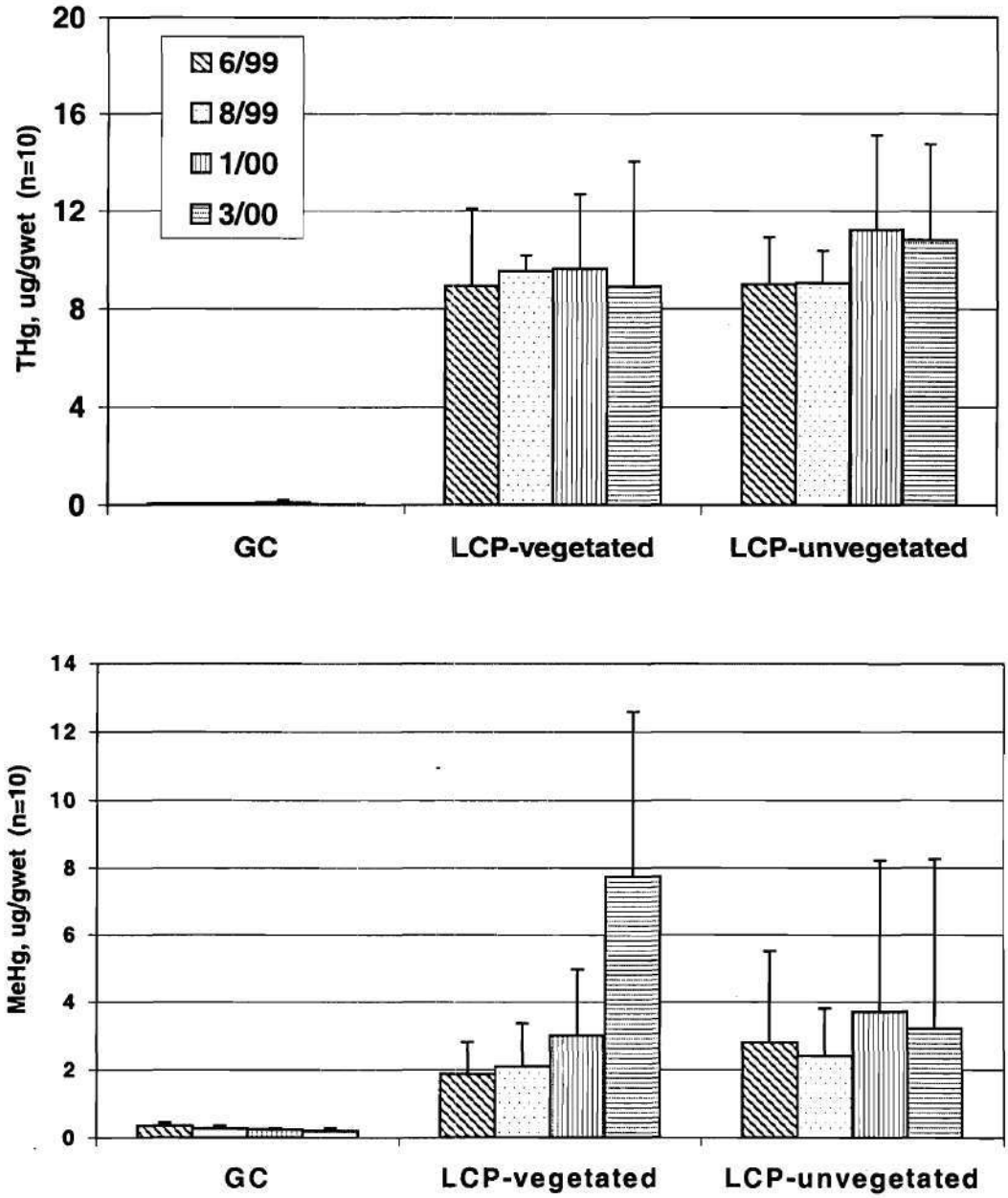

Figure 5.18 Summary of solid-phase total and methyl mercury levels in mesocosm sediments. Levels shown here are on a wet-sediment basis.

average THg was highest in January. Methyl mercury ranged from 0.553 to 17.0 ng/g_{wet}, with an average of 1.87 (± 0.94, n=10) ng/g_{wet} in June, 2.10 (± 1.26, n=10) ng/g_{wet} in August, 3.00 (± 1.97, n=9) ng/g_{wet} in January, and 7.73 (± 4.84, n=10) ng/g_{wet} in March. The wide range of concentrations and large standard deviations were due to differences with depth. Comparing dates, average MeHg was the highest in March.

LCP-unveg. exhibited levels ranging from 4.05 to 20.3 $\mu g/g_{wet}$, with an average of 9.00 (± 1.89, n=10) $\mu g/g_{wet}$ in June, 9.05 (± 1.31, n=10) $\mu g/g_{wet}$ in August, 11.2 (± 3.91, n=10) $\mu g/g_{wet}$ in January, and 10.8 (± 3.93, n=10) $\mu g/g_{wet}$ in March. Average THg concentration was highest in March. Methyl mercury ranged from 0.456 to 15.4 ng/g_{wet}, with an average of 2.80 (± 2.72, n=10) ng/g_{wet} in June, 2.41 (± 1.39, n=10) ng/g_{wet} in August, 3.69 (± 4.52, n=10) ng/g_{wet} in January, and 3.22 (± 5.04, n=10) ng/g_{wet} in March. Similar to LCP-veg., the wide range of concentrations and large standard deviations were due to depth profiles with steep gradients, where MeHg levels were highest in the 0-2 cm intervals. Figure 5.19 shows these depth profiles for LCP-unveg. Comparing dates, average MeHg was highest in January.

Mercury in Porewaters

Figure 5.20 summarizes, in histograms, total and methyl mercury levels found in porewaters over the four sampling dates of this study.

Porewater THg concentrations were higher than expected. To test whether these results were due to procedural problems, sippers were checked for background mercury

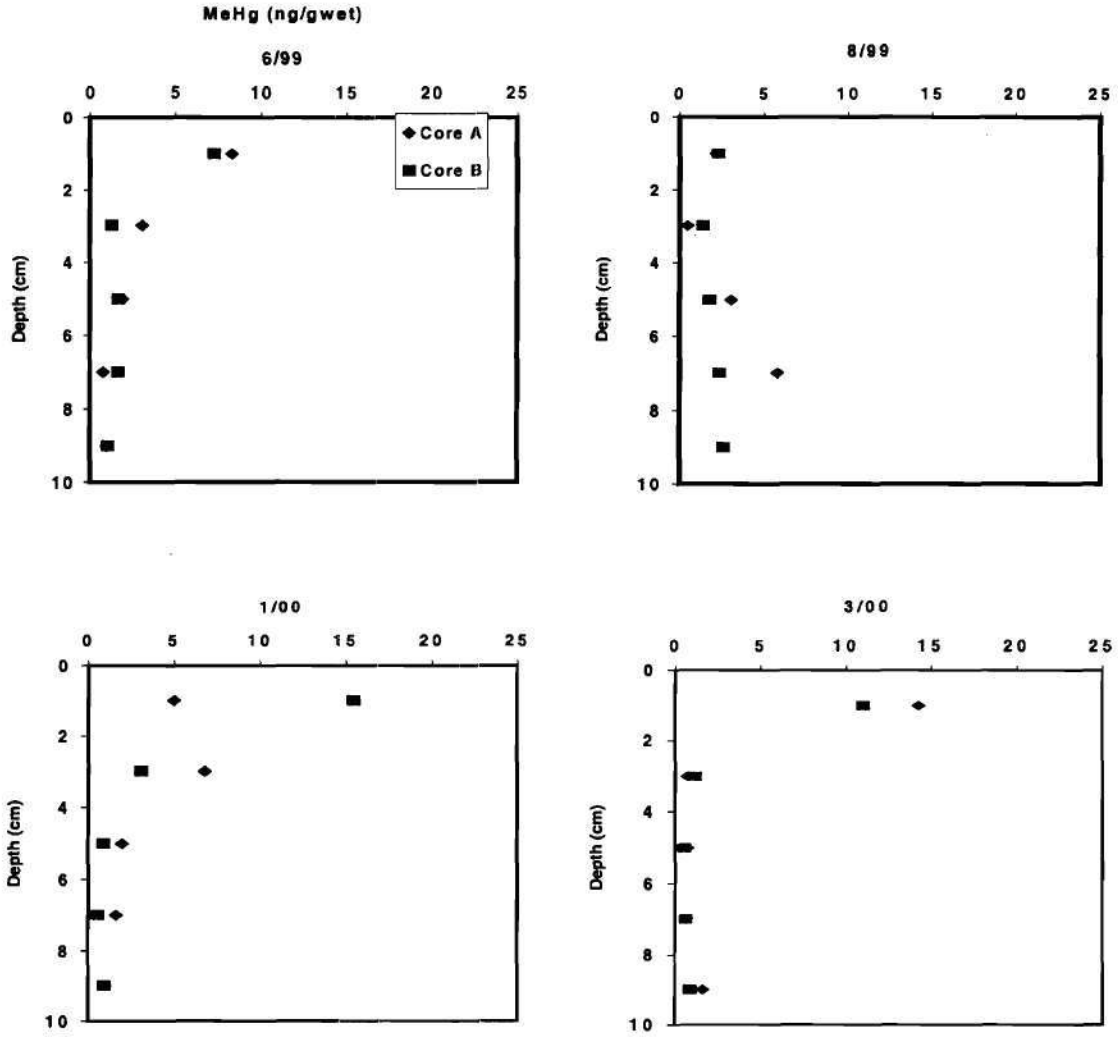

Figure 5.19 Depth profiles of solid-phase methyl mercury in LCP-unveg. mesocosm sediments.

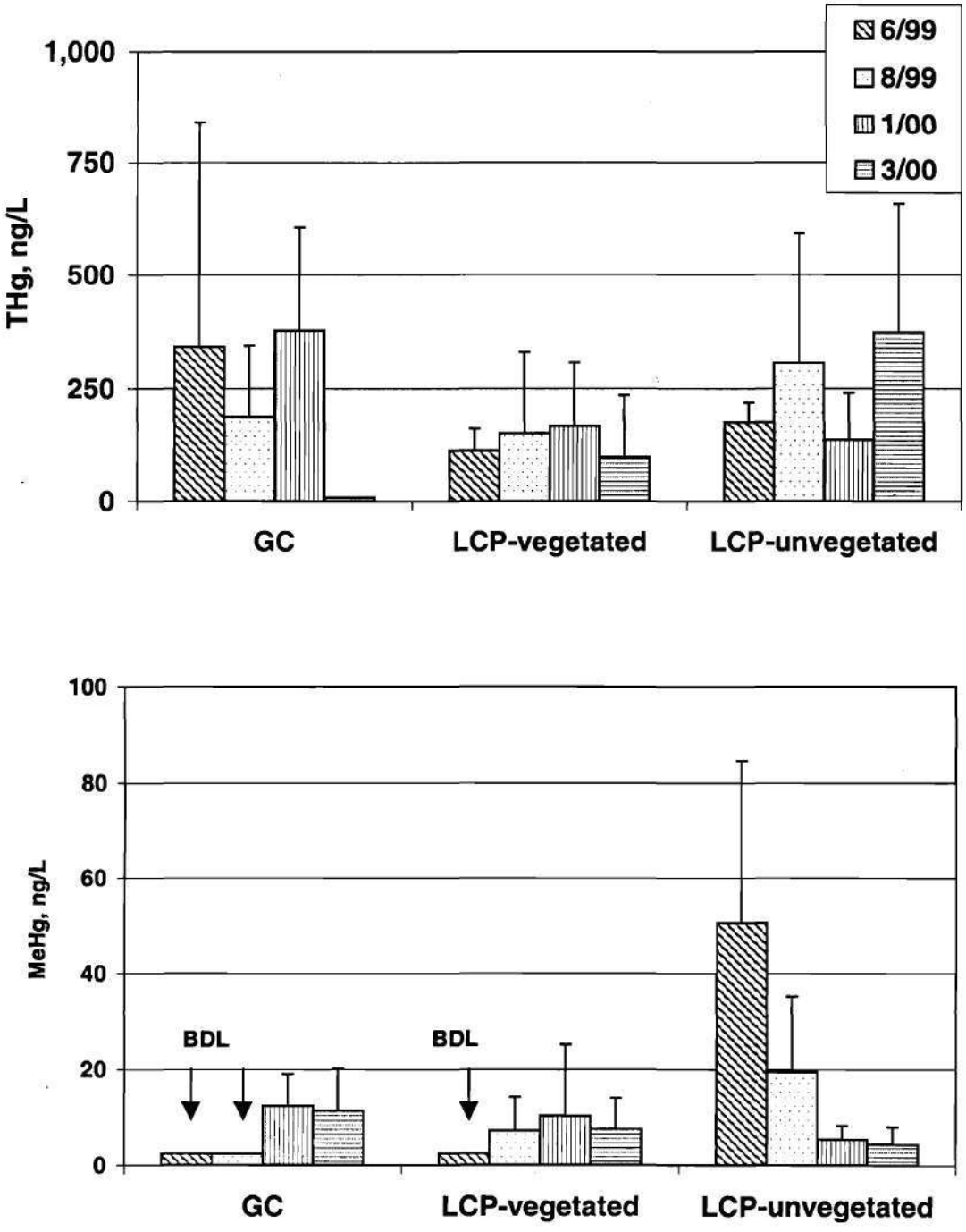

Figure 5.20 Summary of total and methyl mercury levels in mesocosm porewaters.

contamination. To account for residual mercury found in sippers, a series of sipper blanks (or procedural blanks) covering the sippers used in sampling were taken and analyzed. These blanks were collected after the sippers were used in the combined work of Gentzler (1999; three samplings) and this project (four samplings). This totaled seven sampling events.

The sipper blank results showed an average background contamination of 0.156 ($\pm$ 0.067) ng of total mercury from each sipper. This average recovery was subtracted out from total mercury concentrations measured in samples in the following manner:

Equation 5.1:

$$[THg]_{corrected} = \left(\frac{[THg]_{measured} * V}{1000} - \frac{X * V}{7\ mL} \right) * \frac{1000}{V}$$

where:

$[THg]_{corrected}$	=	corrected THg concentration of a porewater sample (ng/L)
$[THg]_{measured}$	=	measured THg concentration of a porewater sample (ng/L)
V	=	sample volume used in analysis (mL)
X	=	average background THg in sipper, equals 0.156 ng

This equation normalizes the average background THg by dividing that residual by the volume used in the systematic blank analysis, 7 mL. The normalized residual in effect represented how much residual was expected from each mL of sipper sample volume and can be multiplied by distinct sample volumes.

Tables 5.7a-b display all porewater THg results, including both $THg_{corrected}$ and $THg_{measured}$ concentrations. Figure 5.20 is derived from $THg_{corrected}$ data. Unexpectedly, GC porewaters showed levels of mercury comparable to LCP porewaters. In GC, total

Table 5.7a Porewater total mercury results, 6/99 and 8/99 samplings.

Date	Mesocosm	Depth [cm]	$THg_{measured}$ [ng/L]	$THg_{corrected}$ [ng/L]
6/99	GC	3	1390	1370
6/99	GC	6	180	158
6/99	GC	10	184	162
6/99	GC	3	90.4	68.1
6/99	GC	6	166	144
6/99	GC	10	175	153
6/99	LCP-veg.	3	181	159
6/99	LCP-veg.	6	181	159
6/99	LCP-veg.	10	135	113
6/99	LCP-veg.	3	105	82.7
6/99	LCP-veg.	6	153	131
6/99	LCP-veg.	10	54.9	32.6
6/99	LCP-unveg.	3	207	185
6/99	LCP-unveg.	6	165	143
6/99	LCP-unveg.	10	166	144
6/99	LCP-unveg.	3	276	254
6/99	LCP-unveg.	6	163	141
6/99	LCP-unveg.	10	208	186
8/99	GC	3	418	396
8/99	GC	6	240	218
8/99	GC	6	108	86
8/99	GC	10	71.3	49.1
8/99	LCP-veg.	3	77.1	54.8
8/99	LCP-veg.	6	380	358
8/99	LCP-veg.	10	64.5	42.2
8/99	LCP-unveg.	3	370	348
8/99	LCP-unveg.	6	549	527
8/99	LCP-unveg.	10	174	152
8/99	LCP-unveg.	3	716	694
8/99	LCP-unveg.	6	138	116
8/99	LCP-unveg.	10	64.4	42.1

Table 5.7b Porewater total mercury results, 1/00 and 3/00 samplings.

Date	Mesocosm	Depth [cm]	$THg_{measured}$ [ng/L]	$THg_{corrected}$ [ng/L]
1/00	GC	1	155	133
1/00	GC	5	602	580
1/00	GC	9	464	442
1/00	GC	1	307	285
1/00	GC	5	160	138
1/00	GC	9	704	682
1/00	LCP-veg.	1	77.3	55.1
1/00	LCP-veg.	5	126	104
1/00	LCP-veg.	9	152	130
1/00	LCP-veg.	1	138	116
1/00	LCP-veg.	5	465	443
1/00	LCP-veg.	9	181	159
1/00	LCP-unveg.	1	76.9	54.6
1/00	LCP-unveg.	5	121	98.7
1/00	LCP-unveg.	9	344	322
1/00	LCP-unveg.	1	68.9	46.6
1/00	LCP-unveg.	5	193	171
1/00	LCP-unveg.	9	154	132
3/00	GC	2	27.4	9.70
3/00	LCP-veg.	2	56.7	34.4
3/00	LCP-veg.	6	31.7	9.70
3/00	LCP-veg.	9	50.4	28.2
3/00	LCP-veg.	2	82.0	59.7
3/00	LCP-veg.	6	112	89.7
3/00	LCP-veg.	9	393	371
3/00	LCP-unveg.	2	636	614
3/00	LCP-unveg.	6	211	189
3/00	LCP-unveg.	9	828	806
3/00	LCP-unveg.	2	410	388
3/00	LCP-unveg.	6	124	102
3/00	LCP-unveg.	9	163	141

mercury ranged from 9.70 to 1370 ng/L, with an average of 341 (± 502, n=6) ng/L in June, 187 (± 157, n=4) ng/L in August, 376 (± 230, n=6) ng/L in January, and 9.70 ng/L (n=1) in March. Comparing dates, average THg concentration (shown in Figure 5.20) was highest in January. Methyl mercury ranged from BDL (2.39) to 24.9 ng/L, with all BDLs in June (n=5) and August (n=6) and an average of 12.3 (± 6.67, n=5) ng/L in January, and 11.4 (± 8.85, n=6) ng/L in March. Average MeHg concentration was highest in January.

LCP-veg. exhibited THg levels ranging from 9.70 to 443 ng/L, with an average of 113 (± 49, n=6) ng/L in June, 152 (± 178, n=3) ng/L in August, 168 (± 139, n=6) ng/L in January, and 98.6 (± 136, n=6) ng/L in March. Average THg was highest in January. Methyl mercury ranged from BDL to 39.5 ng/L, with all BDLs in June (as with GC) (n=6) and an average of 7.27 (± 6.92, n=5) ng/L in August, 10.3 (± 14.9, n=6) ng/L in January, and 7.60 (± 6.41, n=5) ng/L in March. Average MeHg was highest in January.

LCP-unveg. exhibited levels ranging from 42.1 to 806 ng/L, with an average of 175 (± 44.0, n=6) ng/L in June, 306 (± 287, n=5) ng/L in August, 137 (± 102, n=6) ng/L in January, and 373 (± 285, n=6) ng/L in March. Average THg was highest in March. Methyl mercury ranged from BDL to 95.0 ng/L, with an average of 50.6 (± 34.0, n=6) ng/L in June, 19.4 (± 15.7, n=6) ng/L in August, 3.61 (± 2.73, n=5) ng/L in January, and 4.41 (± 3.63, n=6) ng/L in March. Average MeHg was highest in January.

CHAPTER VI

DISCUSSION

Physical Characteristics of Sediments

Physical characteristics of sediments used in this research were discussed in Ch. V. Table 5.2 shows differences in sediment properties between sediments collected from LCP site and sediment collected from Groves Creek. In general, LCP sediment was more porous, less dense, and more organic (higher loss-on-ignition) than sediment from the GC site.

As expected, sediments from both LCP mesocosms had similar physical characteristics. Average values for wet density, moisture content, porosity, and L.O.I. (from Table 5.2) were within five percent of each other. Such similarity (< 5 % difference) would be expected in sediments collected from the same area. With the data obtained in this research, the two LCP mesocosm sediments can be considered the same and compared wholly to GC sediment in the following paragraphs.

Data indicated that wet density was lower while porosity and moisture content were greater in LCP sediment. The greater organic content of LCP may have been the key factor behind this. As mentioned previously, other researchers have estimated organic content with loss-on-ignition techniques (Benoit *el al.*, 1995; Pak and Bartha,

1997; Lord and Church, 1983; Jorgensen, 1977; Gilmour and Riedel, 1995). L.O.I. levels were more than twice as high in LCP sediments compared to GC, leading to less density. Recall from Ch. V that organic materials are significantly less dense than mineral grains; thus, higher-organic LCP sediment was less dense.

Moisture content and porosity, both of which were directly measured, are inherently related in the general sense that void volume used to calculate porosity is filled with water, the mass of which is used to calculate moisture content. Thus, it would be expected that the two LCP sediments had nearly identical data for *both* parameters. Further, GC featured both lower porosity and moisture content.

As discussed previously, particle densities of the sediments overlapped and did not differ by much. It can be concluded that these sediments were physically alike on a dry mineral basis. Sediments were all obtained from Georgia saltmarshes with similar hydrologic regime. Calculated particle densities fell just below the benchmark density of quartz (2.65 g/cm^3), the main component of sand and other earth. With the presence of appreciable organic fractions, saltmarsh sediments reasonably fall just below that benchmark.

Of all physical characteristics discussed here, L.O.I. may have the most importance in research of sulfate reduction and associated biochemical transformations, including co-metabolized mercury methylation. In general, sulfate reduction is fueled by organic compounds and L.O.I. thus provides an estimate of potential sulfate-reducing capacity in the studied sediments. In relation to mercury, Cossa *et al.* (1988) and Benoit *et al.* (1998) theorized that organic particles scavenge Hg from the water column; the

latter researchers positively correlated organic content with total Hg in estuarine sediment. Conversely, in a study of Florida freshwater sediments of 10-50 % organic content, Rood (1996) suggested that mercury retention, as measured by accumulation rates, is not influenced by soil carbon content. More on organic content of LCP and GC sediments is discussed later.

Since they account for the physical nature of sediment, wet density, moisture content, and porosity play a role in movement of water through sediments, especially those of the intertidal saltmarsh regime. Movement of water through mesocosm sediments is discussed in more detail later in the context of a mass balance on system variables and sulfide re-oxidation.

Redox Stratification

Saltmarsh sediment in a natural environment is stratified vertically into microbially-mediated oxidation-reduction zones. Heterotrophic microorganisms create reduced conditions in most coastal sediments below a thin, oxidized surface layer. This stratification allows for the transformation of inorganic and organic compounds through a series of redox processes (Jorgensen, 1977). Redox zones are affected by availability of electron acceptors and donors, bioturbation, and variables such as mixing and input of chemicals from tidal waters and plant roots. In studying saltmarsh mesocosms, redox stratification was viewed in terms of Equation 2.1: organic matter, dissolved parameters (sulfate, sulfide, reduced iron, inorganic carbon, ammonium, pH), and sulfate reduction

rate. Sulfate reduction usually predominates over other redox processes in saltmarsh environments because of the thermodynamics of sulfate (Figure 2.2) and its availability in seawater.

Sulfate reduction consumes sulfate and organic matter and releases inorganic carbon, ammonium, and sulfide into sediment porewater. The resultant concentration profiles of the aforementioned ions are affected by rates of sulfate reduction, mixing, the molecular diffusion rate of each ion, and rates of other reactions or consumption processes occurring in the sediment (Lord and Church, 1983).

Dissolved inorganic carbon and ammonium accumulate in marsh sediment as products of microbial activity. Advection buries the two constituents deeper into the sediment. DIC diffuses into the atmosphere (as CO_2) near the sediment surface and can also be transported to the surface by bioturbation. Ammonium can be oxidized chemically or consumed as a nitrogen source (in vegetated systems) in saltmarsh sediments. Buried ammonium can also be transported by bioturbation to the sediment surface or to root zones, where oxygen and root exudates re-oxidize ammonium and liberate it to the atmosphere.

DIC and ammonium profiles shown in Figures 5.3 and 5.4 exhibited a transformation from a mixed sediment in December 1998 without concentration gradients (Gentzler, 1999) to a more stratified sediment with accumulation of ammonium and DIC with depth, especially in LCP-unveg. DIC and ammonium levels both peaked in summer, coinciding with the time of highest SRR. DIC levels were always lowest at 1-

cm depth and increased with depth, showing the effect of diffusion and subsequent loss as a gas (CO_2).

In LCP-unveg., ammonium showed a trend similar to DIC. In vegetated mesocosms, levels remained low, except for LCP-veg. in August. Koretsky *et al.* (submitted) showed results for ammonium similar to mesocosms in comparing two vegetated sites with an unvegetated site. In that study, samples were taken in winter and summer. Levels increased with depth at three sites, but greater concentrations, nearly 1000 μM, built up at an unvegetated area, compared to two vegetated areas.

Lower ammonium concentrations in vegetated compared to unvegetated suggest that *Spartina* stimulated NH_4^+ oxidation and/or consumption. These data support the assertion that *Spartina* takes up ammonium as a nitrogen source (Sullivan and Daiber, 1974; Linthurst, 1980; Dai and Wiegart, 1997; Koretsky *et al.*, submitted). However, high levels of ammonium in LCP-veg. in August were unexpected and suggest inhibition of plant growth or some other process that allowed ammonium to accumulate. Sampling occurred at the end of vegetative growth, so it is possible that the hindered growth of *Spartina* in LCP sediment was also manifested at the end of the growing season, during reproductive growth. Stressed plants possibly could not reproduce well in the new environment they were placed into.

Sulfate reducing bacteria use sulfate as the terminal electron acceptor in anoxic saltmarsh sediments. Profiles of porewater sulfate typically display decreases with depth as sulfate is utilized in sulfate reduction (Howes *et al.*, 1984; Howarth and Giblin, 1983; Kostka and Luther, 1995). Sulfate concentrations near the surface tend to approximate

that of the overlying water and then decrease with depth. Levels remain high near the surface due to diffusion and advection from overlying water and re-oxidation of sulfide to sulfate in underlying sediment exposed to oxidants. Re-oxidation is discussed in more detail later on.

March 1999 data obtained by Gentzler (1999) and data presented here (Figure 5.6a-d) showed decreases in porewater sulfate with depth. Prior to March 1999, sulfate concentrations failed to show such depletion due to lack of system equilibration (Gentzler, 1999). Concentration gradients with depth from March 1999 to March 2000 suggest development of redox stratification over the sixteen-month sampling period. GC levels decreased less with depth compared to LCP, implying lower SRR in GC. The largest gradient in GC, described in Ch. V, was 1.2 mM/cm in March 2000 (Figure 5.6d). In contrast, LCP gradient reached 5.0 mM/cm in August (Figure 5.6b).

As sulfate is depleted by sulfate reduction, sulfide is produced and can accumulate in sediment porewater. Kostka and Luther (1995) and King (1988) found that dissolved sulfide concentrations increase with depth in saltmarsh sediments. Dissolved sulfide is rapidly trapped in sediment by precipitation with metal ions, such as iron, and a significant portion that remains, up to 90 percent of the sulfide produced, reaches the oxic surface layers of the sediment, where it is oxidized back to sulfate via intermediate oxidation steps (Jorgensen, 1977).

Sulfide profiles from mesocosms in December 1998 showed no appreciable accumulation of sulfide (Gentzler, 1999). Not until March 1999 (Gentzler, 1999) and proceeding dates (Figure 5.7) did sulfide accumulate. LCP-unvegetated showed greatest

sulfide concentrations, reaching millimolar levels in June and August 1999. LCP-vegetated had slightly less accumulation than LCP-unvegetated. GC showed no accumulation of sulfide at any depth.

To compare sulfide accumulation among mesocosms, concentrations can be integrated on an areal basis for the two months of highest sulfide production, June and August. With centrate data integrated to 10 cm, LCP-veg. showed 12.1 $\mu mol/cm^2$ in June and 15.3 $\mu mol/cm^2$ in August, while LCP-unveg. exhibited 21.6 $\mu mol/cm^2$ in June and 8.99 $\mu mol/cm^2$ in August. GC yielded much lower sulfide, 0.18 $\mu mol/cm^2$ in June 0.11 $\mu mol/cm^2$ in August. Sulfide accumulation was significantly greater in LCP sediment, suggesting higher SRR and less re-oxidation than GC.

Hypothetically, sulfide profiles would inversely reflect those of sulfate since sulfate is reduced to sulfide. However, sulfate levels regularly ranged around 30 mM in surface porewaters, while only at several instances did sulfide surpass 2 mM at any depth in the studied 10-cm interval. This non-conservative behavior can be explained by several chemical phenomena. In the presence of oxidants, sulfide can be re-oxidized back to sulfate. This re-oxidation has been mathematically examined in literature and is discussed in context of data of this study later. Also, sulfide can be lost as gaseous H_2S or be sequestered in solid sulfide minerals, including elemental sulfur, iron monosulfide, and pyrite. This interaction with iron is explained next. In addition, it should be added that dissolved sulfide levels and sulfide complexation has recently been shown to control dissolved mercury levels and associated mercury methylation (Benoit *et al.*, 1998). This aspect is also discussed later.

For all sampling dates, including Gentzler (1999), GC showed higher iron(II) concentrations than LCP (Figure 5.8). This signified that iron reduction occurred to a greater extent in GC. Also, Kostka and Luther (1995) suggested that presence of iron(II) in porewaters indicated a prevalence of pyrite and sulfide oxidation. Therefore, presence of iron(II) in GC may have been due to either biological iron reduction or enhanced sediment oxidation. Also, GC sediment may have had a higher natural iron content than LCP. In LCP mesocosms, higher rates of sulfate reduction produced ample sulfide to precipitate porewater iron(II) as solid sulfides, explaining low dissolved iron(II) levels.

This formation of solid sulfides just described was supported by higher AVS and CRS concentrations observed during summer in LCP, as shown in Tables 5.5 and 5.6. Higher sulfide production in June and August precipitated more solid sulfide minerals, including acid-volatile FeS (sulfur valence of -2). Oxidizing conditions further transform sulfides into more stable chromium-reducible pyrite (valence of -1) or elemental sulfur (valence of zero; Kaplan *et al.*, 1963; Troelsen and Jorgenson, 1982). Overall, higher concentrations of AVS and CRS in LCP compared to GC indicated higher SRR in LCP sediment.

To look at the short- and long-term distribution of sulfate reduction end products, collective CRS and AVS data (both colormetric and radiolabel) can be compared. CRS levels obtained colormetrically, which indicate long-term distribution, were two orders of magnitude greater than AVS. For example, CRS for LCP-veg. in June was 273 $\mu mol/cm^3$, while corresponding AVS was 3.50 $\mu mol/cm^3$. Radiolabel determinations, which show short-term distribution, likewise showed much higher CRS, as displayed in

Figure 5.16. Overall, mesocosms showed vastly greater CRS radiolabel pools, averaging more than 80 percent of the total reduced ^{35}S.

Mesocosm findings resembled those of Howarth and Giblin (1979), Howarth and Teal (1983), Howarth and Merkel (1984), and King (1988), who all observed that 65 – 90 % of the short-term end products of sulfate reduction assays were present as CRS in both New England and Georgia sediments. In particular, CRS was found to constitute 62-99 % of the reduced sulfur pool in a Georgia saltmarsh (Howarth and Giblin, 1983). These researchers also experimentally determined that most of this CRS was pyrite (as opposed to elemental sulfur). With pyrite the predominant form of CRS, it can be concluded that pyrite was the major solid sulfide end product, both short- and long-term, of sulfate reduction in mesocosm sediments.

An oxidizing environment, as suggested by a predominance of CRS over AVS, would drive down pH. This is especially true at shallower depths, where reduced sulfur has been re-oxidized to sulfate (Giblin, 1982). pH is an indicator of redox stratification as it reflects sulfide oxidation and aerobic processes closer to the surface and production of bicarbonate (inorganic carbon) from anaerobic respiration (i.e. sulfate reduction) deeper in the sediment. Looking at Equation 2.1 again, more alkalinity is produced than sulfate consumed in sulfate reduction - 52 moles of sulfate yields 67 moles of bicarbonate. In mesocosm sediments, redox stratification indeed formed slight vertical depth gradients in pH - with increase in sediment depth, pH generally increased. For example, in LCP-veg. in August 1999, pH rose from 7.43 at 1 cm to 7.89 at 9 cm. In vegetated saltmarsh systems, Giblin and Howarth (1984), Howes *et al.* (1984), and King

(1988) also found increasing pH gradients with depth. For example, in Howes *et al.* (1984), pH rose from 6.0 at 0-2 cm to 6.9 at 10 cm.

The relatively high pH measurements of LCP-veg. corresponded to high sulfate reduction in August. Bicarbonate produced during sulfate reduction acts as a buffer and pH should fall in the range of 6.9-8.3 (Ben-Yaakov, 1973). Average August measurements for all three mesocosms, shown in Table 5.4, do in fact fall in that range. In addition, average pH increased in all three mesocosms from June to August, indicating an increase in microbial activity through summer. As sulfate reduction was inhibited in winter, pH fell in January and March. Also, values below the theoretical limit of 6.9 (Ben-Yaakov, 1973) could be due to sulfide oxidation.

Kostka and Luther (1995) measured pH of 6.5-7.5 in a Delaware saltmarsh in a vegetated area and 7.0-7.5 in an unvegetated area. These values were quite similar to data here for vegetated and unvegetated systems (Table 5.4).

Differences between GC and LCP sediments have been shown in nearly all physical, chemical, and biological parameters discussed thus far. In summary, GC data suggested that less sulfate reduction occurred compared to LCP. These data match the sulfate reduction rate profiles, which in fact showed lower rates of sulfate reduction in GC.

Sulfate reduction rate profiles for mesocosms changed gradually over the combined period of Gentzler's work (1999) and this study. Figure 6.1 is a time series of SRR profiles for LCP-veg., beginning in December 1998. Over a two-year period, there is a shift from no gradient with depth to a more established vertical stratification.

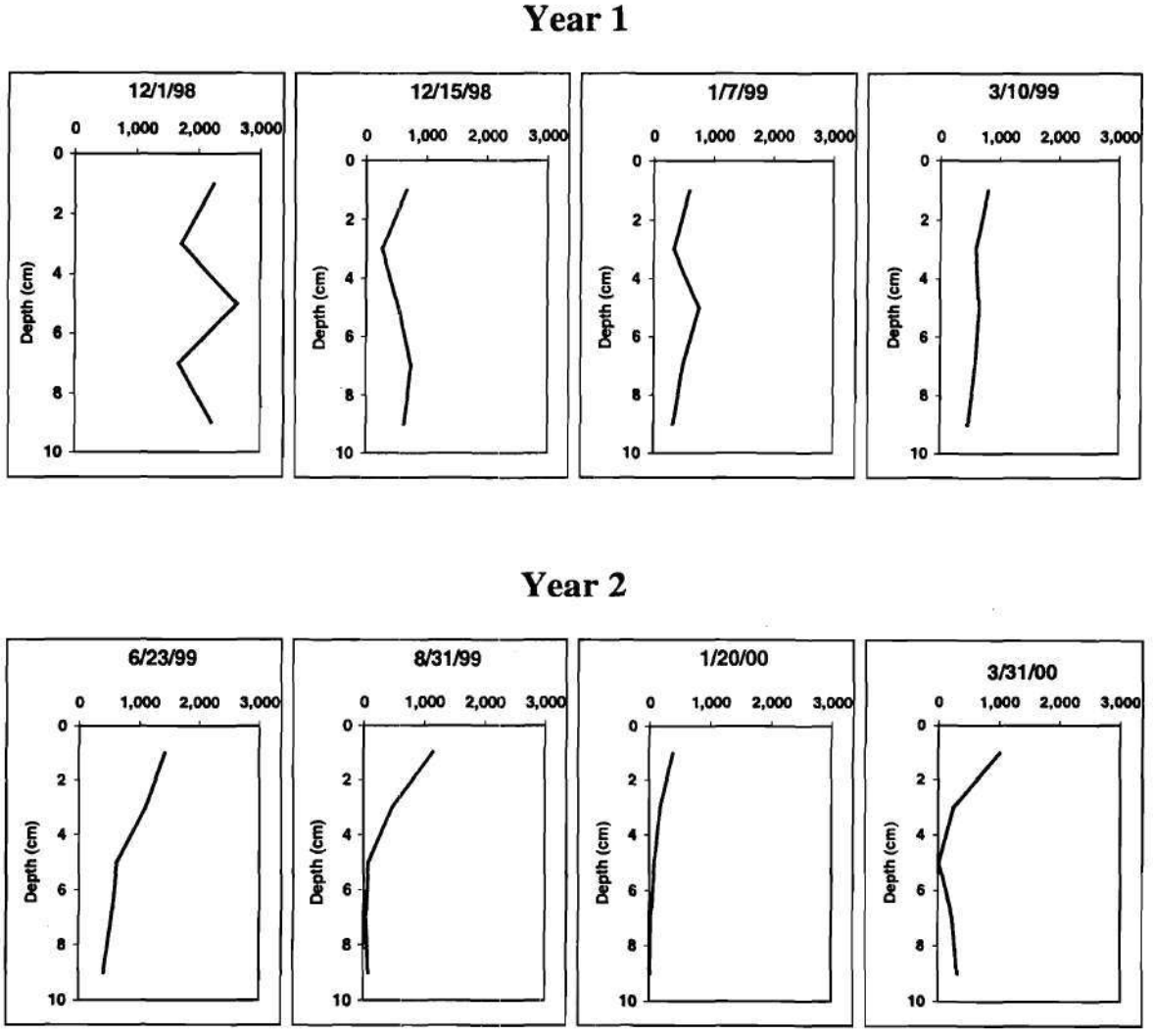

Figure 6.1 Development of SRR stratification in mesocosm sediment over a two-year period. Data shown are SRR in nmol/cm^3-d for LCP-veg.

In natural marshes, maximum sulfate reduction rates have been observed in the top few centimeters of sediment, followed by a decrease with depth to about 10 cm during the summer months (Hines *et al.*, 1989; King, 1988; Kostka *et al.*, submitted; King, 1999). March 1999 through March 2000 sulfate reduction rate profiles for all mesocosms showed similar maxima near the surface and similar decreases with depth. Sulfate reduction rates were higher in LCP mesocosms compared to GC. SRRs for LCP-veg. exceeded LCP-unveg.

Kostka *et al.* (submitted) completed studies of sulfate reduction and porewater chemistry for a saltmarsh on Sapelo Island, Georgia. King (1999) studied sulfate reduction in saltmarsh sediments of Skidaway Island, Georgia. SRR profiles from both studies are shown in Figure 6.2. These profiles show August maximum sulfate reduction rates in the top few centimeters, with a marked decrease with depth to about 10 cm.

Looking at the time series of mesocosm SRRs in Figure 6.1, a consistent decrease with depth was not evident until June 1999. With mesocosm equilibration reached and the growing season in progress, sulfate reduction rates in the top 2 cm increased markedly, exhibiting behavior similar to that found in other Georgia saltmarshes (King, 1988; Kostka *et al.*, submitted; King, 1999).

Most previous research has been conducted on vegetated saltmarshes, so data from the unvegetated mesocosm are examined in light of this. Interestingly, the unvegetated mesocosm showed highest rates on a regular basis. This was surprising in that *Spartina* plants supply labile organic carbon mineralized during sulfate reduction. The high sulfate reduction rates in the unvegetated mesocosm may have been due to

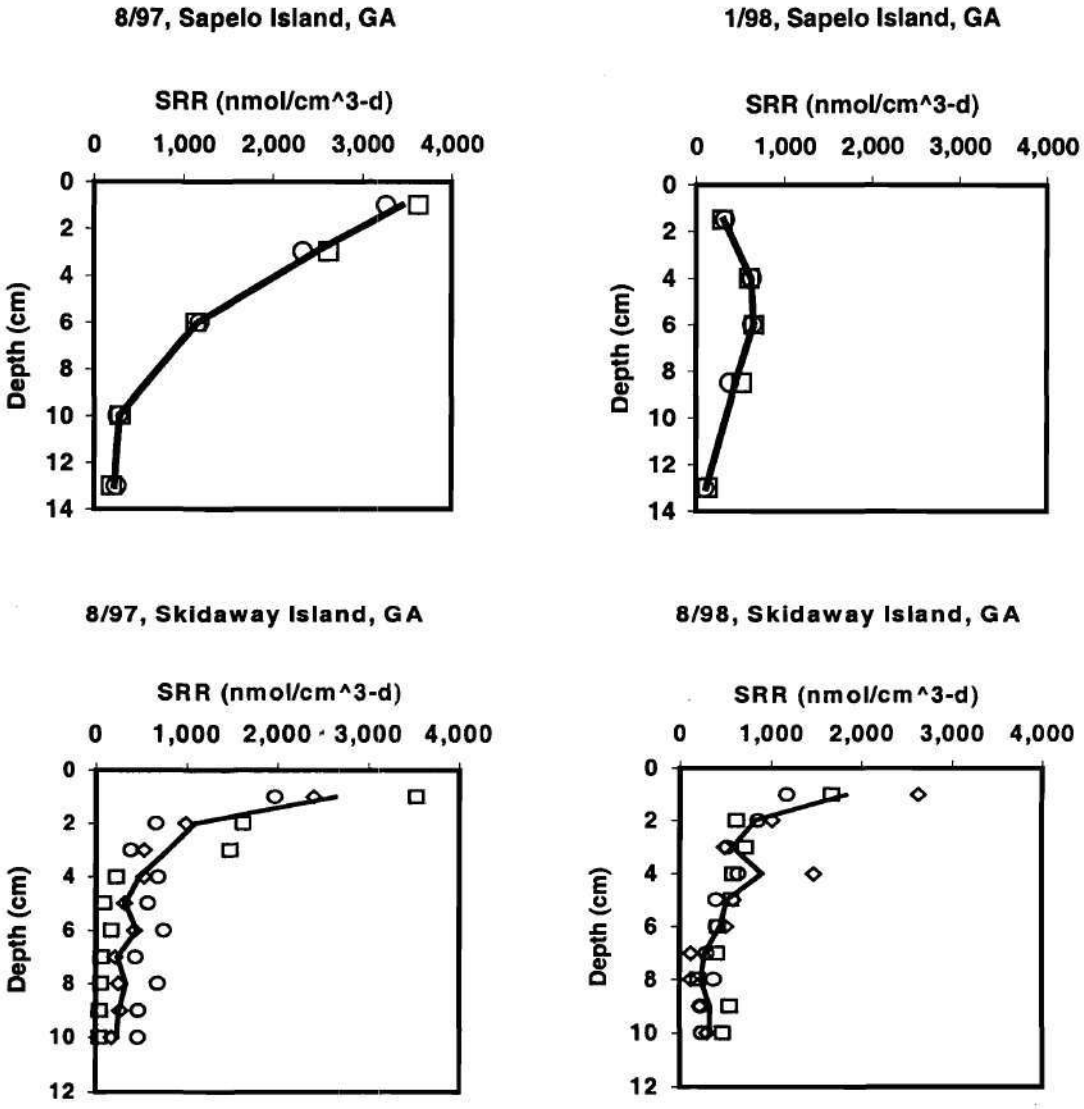

Figure 6.2 Sulfate reduction rates in two Georgia saltmarshes. Sapelo Island data are from Kostka *et al.* (submitted) and Skidaway Island data are from King (1999).

buried *Spartina* detritus (organic matter) in the sediment resulting from sediment collection. This detritus may have supplied additional carbon to be utilized by sulfate reducing bacteria.

The lower values for SRR in GC likely resulted from two main factors: organic carbon availability and oxidizing conditions. As suggested by L.O.I. data, LCP sediment contained twice as much organic carbon available for microbial respiration than GC sediment. Oxidizing conditions, which include bioirrigation and the presence of electron acceptors other than sulfate, affect a host of geochemical data discussed above and are further explained later in context of *Spartina* and macrofauna.

More relationships can be seen with integrated SRRs (Figure 5.14). LCP integrated rates were higher than GC in three out of four samplings, which may have resulted directly from LCP sediments having twice the carbon substrate. Recall from Equation 2.1 that SRR is dependent on this carbon. Also, the fact that SRR in LCP-unveg. remained low in March implies that vegetation in the other two mesocosms stimulated microbial activity as the growing season commenced in the spring. A lack of plant exudates (labile organic carbon) could slow progression of SRR since sulfate-reducing bacteria require such organic inputs.

Other researchers have found 10-cm integrated SRRs up to three times higher in marsh sediments. King (1999) found average rates of 6270 and 6820 nmol/cm^2-d for Skidaway Island sediments in August (consecutive years; sediment temperature = 27°C). Howes *et al.* (1984) reported a rate of 6000 nmol/cm^3-d in a New England salt marsh in September (no temperature given); King (1988) measured a rate of 9400 nmol/cm^2-d in a

South Carolina marsh in August (26°); and King *et al.* (1985) found a rate of 10,700 nmol/cm^2-d in August (no temperature given). In addition, for a Sapelo Island salt marsh, Kostka *et al.* (submitted) reported a rate of 17,100 nmol/cm^2-d in August (30°) and 4860 nmol/cm^2-d in January (11°).

As with any microbial process, temperature is key with sulfate reduction. As expected, SRRs in mesocosms in the warm months of June and August were greater than those measured in January and March. Looking at integrated rates again (Figure 5.14), June had the highest rates for all three mesocosms. GC's integrated SRR of 8230 nmol/cm^2-d for June (sediment temperature = 25.0°C) was nearly six times greater than 1410 nmol/cm^2-d for January (sediment temperature = 12.0°). Figure 6.3 shows how SRR and temperature in all three mesocosms followed similar trends during the course of a year, especially with the sharp dips in the winter. The exception here is how SRR in LCP-unveg. did not increase in the springtime. This was likely due to a lack of plant inputs at the start of the growing season, as explained earlier.

Figure 6.4 combines data from other *Spartina* saltmarshes studied in the literature above and compares those data with mesocosm values. Mesocosms exhibited lower SRR, but a positive correlation to temperature was evident - SRRs increased in these marshes as temperatures increased. The peak measurement from Kostka *et al.* (submitted) suggests that SRR may rise dramatically as temperature nears 30°. Mesocosm sediments never reached this temperature, but 30° may be a threshold at which a significant increase in SRR occurs. A slurry experiment by King *et al.* (1999)

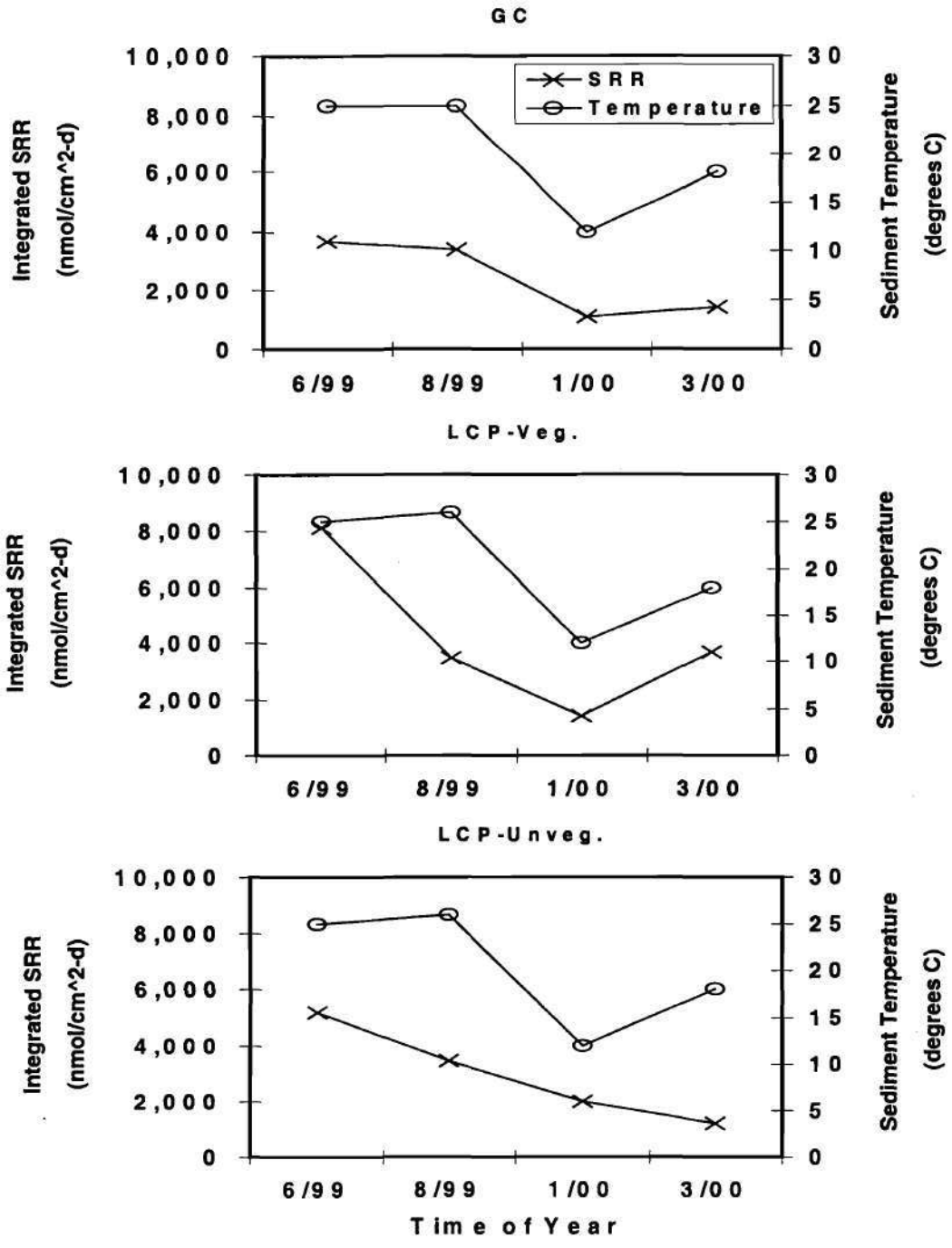

Figure 6.3 Comparison of SRR to time and temperature among mesocosms.

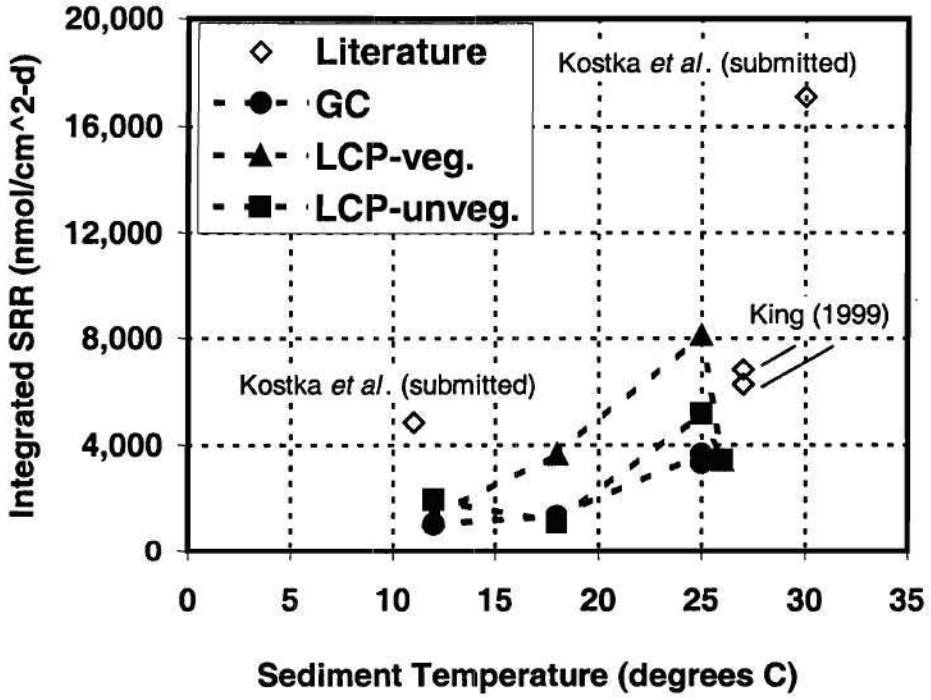

Figure 6.4 The effect of temperature on SRR in vegetated saltmarsh systems.

substantiates this argument; in his experiment, SRR increased approximately eight-fold from 25° to 37°.

Sapelo Island sulfate concentrations from Kostka *et al.* (submitted), shown in Figure 6.5, indicate that the lesser extent of sulfate depletion in January correlated with lower sulfate reduction rates (Figure 6.2). Mesocosm data similarly showed lesser sulfate depletions and SRRs in winter months.

Mercury Levels

Mercury studies in the three mesocosms allow comparisons of mercury species. As shown in Figures 5.17 and 5.19, data were broken down collectively into histograms.

As expected with the control mesocosm, GC exhibited very low levels of solid-phase total and methyl mercury. The 0.023-0.249 $\mu g/g_{wet}$ (equivalent to 0.044-0.473 $\mu g/g_{dry}$) range of concentrations measured for THg is consistent with background abundance described in literature. Oremland *et al.* (1995) found THg concentrations of 0.047-1.460 $\mu g/g_{dry}$ in non-polluted Carson River, Nevada sediment. Kraus *et al.* (1986) observed an average level of 0.22 $\mu g/g_{dry}$ in a *Spartina*-dominated non-polluted creek in New Jersey. Fabris *et al.* (1999) described bay sediments in Australia with levels up to 0.51 $\mu g/g_*$ [note: Fabris *et al.* (1999) did not state whether concentrations were presented on a wet or dry basis]. Gilmour and Riedel (1995) studied a pristine Wisconsin lake with levels of 0.077-0.082 $\mu g/g_{dry}$ in bottom sediments. Winger *et al.* (1993) found an average

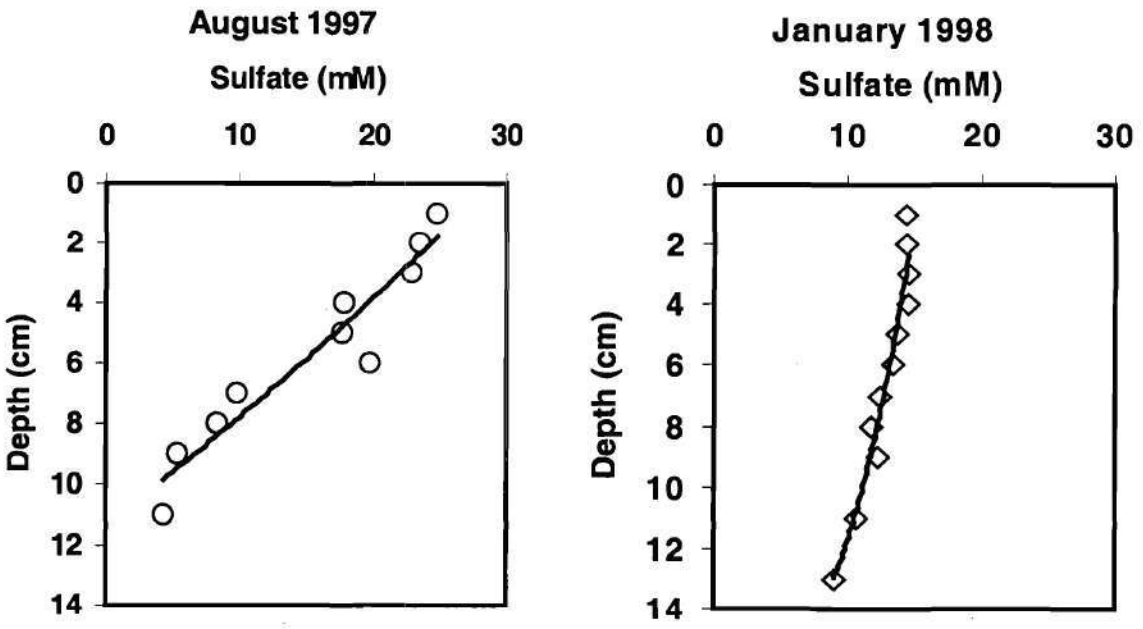

Figure 6.5 Sulfate profiles at Sapelo Island, GA (Kostka *et al.*, submitted).

THg concentration of 0.16 $\mu g/g_*$ in a Florida bay sediment [note: Winger *et al.* (1993) did not state whether concentrations were presented on a wet or dry basis].

Less has been published on background MeHg in sediments. The 0.156-0.470 ng/g_{wet} (0.296-0.893 ng/g_{dry}) range of concentrations for MeHg in GC is much lower than levels found by Gilmour and Reidel (1995), 3.7-4.6 ng/g_{dry}, in a pristine Wisconsin lake sediment. The same researchers found much lower concentrations, 0.01-0.06 ng/g_{dry}, in lake sands, but sands were much different than the fine-grained mesocosm sediments of this study and should not compared.

Higher levels of solid-phase mercury were characteristic of LCP mesocosms. In fact, since the sediments came from a common source (LCP site), concentration ranges for the two mesocosms overlapped considerably. The range of THg in LCP-veg. (3.10–21.3 $\mu g/g_{wet}$) is nearly the same as the range in LCP-unveg. (4.05–20.3 $\mu g/g_{wet}$). The same goes for MeHg (0.553–17.0 ng/g_{wet} in LCP-veg. and 0.456–15.4 ng/g_{wet} in LCP-unveg.).

With risks of biomagnification in food chains, research into mercury speciation is actually more focused on the mobile fraction, e.g. the dissolved phase. Dissolved levels of THg in LCP mesocosms were similar to that of site data, discussed in the next section. The bulk of literature reports porewater THg concentrations in freshwater sediments or saltmarsh sediments from other parts of the country, but not Georgia saltmarshes.

Mercury content in sediments has been tied to organic content (Benoit *et al.*, 1998). Mesocosm data likewise shows that two sediments of similar THg and MeHg

content, LCP-veg. and LCP-unveg., had similar organic content (L.O.I. of 15.59 % and 15.76 %, respectively).

Comparison to LCP Field Data

Field data collected firsthand from the LCP site are available for comparison. Kostka (unpublished) collected samples from LCP in 1998 for porewater chemistry and Hg studies. Figures 6.6-6.9 display data in similar format to those collected in BERM mesocosms. For sake of easier comparison, profiles are shown in the same scale as those of Ch. V.

Three sampling locations were identified at LCP site. Locations SM I and SM II were situated in the south marsh, while NM was located in the north marsh. All locations were vegetated with *Spartina* and visually resembled the LCP-vegetated mesocosm.

LCP site data can first be characterized by mercury content. Figure 6.6 displays average concentrations of Hg in LCP site sediment. All concentrations here are discussed and compared on a wet-sediment basis. THg levels at SM I were much greater than those detected at SM II or NM. Accounting for standard deviation, these differences were significant. In November, SM I had an average THg concentration of 43.3 $\mu g/g_{wet}$, nearly 15 times greater than SM II. In April, SM I had an average concentration of 22.7 $\mu g/g_{wet}$, nearly 20 times greater than NM. Strangely, data show that average MeHg in SM II exceeded SM I in November. This is especially evident in the ratio of MeHg to THg, which is 1.14 % in SM II and 0.05 % in SM I in November.

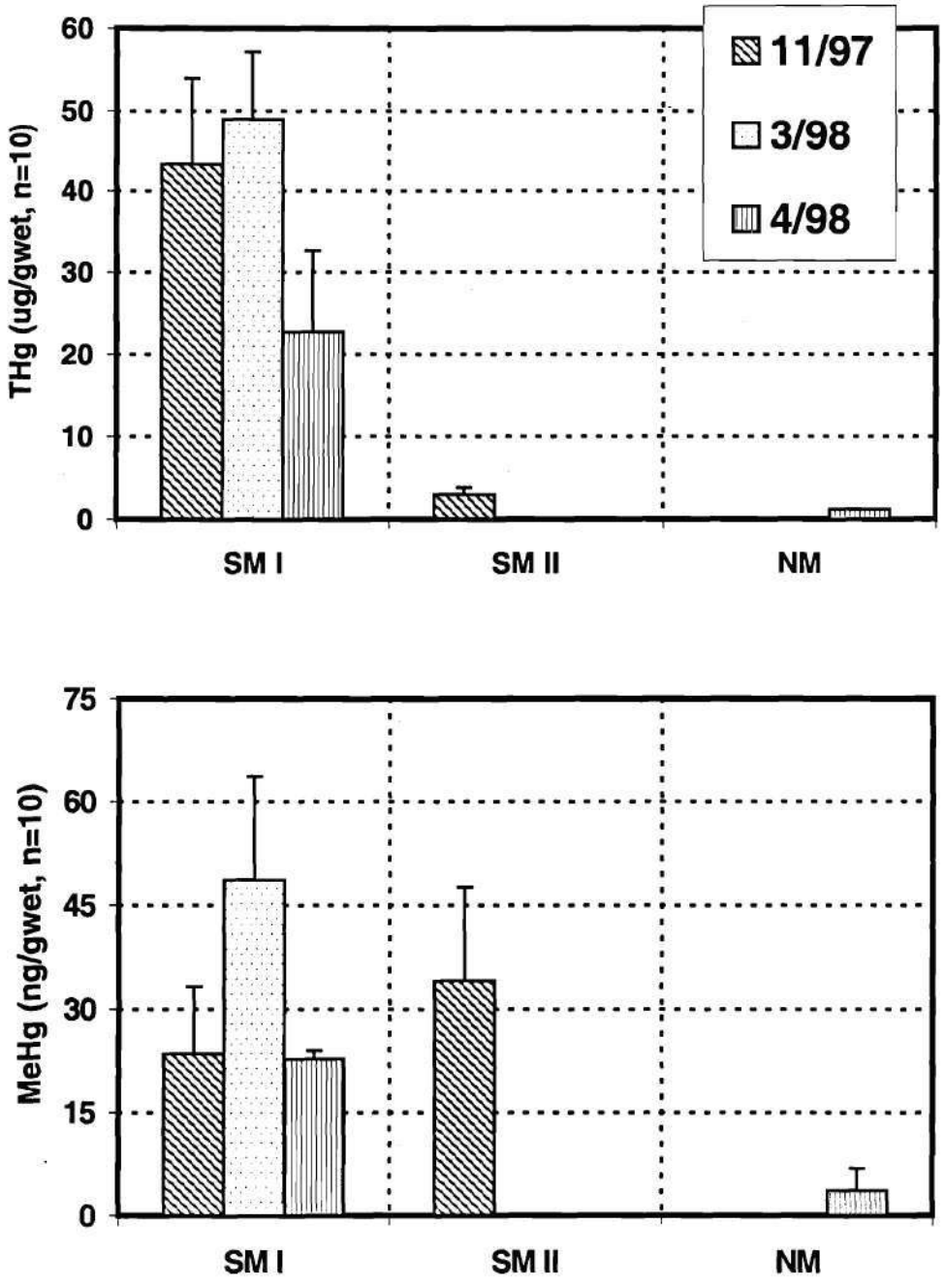

Figure 6.6 Summary of solid-phase total and methyl mercury levels in LCP site sediments (Kostka, unpublished). Data are given on a wet-sediment basis.

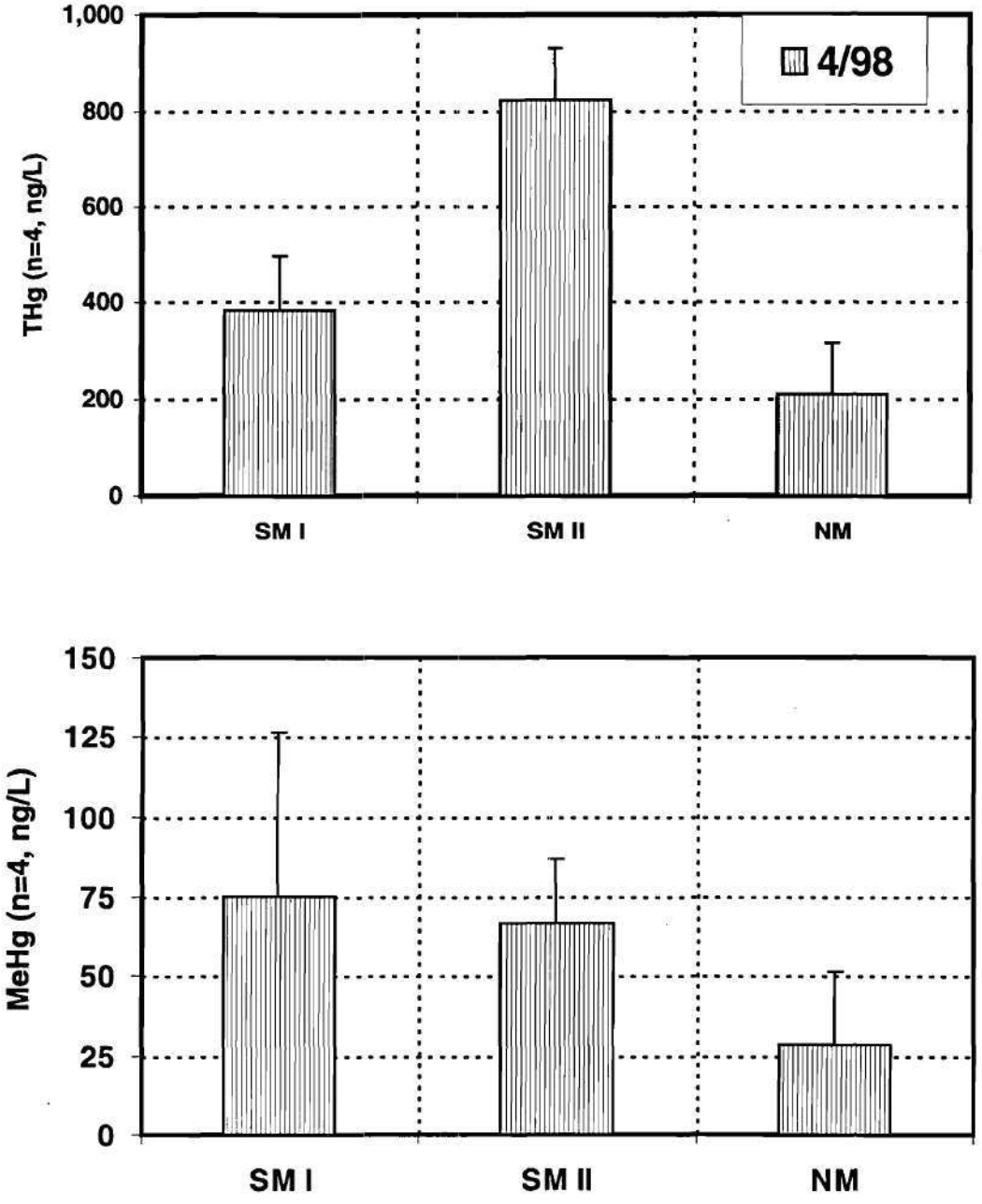

Figure 6.7 Summary of total and methyl mercury levels in LCP site porewaters (Kostka, unpublished).

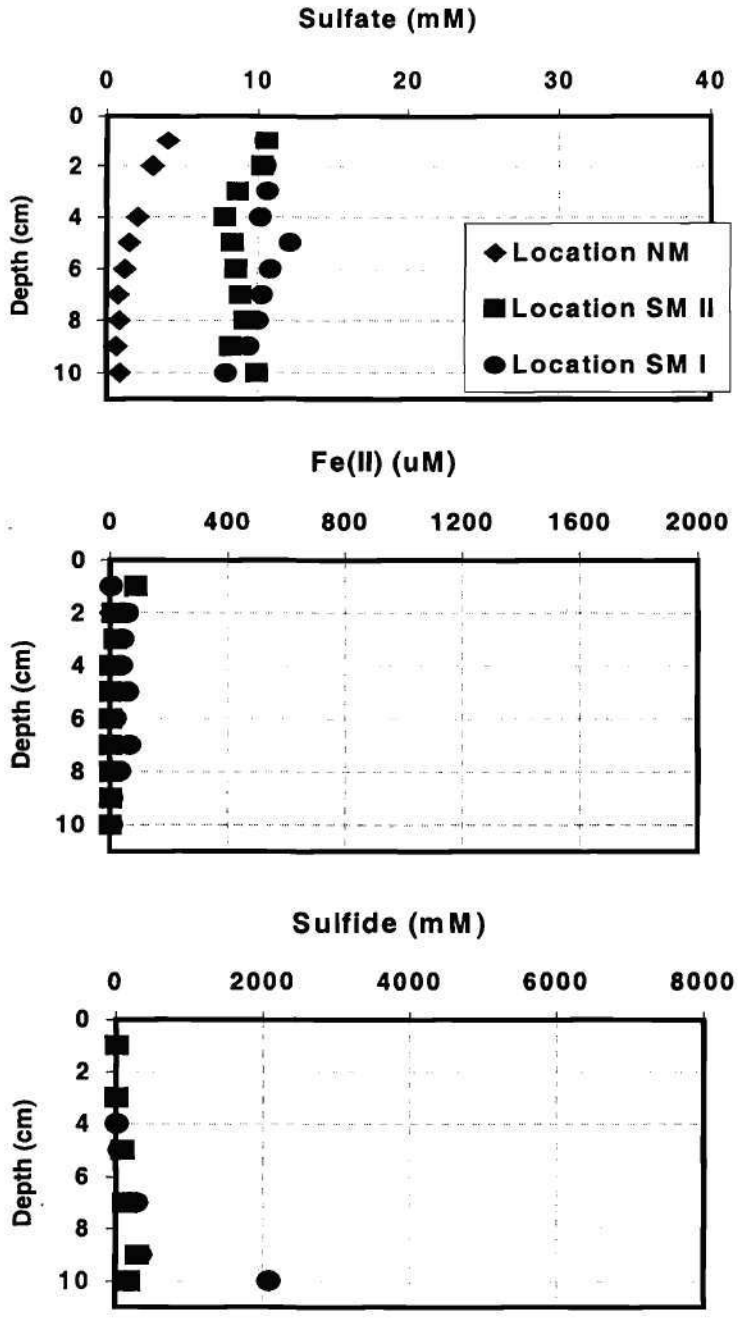

Figure 6.8 Sulfate, iron(II), and dissolved sulfide levels in LCP site porewaters in 4/98 (Kostka, unpublished).

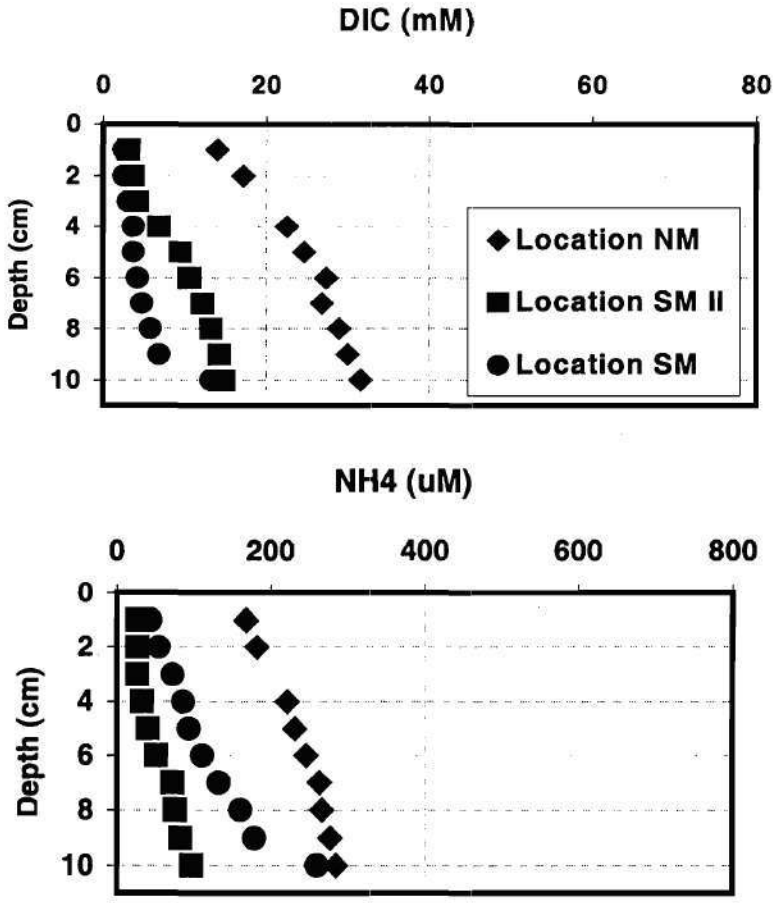

Figure 6.9 DIC and ammonium levels in LCP site porewaters in 4/98 (Kostka, unpublished).

Comparing site data to mesocosms, THg levels in SM I were higher than those detected in LCP mesocosms. For example, the average detection in SM I in March was nearly five times greater than the average detection in LCP-veg. in March. For MeHg, levels in SM I and SM II were higher than any encountered in mesocosms.

Figure 6.7 displays average concentrations of Hg in LCP site porewater. Porewater data were only taken in April. Unlike sediment data, SM I did not have the highest THg detections. SM II, with an average concentration of 824 ng/L, had the highest THg. These levels were significantly higher than SM I and NM. NM had an average concentration of 210 ng/L, one-fourth that of SM II. With MeHg, SM I had the highest average concentration, 74.8 ng/L. NM, with an average concentration of 28.3 ng/L, was one-third that of SM I. However, large standard deviations show that differences in porewater MeHg among the three locations were not significant.

Comparing site data to mesocosms, THg concentrations were within the same order of magnitude, in the hundreds of nanograms per liter. A notable difference is the standard deviation of measurements, which is lower in site data compared to mesocosm data. For example, the standard deviation of SM II measurements was 107 ng/L, which represents 13.0 % of the average concentration. The *lowest* standard deviation of mesocosm measurements was 44.0 ng/L in June for LCP-unveg., which represents 25.1 % of the respective average concentration. In a natural environment, THg site data had lower standard deviation (less variability) than mesocosm data. In the case of MeHg, levels were higher in site data but standard deviations were fairly similar to mesocosms.

Based on the mercury levels just discussed, SM II resembled BERM mesocosms the most, especially LCP-veg. But perhaps the most revealing data are from NM samples. As Figures 6.6 and 6.7 show, NM had the lowest levels of THg and MeHg in both sediment and porewater among the three LCP sampling locations. Nonetheless, porewater levels were still substantial, with 210 ng/L of THg and 28.3 ng/L of MeHg. Even though THg sediment concentrations were low, within one order of magnitude to background according to the literature mentioned above, porewater showed levels consistent with contamination, in the hundreds of nanograms per liter. This repeats a scenario seen with GC mesocosm samples: low Hg in sediment, but unexpectedly high Hg in porewater. More specifically, GC showed an average THg sediment concentration of 0.099 $\mu g/g_{wet}$ and porewater concentration of 376 ng/L in January. Perhaps "background" Hg in porewater is actually higher than previously thought. The bulk of literature reports Hg in freshwater sediments or saltmarsh sediments from other parts of the country; none are from Georgia saltmarshes.

Another interesting relationship arises from plotting the ratio of MeHg to THg in sediment against THg in sediment on a logarithmic scale. Figure 6.10 shows a striking similarity: LCP site data and mesocosm data, independent data sets from both pristine and contaminated environments, show alike inverse relationships between MeHg:THg and THg. In fact, regressions show favorable correlations and similar slopes ($y = 0.0061 x^{-0.5859}$, $R^2 = 0.5291$ from LCP data, and $y = 0.0016 x^{-0.567}$, $R^2 = 0.7894$ from mesocosm data). Apparently, solid-phase MeHg remains at trace levels (parts-per-billion) even as sediments become more and more contaminated.

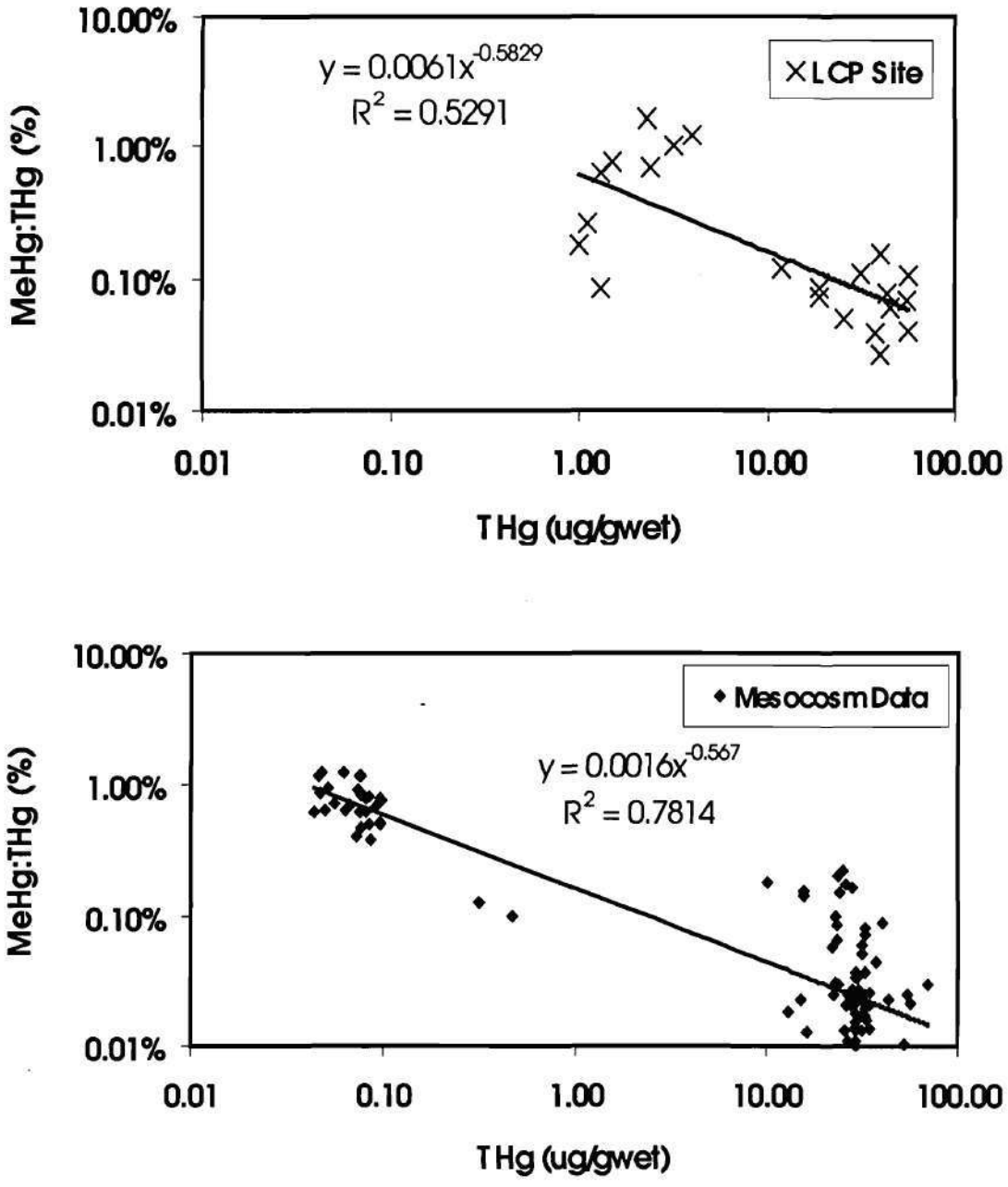

Figure 6.10 Regression plots of MeHg:THg ratio (solid phase) vs. THg in the solid phase.

LCP site geochemistry profiles were taken in April 1999 and are shown in Figures 6.8 and 6.9. Sulfate did not exhibit much gradient with depth, especially at SM II, where concentrations stayed at ~10mM with depth. LCP-veg. likewise did not show notable sulfate gradient in March, but concentrations were higher (18-22 mM).

Fe(II) results were similar for SM II and LCP-veg.; levels were all below 125 μM. Sulfide did not accumulate much at any of the three sites. DIC and ammonium accumulated with depth, especially at NM, but they did not reach the levels in the mesocosms. For DIC, mesocosm levels were up to 2.5 times greater. For ammonium, SM II levels were about half that of mesocosms.

The high level of ammonium in vegetated sediments helps explain another observation from LCP-veg. At every site location (SM I, SM II, and NM), levels increased down to 10 cm. SM II reached nearly 100 μM while SM I and NM exceeded 250 μM. These concentrations were unlike what was found in either vegetated mesocosm for March. However, recall that site samples were collected one month later (April vs. March) than mesocosm samples. Warmer temperatures may have contributed to this increased ammonium. LCP-veg. experienced a similar surge in ammonium in August, as shown in Figure 5.5, but GC did not. Apparently, LCP sediments, contaminated with mercury and high in dissolved sulfide, suppressed growth of *Spartina* once summer set in, keeping ammonium concentrations high. This assertion is also supported by above-ground biomass data, which are discussed next.

Contamination and Growth Inhibition

Accumulation of pollutants may affect microbiological activities in saltmarsh sediments. Changes induced by contaminants in the predominating pathways of terminal carbon flow and nutrient transformations would have serious consequences for the organisms living within sediment and in the water column above (Capone *et al.*, 1983). In studies of organic pollutants, sulfate reduction inhibition has been shown to occur with 1000 $\mu g/g_{dry}$ levels of PCP, toxaphene, naphthalene, and chlordane; 500 $\mu g/g_{dry}$ atrazine; and 100 $\mu g/g_{dry}$ heptachlor (Kiene and Capone, 1984). Capone *et al.* (1983) found that sulfate reduction in Hg-amended sediment was inhibited in both short- and long-term experiments. However, concentrations of Hg used by Capone *et al.* (1983) were 1000 $\mu g/g_{dry}$, whereas LCP sediments in this research contained two orders of magnitude less Hg, up to approximately 70 $\mu g/g_{dry}$. Microbial biomass, measured as ATP, was unaffected by Hg at 10, 100, and 1000 $\mu g/g_{dry}$ levels. Using LCP sediment samples, Winger *et al.* (1993) revealed toxicity to small crustaceans in porewater and sediment with Hg concentrations of 1-27 $\mu g/g_{dry}$, similar to LCP sediments of this study.

Hydrogen sulfide can act as a phytotoxin and inhibit plant growth (Koch *et al.*, 1990). Growth of *Spartina*, expressed as percent survival, number of plants, average maximum height, culm density, and growth rate, was slightly less in LCP than in GC sediment. This inhibition could have resulted from Hg toxicity, from sulfide-induced growth limitation, or from transplantation of *Spartina* plants from their natural GC environment to unfamiliar LCP sediment. Recall from Figure 5.17 that *Spartina* growth in GC was 25 % denser, 22 % taller, and 39 % faster on average. Also, ammonium build-

up in August in LCP-veg. suggested abnormal plant activity, i.e. *Spartina* did not take in necessary nitrogen.

Koch *et al.* (1990) studied the effect of sulfide on *Spartina* from a Louisiana saltmarsh. It was found that growth rate was reduced by adding sulfide to culture media the plants were grown in. Specifically, vegetative plant growth steadily decreased from 0.8 cm/day in aerated sediment to below 0.4 cm/day in sulfide concentrations $\geq$ 2.0 mM. Growth inhibition was also evident at a concentration of 1.0 mM. Further, ^{15}N-tracer experiments showed that NH_4^+ uptake by plant roots was similarly limited by sulfide. The concentration of ammonium in the culture solution was 357 μM, similar to the concentrations found in mesocosm porewaters.

Quantitatively, differences in plant growth between GC and LCP-veg. were substantial enough to suggest plant toxicity. However, since LCP sediment also contained PCBs (Winger *et al.*, 1993), it cannot be determined whether mercury, PCBs, hydrogen sulfides, or a combination of the three, specifically caused this inhibition.

SRRs measured in mesocosm sediments were lower in GC, likely due to organic content and bioirrigation. With SRR higher in LCP sediments, it was evident that Hg levels seen here, up to 70 $\mu g/g_{dry}$, did not dampen SRR.

Effects of Vegetation

Lack of vegetation did not prevent sediment from undergoing stratification. In fact, the unvegetated mesocosm showed more rapid equilibration than the vegetated

mesocosm. In vegetated mesocosms, significant *Spartina* growth did not begin until around the time of the March 1999 sampling. However, greater concentrations of NH_4^+ in LCP-unvegetated compared to the vegetated mesocosms suggest that *Spartina* plants consumed ammonium or injected oxygen into sediments, oxidizing NH_4^+. This supports the lowest NH_4^+ concentrations found in GC, where *Spartina* grew better.

Higher concentrations of sulfide in the unvegetated mesocosm corroborate enhanced oxidation from *Spartina* roots in vegetated mesocosms. The lowest concentrations of sulfide were found in the GC mesocosm, which also showed the most above-ground *Spartina* growth. In addition, the presence of iron(II) in the porewaters of GC indicates a prevalence of pyrite/sulfide oxidation (Kostka and Luther, 1995) assisted by *Spartina* oxidants.

Depth penetration of *Spartina* roots is also important. Schubauer and Hopkinson (1984) measured appreciable *Spartina* root mass down to 50 cm in Georgia salt marshes. As related to sulfate re-generation, which will be discussed in more detail later, these roots could potentially impact sediments the entire length of a core sample (10 cm). *Spartina* root exudates were important in oxidation of the sediments.

In general, changes in microbial process rates and porewater chemistry were expected as the *Spartina* growth cycle continued and sediments were oxidized by a well-established root network.

Presence of Macrofauna

Although not quantified extensively in this study, macrofauna assists in explaining subsurface oxidation of saltmarsh sediments. Further, macrofauna may be affected by vegetation and contamination. In general, macrofaunal presence in mesocosms corroborates findings of geochemical data.

Burrow density in GC was only 6.2 per m^2, much less than the findings of Kostka *et al.* (submitted) of 61-65 per m^2 at Sapelo Island, Georgia saltmarshes. The translocation of sediments from Groves Creek to the mesocosms likely hindered the proliferation of fiddler crabs. But what may be more notable is that all three mesocosms began with no evident macrofaunal life - crabs or snails were purposely left out of the mesocosms. Apparently, macrofauna present in the summer of 1999 either hatched from eggs within translocated sediments or were transported in by wind or birds. Another possibility is that influent seawater carried in eggs.

Considering that all mesocosms basically began without macrofauna, it may be significant that burrows and snails showed up in GC and LCP-veg., but not LCP-unveg. Macrofauna may have utilized *Spartina* detritus as a food source. Fiddler crabs could bioirrigate the sediments, mixing reactive organic matter and oxygen over appreciable depths and thus replenishing sulfate. The higher macrofaunal activity in GC may have been another factor limiting sulfate reduction in that mesocosm.

Mesocosm Dynamics

The BERM presented a means to replicate the natural saltmarsh environment. Tidal waters were controlled and sediment sampling could be easily accomplished. In addition, a gamut of geochemical parameters could be studied at precise depths and viewed in time series or as part of a material balance. Further, the controlled nature of the mesocosms lessened the effects of real-time changes in tidal waters.

Effect of Retention Time

As Ch. III described, water from Skidaway River was continuously pumped to rock filters. After going through these filters, water traveled to another rock filter located within the BERM complex. Water from this filter was continuously pumped to a reservoir, which provided water to mesocosms according to a timed tidal cycle. The reservoir continuously directed overflow back to the filter. Combined with a relatively low flow of water from the river, this recycled overflow provided sufficient water to keep the BERM filter filled.

The overflow system created a retention time or "grace period" which ensured that mesocosms still received water if problems were experienced anywhere between the river and the reservoir. The Skidaway facility was susceptible to power outages or electrical storms that could shut down pumps. Also, algae build-up during warm summer months clogged piping. Third, routine maintenance on pumps and piping required that power and pump be shut-off.

The 5000-L reservoir filled three mesocosms once every 12.75 hours. Each mesocosm (3.05 m in length, 1.52 m in width) filled to a depth of 30.5 cm. Thus, the three mesocosms required a total of 4,240 L per tidal cycle (12.75 hr), which calculates to a flow rate of 8,000 L/d. Although not used in this study, a second reservoir-and-mesocosm system was located at the BERM and maintained similar flow demands. Thus, flow out of the BERM was approximately 16,000 L/d.

The 3,500-L concrete-encased filter provided water to both reservoirs. With a 40 percent porosity, this filter had a bed volume of 1,400 L. Thus, the total volume of influent water (reservoirs + filter) was 5,000 L + 5,000 L + 1,400 L = 11,400 L.

Dividing the total volume of 11,400 L by the demand of 16,000 L/d, this calculates to a retention time, τ, of 0.71 day. Thus, if the rock filters near the river had to be cleaned, and mesocosms relied solely on the BERM filter and reservoir, mesocosms could receive water for up to 0.71 day (17 hours). Depending on the exact timing in comparison to the programmed tidal cycle, this period could accommodate at least one and up to two tidal cycles. In addition, if a lightning strike shut-off power at the BERM filter, and the three mesocosms relied on their reservoir (5,000 L) alone, they could receive water for up to 5,000 L / 8,000 L/d = 0.63 day (15 hours). Again, depending on the exact timing in comparison to the programmed tidal cycle, this period could accommodate at least one and up to two tidal cycles.

The "grace period" system worked - for the length of this study, despite any power outage, clogged pipe, or maintenance, mesocosms never went dry due to problems

with the river intake pump or piping to the BERM filter or piping between the filter and reservoirs.

Mesocosms received a large fraction of water that had been recycled from reservoir overflow rather than raw water directly from the river. Recycle ratios varied week-to-week due to operations and maintenance activities at the river pump, but it was observed that roughly three times as much water came to the BERM filter via reservoir overflow versus raw water from the river. In addition, mixing occurred in the filter and reservoir. In effect, the filter and reservoir behaved as "integrators" when water was not flowing through and filling the mesocosms. Thus, waters reaching mesocosms did not necessarily reflect real-time Skidaway River water. Changes in river water chemistry were dampened and showed up on a gradual basis, e.g. seasonally, which Table 5.3 exhibited. On a given day, an instance of elevated sulfate levels in an advancing incoming-tide salt wedge could not immediately be detected in mesocosm waters. Recall from above that retention time from BERM filter to mesocosms was calculated to be 0.71 day. Retention time from the river, or the time required for a change in river chemistry to affect the mesocosms, was even longer once the rock filters near the river were included into calculations.

Re-oxidation of Sulfide in Surface Sediments

Sulfate reduction is fueled by the steady supply of sulfate in seawater. For intertidal marsh areas, a downward flow of water can transport dissolved oxygen and porewater sulfate to deeper levels and subsequently provide a means for input of

atmospheric oxygen. Aerobic (oxidizing) conditions can potentially keep sulfates relatively high in surface sediments while anaerobic sulfate-reducing bacteria consume sulfates with depth. Based on water diffusion, it might be expected that sulfates in the surface layers of sediment directly correspond to the steady supply of overlying seawater. However, in mesocosm sediments of this study, sulfate in porewaters of surface (top 2 cm) sediments were consistently higher than sulfate levels of the seawater supply for all three mesocosms. More generally, the observed sulfate depletion in porewaters at depth was less than that predicted by measured rates of sulfate reduction and water infiltration. Thus, it is hypothesized that influent oxygenated seawater and subsequent routine exposure of the sediment surface to the atmosphere during low tide of the simulated tidal cycle increased oxidizing conditions to a point where sulfate was re-generated and levels in surface sediments exceeded that of the seawater supply.

Lord and Church (1983), Giblin and Howarth (1984), and Thamdrup *et al.* (1994) previously looked into dynamics of sulfide re-oxidation in saltmarsh environments and associated non-conservative behavior in porewaters. They found that relationships among sulfate levels in porewaters, sulfate reduction rates in sediments, and percolation rates of water through the mesocosm cells quantitatively showed the potential significance of this re-oxidation.

Thamdrup *et al.* (1994) compared porewater concentrations, including SO_4^{2-}, Fe^{2+}, and H_2S, with SRR and concluded that porewater concentrations reflected net outcome of diagenetic processes, not just the result of sulfate reduction alone. For example, the researchers found no detectable H_2S in the top 4 cm of Danish sediments,

even though H_2S was continuously produced by sulfate reduction. The reduced sulfur was at least partially oxidized under anoxic conditions (Giblin and Howarth, 1984).

Giblin and Howarth (1984) used sulfate reduction rates in Georgia sediments to predict porewater concentrations at a given depth. These concentrations differed from observed levels, showing the importance of oxidative reactions in these sediments. The researchers believed both soluble sulfides and pyrite were being oxidized to sulfate, and these processes controlled the chemistry of interstitial water. Chemical oxidation possibly occurred in the following two reactions:

Equation 6.1:

a) $H_2S + 2O_2 \rightarrow SO_4^{2-} + 2H^+$ b) $FeS_2 + 7/2O_2 + H_2O \rightarrow Fe^{2+} + 2SO_4^{2-} + 2H^+$

Lord and Church (1983) stipulated that an upper zone from 0 to 7 cm experienced re-generation of sulfate from sulfide oxidation reactions. These reactions were greater than or equal to sulfate reduction rates and were believed to occur in oxidizing microenvironments which surrounded the *Spartina* root system. Their data from a New England saltmarsh showed indeed that a net enrichment of sulfate occurred. Despite influent seawater with a sulfate concentration of 38 mM, levels were found up to 45 mM to a depth of 7 cm. This phenomena also occurred in BERM mesocosm sediments. For example, in January 2000, influent seawater had sulfate levels of 18.8-19.4 mM, while depths of 1-5 cm had levels up to 28.0 mM in GC.

With porewater chemistry measured, a material balance approach allowed calculation of potential sulfate re-oxidation rates in mesocosm sediments. Relevant terms used in the material balance are defined below:

- Sediment Lift, i – a subsample of a whole sediment core with radius = 1 cm, length = 2 cm
- Underdrain Volume, V – volume of water flushed downward through a mesocosm over one complete tidal cycle; collected during low-tide period in the manner described in Ch. IV
- Porosity, ϕ – ratio of volume void space to total wet sediment volume
- Face Velocity, v_f – velocity of water based on a change of volume over a period of time, normalized to cross-sectional area, i.e. volume of flow per unit cross-sectional area per unit time; comparable to Darcy velocity
- Pore Velocity, v_p – average linear velocity of water through pore spaces of sediment matrix; $v_p = v_f / \phi$
- t_1 – length of time in which the sediment surface is flooded during one tidal cycle; equals 6.75 hr. in all cases
- T – length of time of one complete tidal cycle; equals 12.75 hr. in all cases
- t* – time it takes for a sediment lift to drain completely at a downward pore velocity after the flood period is complete; varies for each mesocosm
- t_2 – length of time in which the sediment surface is free of overlying water during one tidal cycle; equals 6 hr.; $t_2 = T - t_1$

- S_{sw} – sulfate concentration in influent or overlying seawater
- S_i – porewater sulfate concentration of lift i
- S_{i-1} – porewater sulfate concentration of lift directly overlying lift i .

To assess the overall reactions and processes involved, a mass balance on sulfate for a complete tidal cycle can be performed. Using times and volumes just discussed, rates of reaction, i.e changes in concentration of sulfate over time, are next needed. Pertinent reactions in the material balance are transport, sulfate reduction, and sulfide re-oxidation. Transport took place via advection of sulfate from influent seawater and from porewater seepage lift-to-lift. Sulfate reduction, measured as SRR, occurred within each lift and is considered continuous over a complete tidal cycle; i.e., sulfate reduction always occurred in a sediment lift, not just during high tide. Sulfide re-oxidation, or SOR, occurred due to presence of oxygen in: influent water, *Spartina* stem air channels and root zone exudates, air that diffused into exposed surface sediments at low tide, and bioirrigated sediment. Also, as Equation 6.1 suggested, pyrite possibly was oxidized to sulfate. Sulfide re-oxidation rate addresses the increase of sulfate levels in surface sediments (when compared to overlying water) and is considered continuous over the complete tidal cycle; i.e. re-oxidation occurred via air exposure during low tide or replenishment of sulfate and oxygen during high tide.

A sulfate mass balance was performed on a lift-to-lift basis using [(dS/dt)*V*t] as the integral mass term. Available data were porewater sulfate concentrations (obtained per lift from a single core per mesocosm), sulfate reduction rates (determined per lift

from duplicate cores per mesocosm), and underdrain volumes (measured for each mesocosm during low-tide period). There were two caveats in this approach: sulfate levels and times of reaction.

For the surface (0-2 cm) lift, S_{sw} represented the sulfate level of overlying seawater from influent. S_i represented sulfate level in porewater of the surface lift and was indicative of sulfate transported downward to the underlying lift. For subsequent (2-10 cm) lifts, S_{i-1} represented sulfate level in porewater transported out of the overlying lift into the current lift and S_i represented the sulfate level in porewater of the current lift.

A critical step was establishing the time periods over which the various reactions and processes occurred in the tidal cycle. SRR and SOR were considered continuous reactions, occurring over the complete tidal cycle, and were thus assigned time T. Advection of sulfate was affected by the advancing water front – once water drained from a lift entirely, porewater exhaustion was reached and the advection term went to zero. The term t* accounted for this exhaustion and was calculated from pore velocity. Pore velocity was calculated from measured underdrain volume and porosity. Below a certain depth, for a given pore velocity, exhaustion does not occur and t* reached t_2. In summary, lifts affected by porewater exhaustion (the "vadose" zone) were treated differently than lifts not affected (the "saturated" zone).

To begin the mass balance approach, flow of water through each mesocosm was calculated as face velocity. Water flushed through each mesocosm differently due to variations in sediment origins and physical properties as well as the presence or lack of vegetation. Volume of water collected from the GC underdrain averaged 114 L; for

LCP-vegetated and LCP-unvegetated, the volumes were 174 and 257 L, respectively. These values gave face velocities of 0.194, 0.297, and 0.438 cm^3/cm^2-hr. Converted to pore velocity, these values were 0.283, 0.351, and 0.511 cm/hr.

The disparity in velocities further shows physical differences among the mesocosms. Comparing pore velocities, water flowed through LCP-unvegetated sediment pores 1.8 times faster than GC and 1.2 times faster than LCP-vegetated. This may have resulted from the stabilization effect of *Spartina* vegetation and sponge-like behavior of root material. Water flowed more readily in unvegetated sediment. More rapid flow affected chemical transport and mass balance of the system by more quickly exhausting the porewater in surface sediment lifts. Thus, t* is shortest for LCP-unvegetated.

When $t^* < t_2$, porewater was exhausted and mass balance was re-evaluated since advection no longer existed (as mentioned above). Face velocity and porosity were known, so t* was calculated a priori by $t^* = 2\,\phi / v_f$ (simply based on a lift of length = 2 cm).

The input of sulfate into a lift plus the newly reacted / generated sulfate from re-oxidation equals the output of sulfate from the lift plus the newly reacted / reduced sulfate:

Equation 6.2:

$$S_{i-1}*v_f*\pi*t_1 + SOR*2\pi*T = S_i*v_f*\pi*(t_1+t_*) + SRR*2\pi*T\ .$$

Rearranged and simplified, this mass balance yields the following equation for lifts affected by porewater exhaustion:

Equation 6.3a:

$$SOR = SRR + (v_f\ t_1 / 2\ T)\ (S_1 - S_o) + S_1\ \phi / T\ ,$$

and the following equation for remaining lifts:

Equation 6.3b:

$$SOR = SRR + (v_f / 2)\ (S_2 - S_1)\ .$$

Table 6.1 displays re-oxidation rates calculated as above. As suspected, SORs were substantial in surface sediments. In nearly every instance, SORs were substantial in the 0-2 cm lift and to a lesser degree in the 2-4 cm lift. SOR then generally diminished in most lifts below 4 cm.

The possible reasons behind this surface re-oxidation were mentioned earlier. Influent water, *Spartina* stem air channels and root zone exudates, air that diffused into exposed surface sediments at low tide, bioirrigated sediment, or oxidative reactions could drive SOR. The case of influent water can be studied in more detail since the volume of

Table 6.1 Sulfide re-oxidation calculations for mesocosm sediments.

		GC Mesocosm pore velocity = 0.283 cm^3/cm^2-hr vadose zone = 1.70 cm			LCP-veg. Mesocosm pore velocity = 0.351 cm^3/cm^2-hr vadose zone = 2.11 cm			LCP-unveg. Mesocosm pore velocity = 0.511 cm^3/cm^2-hr vadose zone = 3.06 cm		
		Sulfate [mM]	SRR [nmol/cm^3-d]	SOR [nmol/cm^3-d]	Sulfate [mM]	SRR [nmol/cm^3-d]	SOR [nmol/cm^3-d]	Sulfate [mM]	SRR [nmol/cm^3-d]	SOR [nmol/cm^3-d]
6/99										
	influent	22.4			22.4			22.4		
	0-2 cm	29.1	40 - 574	27,000 - 28,000	27.6	1220 - 1640	33,300 - 33,700	26.0	593 - 1580	31,800 - 32, 800
	2-4 cm	27.3	141 - 519	0	21.0	693 - 1520	5350 - 6170	21.7	319 - 491	6,360 - 6,530
	4-6 cm	28.4	121 - 293	2750 - 2900	15.5	531 - 729	0	16.9	198 - 363	0
	6-8 cm	28	288 - 701	0 - 263	14.3	302 - 770	0	11.5	228 - 589	0
	8-10 cm	27.9	435 - 630	0	9.3	362 - 464	0	7.2	0 - 350	0
8/99										
	influent	24.1			24.1			24.1		
	0-2 cm	33.5	218 - 921	33,800 - 34,500	25.9	742 - 1570	25,200 - 26,000	14.2	370 - 440	0
	2-4 cm	34.1	26 - 237	1,490 - 1,700	8.0	355 - 596	0	20.6	204 - 334	34,900 - 35,000
	4-6 cm	32.4	83 - 233	0	3.3	51 - 113	0	25.1	388 - 673	24,300 - 24,600
	6-8 cm	27	233 - 629	0	0.9	6 - 74	0	8.6	141 - 574	0
	8-10 cm	25.2	155 - 483	0	0.5	10 - 149	0	4.3	143 - 208	0
1/00										
	influent	19.1			19.1			19.1		
	0-2 cm	24.8	17 - 81	23,500 - 23,600	25.4	23 - 756	32,500 - 33,200	24.0	87 - 669	33,400 - 34,000
	2-4 cm	28.0	200 - 331	7,530 - 7,670	26.4	164 - 188	3,780 - 3,800	24.2	176 - 265	20,700 - 20,800
	4-6 cm	25.3	148 - 159	0	23.3	30 - 148	0	23.7	236 - 323	0
	6-8 cm	21	35 - 152	0	20.8	25 - 35	0	20.3	0 - 43	0
	8-10 cm	20.1	0	0	20.2	0 - 37	0	14.1	48 - 162	0
3/00										
	influent	18.5			18.5			18.5		
	0-2 cm	23.4	151 - 292	21,600 - 21,800	23.1	847 - 1190	28,400 - 28,700	21.2	0 - 662	25,000 - 25,600
	2-4 cm	22.6	185 - 253	0	21.6	146 - 365	0	31.2	97 - 132	53,600
	4-6 cm	22.7	147 - 225	511 - 590	23.4	0 - 23	6,400	19.2	78 - 199	0
	6-8 cm	21	8 - 39	0	22.1	0 - 471	0	17.6	0	0
	8-10 cm	28.5	17 - 87	17,700	25.9	362 - 464	13,600 - 14,200	10.1	0 - 21	0

water going through the system was quantified. This influent water was assumed to be saturated with respect to dissolved oxygen, which is dependent on temperature and salinity (Colt, 1984). With temperature, salinity, and quantity of water known, the mass of dissolved oxygen made available each tidal cycle can be calculated. In addition, the mass of oxygen required for a given SOR can be back-calculated as follows.

Equation 6.4:

$$\text{Mass } O_2 \text{ required (mg)} = \frac{SOR * T * A * L * M}{24 \text{ hrs} * 10^6}$$

where:

SOR	=	sulfide re-oxidation rate (nmol/cm^{3}-day)
T	=	length of time of one complete tidal cycle; equals 12.75 hrs
A	=	surface area of mesocosm; equals 46,452 cm^2
L	=	length of sediment lift; equals 2 cm
M	=	mass of oxygen in nmol of sulfate; equals 64 ng .

The mass of dissolved oxygen available can be compared to the mass O_2 required per SOR. These comparisons showed that only about one percent of sulfide re-oxidation can be traced to oxygen in influent water. Much more O_2 than that dissolved in water was needed.

It is notable that SOR occurred to a similar degree in both vegetated and unvegetated systems here. So, in finding the reasoning behind SOR, this uniformity among the three mesocosms rules out *Spartina* and bioirrigation, which were present in only two mesocosms. This leaves air diffusion and oxidative reactions. With SOR

dominant closer to the surface (0-4 cm depths), the short distance is conducive for air diffusion. Subsequently, as Giblin and Howarth (1984) suggested, the infusion of oxygen can trigger oxidative reactions, including the oxidation of chromium-reducible sulfur (pyrite), which is prevalent in all mesocosm sediments, including 0-4 cm depths.

Vadose zones, as calculated by pore velocities, were in fair agreement with the 0-4 cm SOR maxima. By definition, the vadose zone was the depth to which porewater exhaustion occurred. In following, this would be the depth to which air could diffuse and oxygenate the sediment. As indicated in Table 6.1, the vadose zones for GC, LCP-veg., and LCP-unveg. were 1.70 cm, 2.11 cm, and 3.06 cm, respectively. These depths corroborate the 0-4 cm intervals of highest SOR.

It thus appears that air diffusion into porous marsh sediments and possibly subsequent chemical oxidation were at least partially responsible for high SORs. Air diffusion could occur during the low-tide period and a pore volume of air, with a nominal partial pressure of oxygen of 21 %, could permeate the vadose zone every tidal cycle. It is known from the ideal gas law that one mole of air occupies 22.4 L of space (at 0° C). Thus, the mass of oxygen that could enter the vadose zone can be calculated as follows:

Equation 6.5:

$$\text{Mass } O_2 \text{ in vadose zone (mg)} = \frac{\phi * L_v * A * P_{O2} * MW_{O2}}{22.4 \text{ L/mol}}$$

where:

ϕ = sediment porosity (%)

L_v	=	depth of vadose zone (cm)
A	=	surface area of mesocosm; equals 46,452 cm^2
P_{O2}	=	partial pressure of oxygen (%)
MW_{O2}	=	molecular weight of O_2; equals 32 g/mol

Calculations for each mesocosm show that even oxygen diffusion into the vadose zone did not meet the amount required by SOR. At its best, oxygen diffusion accommodated 31 % of SOR oxygen demand, assuming one pore volume of air diffuses in. It is also possible that, as oxygen is consumed, more diffuses in.

One last factor that can be looked at is plant O_2 input. Again, only two mesocosms had *Spartina*, but all three did experience algal growth on the sediment surface. Without the shade of *Spartina* plants, algae grew especially well in LCP-unveg. during the hot, sunny months of June – September. An effort was made to remove these mats, but the growth likely was able to contribute oxygen to surficial sediment, perhaps sediment in the 0-4 cm depth interval, where high SOR was calculated.

In current research at the University of Georgia, presented in a web page at gce-lter.marsci.uga.edu/lter/files/misc/GCE_Yr1_annual_rept.pdf, a gross primary production of 12 mmol O_2/m^2-h has been measured in unvegetated intertidal mudflats and tidal creeks. This value can be used as another input of oxygen into mesocosm sediments. Oxygen input attributed to surficial algae is assumed the same for each mesocosm since surface area and tidal cycle is identical for every mesocosm. Calculations show that as much as 29 % of the SOR oxygen demand is satisfied by algal input.

The summation of the addressed oxygen inputs yields up to 61 % of SOR demand. So, the material balance is still not satisfied. Data from this project show no

other quantifiable means of oxygen delivery into the subsurface. However, in this dynamic environment, another possibility is that the subsurface receives additional pore volumes of air. The previous calculation assumed only pore volume. As oxygen is consumed, its partial pressure dips below the ambient 21 % and a diffusive gradient is created, enhancing transport of O_2 into the sediment. Further, thermal energy from the sun influences oxygen fate, such as decreasing dissolved oxygen or increasing microbial activity.

This approach does have inherent uncertainties, mainly with the way in which sulfate concentrations are used. First, SRR, SOR, and sulfate concentration were not obtained independent of one another. Recall from Equations 4.1 and 6.1 that porewater sulfate is an input parameter in the calculations of SRR and SOR. Also, SRR is an input parameter in the calculation of SOR. Second, any solid-phase sulfate that may go into solution is unaccounted for. Porewater sulfate, not total sulfate in sediment, was measured and applied in the equations. The presence of gypsum, for example, would widen the gap in the material balance.

Relationships Between Sulfate Reduction, Sulfide, and Hg Availability

To investigate the relationship between transformation processes and mercury contamination, sulfate reduction rate data from this research were compared with mercury levels found in the same sediments. Data to a depth of 10 cm were viewed from

each mesocosm for both THg and MeHg. The strongest correlation is shown in Figure 6.11, which compares integrated SRR data with porewater MeHg.

As already stated, the mobile fraction of MeHg is the main contaminant of concern because of its likeliness to biomagnify in the food chain. What Figure 6.11 suggests is that exposed, unsequestered, unrooted sediments are a source of mobile MeHg, while vegetated sediments limit the availability of the contaminant. This point is further supported by Figure 6.12, which shows that methyl mercury speciation (MeHg:THg ratio) increased with SRR in the unvegetated system. Although it is likely that SRB-mediated mercury methylation occurs in both environments, the presence of plants brings an infusion of oxidants into the vegetated subsurface. These oxidants may promote oxidative demethylation, which in turn may bring about decreased levels of MeHg.

The behavior of mercury can also be viewed in the context of sulfide. Studies on sulfide controls on mercury speciation and bioavailability have suggested that dissolved sulfide varies inversely with methyl mercury production (Benoit *et al.*, 1999; Benoit *et al.*, 1998; Benoit *et al.*, 1999). This may occur when speciation of Hg at high sulfide concentrations shifts away from lipid-soluble, bioavailable HgS^0 towards disulfide complexes, a charged species that remains in the dissolved phase and is less likely to diffuse across the SRB cell membranes in mercury methylation. This possibly explains the high levels of dissolved THg measured in the mesocosms, which had sulfide levels much higher than those in the above-referenced literature. Literature sulfide levels in the above-mentioned studies ranged up to 65 μM; GC is the only mesocosm that does not

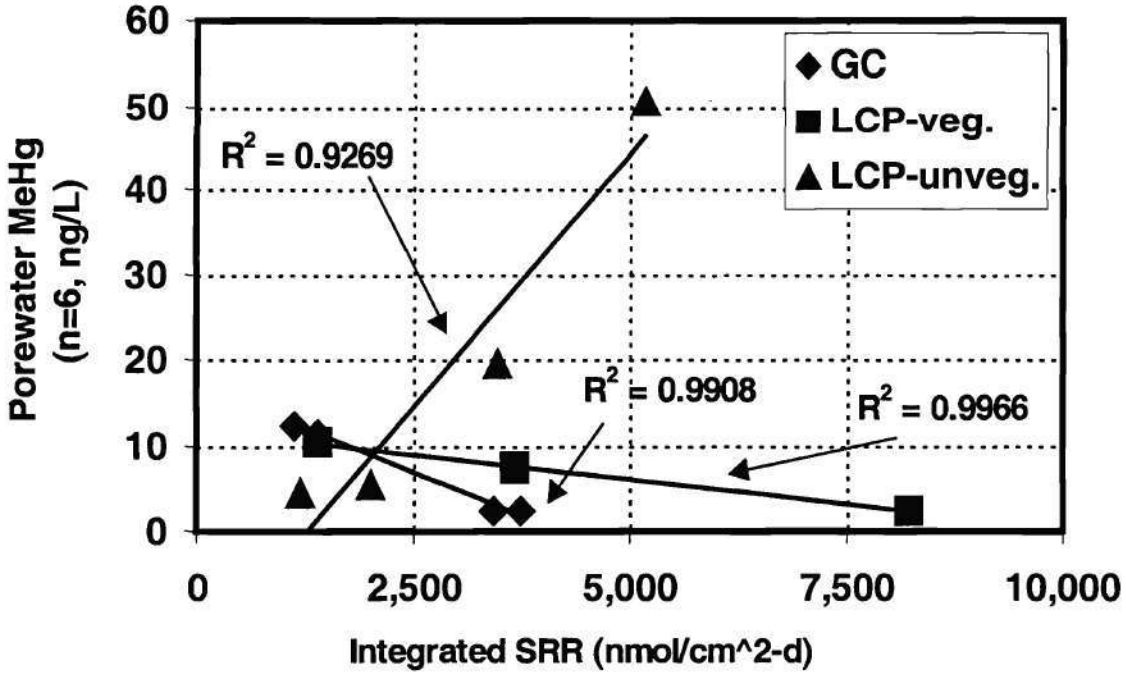

Figure 6.11 The effect of SRR on MeHg in vegetated and unvegetated systems.

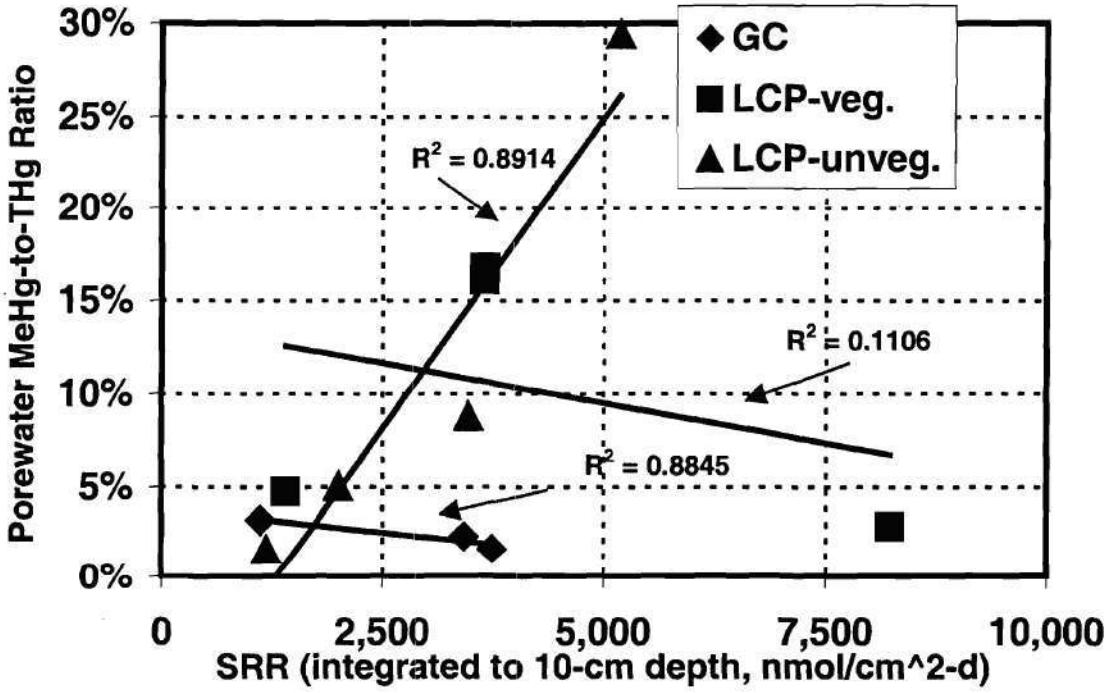

Figure 6.12 The effect of SRR on Hg speciation in vegetated and unvegetated systems.

exceed this consistently. So, high dissolved levels of THg and sulfide could indicate that mercury methylation is not occurring to a great degree. However, LCP-unveg., which showed appreciable sulfide as well as elevated MeHg, was not consistent with this assessment of sulfide control. In general, mesocosm data are consistent with the idea that dissolved sulfide increases dissolved THg, but not with the idea that dissolved sulfide limits THg production.

Occurrence of Mercury Demethylation

As mentioned in Ch. II, oxidative demethylation has been shown to occur in sediments. However, only little information exists as to what environmental conditions favor either organomercurial lyase or oxidative demethylation at *in-situ* Hg concentrations. Oremland *et al.* (1995) found oxidative demethylation (OD) to occur in sediments contaminated with THg in the range of 3.14–44.3 $\mu g/g_{dry}$, similar levels as mesocosm sediments. Marvin-Dipasquale and Oremland (1998) additionally found OD occurring in sediments contaminated with MeHg in the 1–18 ng/g_{dry} range, also within the range of mesocosm sediments. In general, OD is not well-defined in terms of environmental indicators and literature focuses on CO_2 production as the chief indicator of OD. Measurements of inorganic carbon in this study consistently showed millimolar-range ΣCO_2 in porewaters, the result of the dominant respiratory process in saltmarsh sediment, i.e. sulfate reduction. Other favorable conditions have not been reproduced or defined in the same definitive way that a sulfate-rich saltmarsh environment has been

well-documented to support sulfate reduction. Marvin-Dipasquale and Oremland (1998) did observe that additions of sulfate to sediment incubations increased both total MeHg degradation and CO_2 production, showing that sulfate positively affected OD. This is consistent with the concept that, in OD, MeHg acts as a one-carbon analog in the dominant respiratory process operative in the environment studied and the products formed from MeHg are reflective of this process. In other words, OD should produce CO_2 in a sulfate-reducing saltmarsh system.

Ch. VI proposes that sulfide re-oxidation readily occurred in mesocosm sediments. In addition, Figure 6.11 suggests that it was very likely that seasonal changes in MeHg production were due to plant influences. With *Spartina* releasing labile organic carbon and oxidants during the summer months (vegetative growth), it is likely that the bacterial population present in 0-10 cm depths of mesocosm sediments was composed of anaerobes besides sulfate-reducers, such as nitrate- and metal-reducing species that have shown the ability to demethylate (Oremland *et al.*, 1995). Although mercury methylating SRB are active throughout the warmer months when sulfate reduction rates are peaking, demethylators likewise are vigorous as plants are actively supplying organic compounds below-ground. In LCP-unveg. mesocosm, the linear *increase* of MeHg concentrations with sulfate reduction rates may be linked to the activity of solely-mercury-methylating SRB. With the vegetated mesocosms, the linear *decrease* of MeHg concentrations with sulfate reduction rates may very well be indicative of diverse microbial activity, including demethylation. MeHg levels increased in these vegetated mesocosms in the

colder months when SRRs were lower and plants were not growing and thus not providing oxidants to support a diverse bacterial population.

In summary, data suggest that mercury methylation is active throughout the warmer months of the year, but demethylation may be most active at the same time within the sediments when plants are supplying organic compounds and oxidants below-ground. The mesocosms corroborated the results reported by Weber *et al.* (1998). The investigators found non-detect levels of MeHg in porewater during the growing season of *Spartina*, but elevated detections during proceeding months. However, Weber *et al.* (1998) used slurries and this mesosocm study marks the first time that veritable vegetated systems (and not laboratory slurries) have yielded results to indicate that seasonal changes in production of methyl mercury are due to plant physiology.

Core Centrate vs. Sipper Porewater Sampling

In porewater studies, the use of cores allowed parameters to be measured at precise depths from 0 to 10 cm. Each core sample was the centrate of a 2-cm lift of a core and a core data set represented a column of sediment at one location in a mesocosm. Consequently, a core data set generally produced a smooth depth profile for geochemical parameters.

With sipper sampling, each individual device sampled from one depth. One set of sipper data, i.e. samples from 3 cm, 6 cm, and 10 cm, was collected from three different positions within the overall area of a mesocosm; one set was not a continuous depth

sample. This was done because close placement of sippers to one another may have caused vertical movement of water from one sipper's confined area to another. Sippers drew in porewater from a sample tube extending to a certain depth, but the surrounding porous collar was 3.5 cm in length, allowing intrusion of porewater from depths just above and below the tube end. Consequently, sipper data sets did not yield depth profiles identical to core data sets.

A sipper typically yielded up to 7 mL of porewater per sample. Further, it was assumed that the sample tube end drew in water from approximately 1 cm above and below it. These data, along with the 2-cm diameter of a sipper stake and the porosity of the respective mesocosm sediment, can be used to calculate a "zone of influence" for a sipper, i.e. the annular space from which a sipper draws porewater. For GC, this zone was 0.62 cm radially from the porous collar. For LCP mesocosms, the zone was 0.52 cm radially. Including the sipper stake diameter, each sipper in GC covered roughly a 3.24-cm-diameter circular area, while each sipper in LCP mesocosms covered a 3.04-cm-diameter circular area.

Contrarily, a core sample covered only a 2-cm-diameter circular area. Thus, a sipper sample covered an area about 2.5 times greater than a core sample. Combined with the aforementioned fact that it took three separate sippers, each at a different location, to account for one sipper profile (3, 6, and 10 cm), it is not surprising that sipper profiles were not identical to core profiles.

An advantage of sippers was sample volume. As already mentioned, a typical sampling yielded 7 mL. Even with 100 % recovery of centrate (which is highly unlikely;

50 % is more reasonable), a core lift cannot yield this much volume. For example, a core lift from GC (length = 2 cm, $\phi = 0.681$) could yield 4.3 mL (if centrate recovery was 100 %).

In general, sippers are most useful when 5–10 mL of porewater are needed. After this much volume is taken, the sipper collar should be cleaned in order to continue timely sample collection. For studies that require several analyses or multiple aliquots or splits, sippers are ideal. However, when precise depths are more important, cores are the better choice. When both multiple aliquots and precise depths are needed, cores of a size larger than those used in this study are recommended. The problem with larger cores is destruction and disturbance in the study environment; large cores are not recommended in limited-size environments (such as the BERM mesocosms of this study).

Implications and Extensions on Similar Research

Discussion above has described ample research related to redox stratification and mercury availability. Certain literature or proposed research can be extended into this work.

King (1999) modeled mercury methylation rate based on SRR and the composition of SRB communities. Using this model, SRR data from this project and identification of SRB communities allow for estimates of mercury methylation rate. Recall that the mesocosms have shown SRB consortia similar to that of the native marsh (Frischer *et al.*, 2000).

Although more laborious than SRR, mercury methylation and demethylation rates can be measured directly and then compared to MMR estimates.

With the capability to direct effluent to a holding tank, mass balances on system parameters can be performed on more than a 10-cm scale. For example, large quantities of influent and effluent and several samples at depth can be taken for mercury analysis.

In the absence of biological activity, sulfate and chloride are found in seawater at a constant ratio. Sulfate is biologically active, but chloride is not. Thus, core centrate samples to varying depths can be analyzed for sulfate and salinity and sulfate depletion (due to microbiological activity) can be calculated. This method can also be employed in the sulfate mass balance explained in this thesis.

Kostka *et al.* (submitted) measured solid-phase iron and compared those measurements with sulfur geochemistry. With the anomaly of porewater sulfate, sulfide, and iron(II) levels between GC and LCP and the lower SRR in GC, mesocosm sediments would be prime candidates for solid-phase iron determinations.

Spartina has been shown to take up Hg from contaminated sediments and excrete the metal through leaves or transpire the volatile metal into the atmosphere (Kraus *et al.*, 1986; Leonard *et al.*, 1998; Rugh *et al.*, 1998). In addition to porewater and sediment, plant tissue could also be analyzed for Hg concentration. MeHg, beng lipophilic, would not accumulate in plant tissue. To investigate loss of mercury via transpiration, a mesocosm could be retrofitted with a structure to enclose plants. Instrumentation such as an annular denuder could be employed for measurement of mercury in air entrapped in the structure. The annular denuder, described on a web page at

www.arctic.noaa.gov/essay_lindberg.html#footnote1, allows for measurement of both elemental and reactive Hg.

Being lipophilic, MeHg could affect macrofauna in contaminated sediments. Observations in this project indicated diminished numbers of snails and crab burrows in LCP compared to GC. With MeHg known to bioaccumulate readily (Winger *et al.*, 1993), snail and crab specimens could be studied for Hg content.

Mesocosms were able to model vertical flows of tidal waters through sediments. However, horizontal flows, such as the movement of water laterally from the saltmarsh to tidal creeks, may be just as important in the transport of nutrients and/or pollutants. To accommodate horizontal flow, mesocosms could be constructed to include two regimes, both a saltmarsh and an adjacent tidal creek.

CHAPTER VII

CONCLUSIONS

This study was undertaken to determine the effectiveness of three simulated saltmarsh systems in their ability to simulate the natural saltmarsh. Microbial process rates and sediment geochemistry were measured with depth and compared to data from natural marsh. Once equilibrated, these mesocosms became beneficial tools for gaining knowledge about redox chemistry and fate of mercury contamination in saltmarsh environments.

The following conclusions related to redox stratification, *Spartina* influence, and associated mercury bioavailability in the top 10 cm of saltmarsh sediments were reached based on this research:

1) Redox stratification for mesocosms in the form of geochemical data indicated equilibration. After an equilibration time of four months, sulfate reduction rates peaked at the surface and decreased with depth. For associated porewater chemistry, sulfate decreased with depth as it was consumed in sulfate reduction and sulfide showed minor accumulation as a product of sulfate reduction. Likewise, DIC and ammonium increased with depth as products of sulfate reduction.

2) LCP sediments were characterized by higher porosity and greater organic content than GC sediment.

3) As shown by sulfate reduction rates and associated porewater chemistry profiles, GC sediment chemistry differed from LCP. Most notably, iron(II) levels were higher and SRRs were lower in GC. Further, LCP had higher CRS and sulfide concentrations. It is likely that GC sediment had a naturally high iron content, allowing for significant iron reduction in the sediment.

4) Oxygen delivered into the sediment subsurface re-oxidized a significant portion of dissolved sulfide produced by sulfate reduction. In the top 4 cm, this occurred at a rate two orders of magnitude greater than sulfate reduction. Calculations showed that a significant amount of oxygen impacts the saltmarsh, more than that which can be accounted for by *Spartina*, dissolved oxygen in influent seawater, or oxygen diffused into the vadose zone.

5) The most obvious effect of *Spartina* was the uptake of ammonium from sediment porewaters. It can be inferred that the plants utilized ammonium as a nitrogen source.

6) As expected, sulfate reduction rates showed positive correlation with organic carbon in the sediments and with temperature.

7) SRR was slower to develop in the springtime in the unvegetated mesocosm. This was likely due to the lack of plant inputs at the beginning of the growing season. Unvegetated marsh sediments depended more on temperature than vegetated sediments.

8) SRRs in mesocosm sediments generally remained lower than what is reported in natural settings.

9) Total mercury levels up to 70 $\mu g/g_{dry}$ and methyl mercury levels up to 56 ng/g_{dry} showed little to no effect on *Spartina* growth and sulfate reduction. The lower *Spartina* biomass in LCP sediment is more likely due to higher levels of sulfide in LCP.

10) Pyrite was the dominant short- and long-term end product of sulfate reduction in both of these Georgia saltmarsh sediments.

11) Mesocosm porewaters showed greater variability in total mercury concentration than samples taken in a natural environment, such as those taken at LCP site directly.

12) Background total mercury for Georgia saltmarsh porewaters may be in the proximity of 100 ng/L, higher than previously reported. Background total mercury in porewater may be more site-specific than previously indicated.

13) High sulfide levels produced in the saltmarsh environment may have kept dissolved THg levels high. At such high sulfide concentrations, dissolved mercury is unable to diffuse across SRB cell membranes and remains in solution.

14) The ratio of MeHg to THg concentration in the solid phase varies inversely with THg in the solid phase. MeHg may naturally only reach low parts-per-billion levels, even in sediments heavily contaminated with Hg (> 100 ppm).

15) *Spartina* organic inputs may support a population of SRB capable of both methylation and demethylation. These bacteria may carry out demethylation via

the oxidative demethylation route. This study marks the first in which a natural environment has shown that seasonal changes in production of methyl mercury are attributed to plant physiology.

16) The sipper porewater collection technique is appropriate when 5–10 mL of sample from a relative depth are needed.

REFERENCES

Abram, J. W. and D. B. Nedwell (1978). "Inhibition of methanogenesis by sulfate-reducing bacteria competing for transferred hydrogen." Arch. Microbiol. 117(1): 89-92.

Alongi, D. M. (1998). Coastal Ecosystem Processes. New York, New York, CRC Press.

Andersson, I., H. Parkman, et al. (1990). "The role of sediments as sinks or source for environmental contaminants: a case study of mercury and chlorinated organic compounds." Limnologica 20: 347-359.

Ankley, G. T., D. Di Toro, et al. (1996). "Technical basis and proposal for deriving sediment quality criteria for metals." Environmental Toxicology and Chemistry 15(12): 2056-2066.

Atlas, R. M. and R. Bartha (1998). Microbial Ecology: Fundamentals and Applications. Redwood City, CA, Benjamin/Cummings Publishing Inc.

Bak, F. and N. Pfennig (1991). "Microbial sulfate reduction in littoral sediment of Lake Constance." FEMS Mivrobiol. Ecol. 85: 31-42.

Bak, F. and N. Pfennig (1991). "Sulfate-reducing bacteria in littoral sediment of Lake Constance." FEMS Microbiology Ecology 85: 43-52.

Baker, M. D., W. E. Innis, et al. (1983). "Effect of pH on the methylation of mercury and arsenic by sediment microorganisms." Environ. Toxicol. Lett. 4: 89-100.

Baldi, F., M. Filippelli, et al. (1989). "Biotransformation of mercury by bacteria isolated from a river collecting cinnabar mine waters." Microbial Ecology 17: 263-274.

Barkay, T., M. Gillman, et al. (1997). "Effects of dissolved organic carbon and salinity on bioavailability of mercury." Applied and Environmental Microbiology 63(11): 4267-4271.

Benoit, J. M., C. Gilmour, et al. (1998). "Behavior of mercury in the Patuxent River estuary." Biogeochemistry 40: 249-265.

Benoit, J. M., C. C. Gilmour, et al. (1999). "Sulfide controls on mercury speciation and bioavailability to methylating bacteria in sediment pore waters." Environ. Sci. Technol. 33: 951-957.

Benoit, J. M., R. P. Mason, et al. (1999). "Estimation of mercury-sulfide speciation in sediment pore waters using octanol-water partitioning and implications for availability to methylating bacteria." Environmental Toxicology and Chemistry 18(10): 2138-2141.

Ben-Yaakov, S. (1973). "pH buffering of pore water of recent anoxic marine sediments." Limnology and Oceanography 18: 86-94.

Berdicevsky, I., H. Shoyerman, et al. (1979). "Formation of methylmercury in the marine sediment under *in Vitro* conditions." Environmental Research 20: 325-334.

Berman, M. and R. Bartha (1986). "Control of the methylation process in a mercury-polluted aquatic sediment." Environmental Pollution (Series B) 11: 41-53.

Berman, M. and R. Bartha (1986). "Control of the Methylation Process in a Mercury-polluted Aquatic Sediment." Environmental Pollution, Series B: Chemical and Physical 11(1): 41-53.

Berman, M. and R. Bartha (1986). "Levels of chemical versus biological methylation of mercury in sediments." Bulletin of Environmental Contamination and Toxicology 36: 401-404.

Berman, M., T. Chase, et al. (1990). "Carbon flow in mercury biomethylation by *Desulfovibrio desulfuricans*." Applied and Environmental Microbiology 56: 298-300.

Bertrillison, L. and H. Y. Neujahar (1971). "Methylation of mercury compounds by methylcobalimin." Biochem. 10: 2805-2809.

Betts, K. S. (1999). "Technology Update: Bioengineered bacteria show promise in mercury removal." Environmental Science & Technology: 299A.

Biester, H. and H. Zimmer (1998). "Solubility and changes of mercury binding forms in contaminated soils after immobilization treatment." Environmental Science Tech. 32: 2755-2762.

Bisogni, J. J. and A. W. Lawrence (1975). "Kinetics of microbial methylation in aerobic and anaerobic aquatic environments." Journal of Water Pollution Control Federation 47: 135-139.

Bloom, N. S., G. A. Gill, et al. (1999). "Speciation and cycling of mercury in Lavaca Bay, Texas, sediments." Environ. Sci. Technol. 33: 7-13.

Bloom, N. S. and G. J. Watras (1989). "Effects of salinity on methylation of mercury." Sci. Total Environ. 87: 199-208.

Blum, J. E. and R. Bartha (1980). "Effects of salinity on methylation of mercury." Bulletin of Environmental Contamination and Toxicology 25: 404-408.

Bodek, I., W. J. Lyman, et al. (1988). Environmental Inorganic Chemistry: Properties , Processes, and Estimation Methods. New York, Pergamon Press.

Bono, A. and A. Mucci (1995). Partitioning of mercury in solid components of the Sagueney fjord sediments, Abstract. 4th International Symposium on Model Estuaries, Nantes, France.

Brady, N. C. and R. R. Weil (1996). The Nature and Properties of Soils. Upper Saddle River, New Jersey, Prentice Hall.

Breitburg, D. L., J. G. Sanders, et al. (1999). "Variability in response to nutrients and trace elements, and transmission of stressor effects through an estuarine food web." Limnol. Oceanogr. 44: 837-863.

Brock, T. D., M. T. Madigan, et al. (1992). Biology of Microorganisms. Englewood Cliffs, New Jersey, Prentice-Hall, Inc.

Brosset, C. and E. Lord (1995). "Methylmercury in ambient air. Method of determination and some measurement results." Wat. Air Soil Pollut. 82: 739-750.

Brown, N. L., P. A. Lund, et al. (1989). Mercury Resistance in Bacteria. Genetics of Bacterial Diversity. D. A. Hopwood and K. F. Chater. New York, Academic Press: 175-195.

Bubb, J. M., T. P. Williams, et al. (1993). "The behaviour of mercury within a contaminated tidal river system." Wat. Sci. Technol. 28: 329-338.

Buzzelli, C. P., R. L. Wetzel, et al. (1998). "Dynamic simulation of littoral zone habitats in lower Chesapeake Bay. II. Seagrass habitat primary production and water quality relationship." Estuaries 21: 673-689.

Canfield, D. E. and D. J. Des Marais (1991). "Aerobic sulfate reduction in microbial mats." Science 251: 1471.

Canfield, D. E. and B. Thamdrup (1996). "Fate of elemental sulfur in an intertidal sediment." FEMS Microbiology Ecology 19: 95-103.

Capone, D. G., D. D. Reese, et al. (1983). "Effects of metals on methanogenesis, sulfate reduction, carbon dioxide evolution, and microbial biomass in anoxic saltmarsh systems." Applied and Envionmental Microbiology 45: 1586-1591.

Carlson Jr., P. R. and J. Forest (1982). "Uptake of dissolved sulfide by *Spartina alterniflora*: evidence from natural sulfur isotope abundance ratios." Science 216: 633-635.

Casas, A. M. and E. A. Crecelius (1994). "Relationship between acid volatile sulfide and the toxicity of zinc, lead and copper in marine sediments." Environmental Toxicology and Chemistry 13(3): 529-536.

Choi, S.-C. and R. Bartha (1993). "Cobalamin-mediated mercury methylation by *Desulfovibrio desulfuricans* LS." Applied and Environmental Microbiology 59(1): 290-295.

Choi, S.-C. and R. Bartha (1994). "Environmental factors affecting mercury methylation in estuarine sediments." Bulletin of Environmental Contamination and Toxicology 53: 805-812.

Choi, S.-C., T. Chase Jr., et al. (1994). "Enzymatic catalysis of mercury methylation by *Desulfovibrio desulfuricans* LS." Applied and Environmental Microbiology 60(4): 1342-1346.

Choi, S.-C., T. Chase Jr., et al. (1994). "Metabolic pathways leading to mercury methylation in *Desulfovibrio desulfuricans* LS." Applied and Environmental Microbiology 60(11): 4072-4077.

Cline, J. D. (1969). "Spectrophotometric determination of hydrogen sulfide in natural waters." Limnol. Oceanogr. 14: 454-458.

Coleman, M. L., D. B. Hedrick, et al. (1993). "Reduction of Fe(III) in sediments by sulphate-reducing bacteria." Nature 361: 436-438.

Colt, J. (1984). Computation of Dissolved Gas Concentrations in Water as Functions of Temperature, Salinity, and Pressure. Bethesda, MD, American Fisheries Society. Report No. 14.

Compeau, G. and R. Bartha (1983). "Effects of sea salt anions on the formation and stability of methylmercury." Bulletin of Environmental Contamination and Toxicology 31: 486-493.

Compeau, G. C. and R. Bartha (1984). "Methylation and demethylation of mercury under controlled redox, pH, and salinity conditions." Applied and Environmental Microbiology 48(6): 1203-1207.

Compeau, G. C. and R. Bartha (1985). "Sulfate-reducing bacteria: principal methylators of mercury in anoxic estuarine sediments." Applied and Environmental Microbiology 50(2): 498-502.

Cooper, D. C. and J. W. Morse (1998). "Biogeochemical controls on trace metal cycling in anoxic marine sediments." Environ. Sci. Tech. 32: 327-330.

Cossa, D., C. Gobeil, et al. (1988). "Dissolved mercury behaviour in the St. Lawrence estuary." Estuarine Coastal Research Science(26): 227-230.

Craig, P. J. and M. M.A. (1986). "Total methyl mercury and sulphide levels in British estuarine sediments-III." Water Res. 20: 1111-1118.

Craig, P. J. and P. A. Moreton (1984). "The role of sulphide in the formation of dimethyl mercury in river and estuary sediments." Mar. Pollut. Bull. 15: 406-408.

Dai, T. and R. G. Wiegart (1997). "A field study of photosynthetic capacity and its response to nitrogen fertilization in *Spartina alterniflora*." Estuarine, Coastal, and Shelf Science(45): 273-283.

Davis, J. (1999). Brunswick chemical execs sentenced. Atlanta Journal-Constitution. Atlanta: B1,B5.

Devereux, R., M. R. Winfrey, et al. (1996). "Depth profile of sulfate-reducing bacterial ribosomal RNA and mercury methylation in an estuarine sediment." .

Di Toro, D. M., J. D. Mahony, et al. (1992). "Acid volatile sulfide predicts the acute toxicity of cadmium and nickel in sediments." Environmental Sci. Technology 26: 96-101.

Di Toro, D. M., J. D. Mahony, et al. (1990). "Toxicity of cadmium in sediments: the role of acid volatile sulfide." Environmental Toxicology and Chemistry 9: 1487-1502.

Dilling, W. and H. Cypionka (1990). "Aerobic respiration in sulfate-reducing bacteria." FEMS Microbiol. Lett. 71: 123-127.

Dunnette, D. A., D. P. Chynoweth, et al. (1985). "The source of hydrogen sulfide in anoxic sediment." Water Resources 19: 875-884.

Engle, M. A., M. S. Gustin, et al. (2001). "Quantifying natural source mercury emissions from the Ivanhoe Mining District, North-Central Nevada, USA." Atmospheric Environment.

Fabris, G. J., C. A. Monahan, et al. (1999). "Heavy metals in waters and sediments of Port Phillip Bay, Australia." Mar. Freshwater Res. 50: 503-513.

Fossing, H. and B. B. Jjrgensen (1989). "Measurement of bacterial sulfate reduction in sediments: evaluation of a single-step chromium reduction method." Biogeochemistry 8: 205-222.

Frischer, M. E., J. M. Danforth, M. A. Healy, and F. M. Saunders. (2000). "Whole cell versus total RNA extraction for the analysis of microbial community structure using 16S rRNA targeted oligonucleotide probes in saltmarsh sediments." Applied Environmental Microbiology 66: 3037-3043.

Frund, C. and Y. Cohen (1992). "Diurnal cycles of sulfate reduction under oxic conditons in cyanobacterial mats." Appl. Environ. Microbiol. 58: 70-77.

Gagnon, C., E. Pelletier, et al. (1996). "Diagenetic behavior of methylmercury in organic-rich coastal sediments." Limnol. Oceanogr. 41: 428-434.

Gallagher, J. L., R. J. Reimold, et al. (1980). "Aerial-production, mortality, and mineral accumulation-export dynamics in *Spartina alterniflora* and *Juncus roemerianus* plant stands in a Georgia salt marsh." Ecology 61: 303-312.

Gardiner, E. E. (1972). "Differences between ducks, pheasants, and chicken tissue mercury retention, depletions and tolerance to increasing dietary mercury." Canadian Journal of Animal Science 52: 419-427.

Gentzler, S. A. (1999). "Equilibration of a simulated saltmarsh sediment ecosystem: effects of contamination and vegetation on system equilibrium." Special Research Project in Environmental Engineering, School of Civil and Environmental Engineering, Georgia Institute of Technology, Atlanta, Georgia.

Giblin, A.E. (1982). "Uptake and remobilization of heavy metals in salt marshes." Ph.D Thesis in Ecology, Boston University Marine Program, Woods Hole, Massachusetts.

Giblin, A. E. and R. W. Howarth (1984). "Porewater evidence for a dynamic sedimentary iron cycle in salt marshes." Limnology and Oceanography (29): 47-63.

Gibson, G. R. (1990). "A review: physiology and ecology of sulfate-reducing bacteria." J. Appl. Bacteriol. 69: 769-797.

Gilmour, C. C., E. A. Henry, et al. (1992). "Sulfate stimulation of mercury methylation in freshwater sediments." Environ. Sci. Technol. 26: 2281-2287.

Gilmour, C. C. and G. S. Riedel (1995). "Measurement of Hg methylation in sediments using high specific-activity ^{203}Hg and ambient incubation." Water, Air, and Soil Pollution 80: 747-756.

Gilmour, C. C., G. S. Riedel, et al. (1998). "Methylmercury concentrations and production rates across a trophic gradient in the northern Everglades." Biogeochemistry 40: 327-345.

Gilmour, C. G. and D. G. Capone (1987). "Relationship between Hg methylation and the sulfur cycle in estuarine sediments." EOS Trans. Amer. Geo. Union 68: 1718-1725.

Gilmour, G. C. and E. A. Henry (1991). "Mercury methylation in aquatic systems affected by acid deposition." Environ. Pollut. 71: 131-169.

Good, R. E., N. F. Good, et al. (1982). A review of primary production and decomposition dynamics of the belowground marsh component. Estuarine Comparisons. V. S. Kennedy. New York, Academic Press. 2: 241-254.

Grice, G. D. and M. R. Reeve (1982). Chapter 1: Introduction and decription of experimental ecosystems. Marine Mesocosom - Biological and Chemical Research in Experimental Ecosystems. G. D. Grice and M. R. Reeve. New York, Springer-Verlag: 1-10.

Hall, O. J. and R. C. Aller (1992). "Rapid, small-volume, flow injection analysis for CO2 and $NH4^+$ in marine and freshwaters." Limnol. Oceanogr.: 1113-1119.

Hansen, T. A. (1988). "Physiology of sulfate-reducing bacteria." Microbiol. Sci. 5: 81-84.

Hao, O. J., J. M. Chen, et al. (1996). "Sulfate-reducing bacteria." Crticial Review in Environmental Science and Technology 26(1): 155-187.

Heinz, G. (1974). "Effects of low dietary levels of methylmercury on mallard reproduction." Bulletin of Environmental Contamination and Toxicology 13: 554-559.

Hines, M. E., G. T. Banta, et al. (1994). "Acetate concentrations and oxidation in salt marsh sediments." Limnol. Oceanogr. 39: 140-148.

Hines, M. E., R. S. Evans, et al. (1999). "Molecular phylogenetic and biogeochemical studies of sulfate-reducing bacteria in the rhizosphere of Spartina alterniflora." Applied and Environmental Microbiology 65(5): 2209-2216.

Hines, M. E., S. L. Knollmeyer, et al. (1989). "Sulfate reduction and other sedimentary biogeochemistry in a northern New England salt marsh." Limnol. Oceanogr. 34: 578-590.

Horvat, M., V. Mandic, et al. (1994). "Working methods paper: Certification of methylmercury compounds concentration in marine sediment reference material, IAEA-356." Appl. Organomet. Chem. 8: 533-540.

Hosokawa, J. (1993). "Remediation work for mercury contaminated bay experiences of Minamata Bay Project, Japan." Water Science Technology 28: 338-348.

Howarth, R. W. (1993). Chapter 10: Microbial processes in salt-marsh sediments. Aquatic Microbiology: an ecological approach. T. E. Ford. Massachusetts, Blackwell Scientific Publications, Inc.: 239-259.

Howarth, R. W. and A. Giblin (1983). "Sulfate reduction in the salt marshes at Sapelo Island, Georgia." Biogeochemistry 1: 5-27.

Howarth, R. W. and B. B. Jorgensen (1984). "Formation of ^{35}S-labelled elemental sulfur and pyrite in coastal marine sediments (Limfjorden and Kysing Fjord, Denmark) during short-term $^{35}SO_4^{2-}$ reduction measurements." Geochim. Cosmochim. 48: 1807-1818.

Howarth, R. W. and S. Merkel (1984). "Pyrite formation and the measurement of sulfate reduction in salt marsh sediments." Limnol. Oceanogr. 29: 598-608.

Howarth, R. W. and J. M. Teal (1979). "Sulfate reduction in a New England salt marsh." Limnology and Oceanography 24(6): 999-1013.

Howes, B. L. (1985). "Effects of sampling technique on measurement of porewater constituents in salt marsh sediments." Limnol. Oceanogr. 30: 221-227.

Howes, B. L., J. W. H. Dacey, et al. (1984). "Carbon flow through oxygen and sulfate reduction pathways in salt marsh sediments." Limnol. Oceanogr. 29(5): 1037-1051.

Howes, B. L., R. W. Howarth, et al. (1981). "Oxidation-reduction potential in a saltmarsh: spatial patterns and interactions with primary production." Limnol. Oceanogr. 34: 578-590.

Hunt, C. D. and D. L. Smith (1982). Chapter 8: Controlled marine ecosystems - a tool for studying stable trace metal cycles: long-term response and variability. Marine Mesocosm

- Biological and Chemical Research in Experimental Ecosystems. G. D. Grice and M. R. Reeve. New York, Springer-Verlag: 63-80.

Hurley, J. P., S. E. Cowell, et al. (1998). "Tributary loading of mercury to Lake Michigan: Importance of seasonal events and phase partitioning." Science of the Total Environment(213): 129-137.

Isaksen, M. F., F. Bak, et al. (1994). "Thermophilic sulfate-reducing bacteria in cold marine sediment." FEMS Microbiology Ecology 14: 1-8.

Jenson, S. and A. Jernelov (1969). "Biological methylation of mercury in aquatic organisms." Nature (London) 223: 753-755.

Jorgensen, B. B. (1977). "The sulfur cycle of a coastal marine sediment (Limfjorden, Denmark)." Limnol. Oceanogr. 22(5): 814-831.

Jorgensen, B. B. (1978). "A comparison of methods for the quantification of sulfate reduction in coastal marine sediments. II. Estimation from chemical and bacteriological field data." Geomicrobiology Journal 1: 49-64.

Jorgensen, B. B. (1982). "Mineralization of organic matter in the sea bed - the role of sulphate reduction." Nature 296: 643-645.

Jorgensen, B. B. and F. Bak (1991). "Pathways and microbiology of thiosulfate transformations and sulfate reduction in a marine sediment (Kattegat, Denmark)." Applied and Environmental Microbiology 57: 847-856.

Jorgensen, B. B., M. Bang, et al. (1990). "Anaerobic mineralization in marine sediments from the Baltic Sea-North Sea transition." Mar. Ecol. Progr. Ser. 59: 39-54.

Kaplan, I. R., K. O. Emery, et al. (1963). "The distribution and isotopic abundance of sulfur in recent marine sediments off southern California." Geochemica Cosmochimica Acta(27): 297-331.

Kepkay, P. E. and F. O. Anderson (1985). "Aerobic and anaerobic metabolism of a sediment enriched with *Spartina* detritus." Mar. Ecol. Prog. Ser. 21: 153-161.

Kiene, R. P. and D. G. Capone (1984). "Effects of organic pollutants on methanogenesis, sulfate reduction, and carbon dioxide evolution in saltmarsh sediments." Marine Environ. Research 13: 141-160.

King, G. M. (1983). "Sulfate reduction in Georgia salt marsh soils: an evaluation of pyrite formation using ^{35}S and ^{55}Fe tracers." Limnol. Oceanogr. 28: 987-995.

King, G. M. (1988). "Patterns of sulfate reduction and sulfur cycle in a South Carolina salt marsh." Limnol. Oceanogr. 33: 376-390.

King, G. M., B. L. Howes, et al. (1985). "Short-term endproducts of sulfate reduction in a salt marsh: formation of acid volatile sulfides, elemental sulfur, and pyrite*." Geochimica et Cosmochimica Acta 49: 1561-1566.

King, G. M., M. J. Klug, et al. (1982). "Relations of soil water movement and sulfide concentrations to *Spartina alterniflora* production in a Georgia saltmarsh." Science 218: 61-63.

King, J. (1999). "Quantitative assessment of mercury methylation by phylogenetically diverse consortia of sulfate-reducing bacteria in salt marsh systems." Ph.D Thesis in Environmental Engineering, School of Civil and Environmental Engineering, Georgia Institute of Technology, Atlanta, Georgia.

King, J. K., F. M. Saunders, et al. (1999). "Coupling mercury methylation rates to sulfate reduction rates in marine sediments." Environmental Toxicology and Chemistry 18(7): 1362-1369.

King, J. K., J.B. Gladden, et al. (2001). Mercury Removal, Methylmercury Formation, and Sulfate-Reducing Bacteria Profiles in Wetland Mesocosms Containing Gypsum-Amended Sediments and *Scirpus californicus*. WSRC-TR-2001-00063, Department of Energy, Oak Ridge, TN.

Koch, M. S., I. A. Mendelssohn, et al. (1990). "Mechanism for the hydrogen sulfide-induced growth limitation in wetland macrophytes." Limnol. Oceanogr. 35: 399-408.

Koretsky, C. M., P. Van Cappellan, et al. (submitted). "Spatial and temporal trends in sediment biogeochemistry: Sapelo Island, Georgia." Geochimica et Cosmochimica Acta.

Korthals, E. T. and M. R. Winfrey (1987). "Seasonal and spatial variations in mercury methylation and demethylation in an oligotrophic lake." Appl. Environ. Microbiol. 53: 2397-2404.

Kostka, J. E. and G. W. Luther (1994). "Partitioning and speciation of solid phase iron in saltmarsh sediments." Geochim. Cosmoch. 58: 1701-1710.

Kostka, J. E. and G. W. Luther (1995). "Seasonal cycling of Fe in saltmarsh sediments." Biogeochemistry 29: 159-181.

Kostka, J. E., B. Gribsholt, et al. (2002). "The rates and pathways of carbon oxidation in bioturbated saltmarsh sediments.".Limnol. Oceanogr. 47: 230-240.

Kostka, J. E., A. Roychoudhury, et al. (submitted). "Rates and controls of sulfate reduction across gradients in space and time in Georgia saltmarsh sediments." Biogeochemistry.

Krabbenhoft, D. P., C. C. Gilmour, et al. (1998). "Methyl mercury dynamics in littoral sediments of a template seepage lake." Can. J. Fish. Aquat. Sci. 55: 835-844.

Krekeler, D., A. Teske, et al. (1998). "Strategies of sulfate-reducing bacteria to escape oxygen stress in a cynobacterial mat." FEMS Microbiology Ecology 25: 89-96.

Leemakers, W., M. Elskens, et al. (1993). "Geochemistry of mercury in an intertidal flat of the Scheldt Estuary." Netherl. J. Aquat. Ecol. 27: 267-277.

Li, J.-h., K. J. Purdy, et al. (1999). "Seasonal changes in ribosomal RNA of sulfate-reducing bacteria and sulfate reducing activity in a freshwater lake sediment." FEMS Microbiology Ecology 28: 31-39.

Lilley, A. K., M. J. Bailey, et al. (1996). "Diversity of mercury resistance plasmids obtained by exogenous isolation from bacteria of sugar beet in three successive years." FEMS Microbiology Ecology 20: 211-227.

Linthurst, R. A., Ed. (1980). An evaluation of aeration, nitrogen, pH, and salinity as factors affecting *Spartina alterniflora* growth: a summary. Kennedy, V.S., Academic Press.

Lord III, C. J. and T. M. Church (1983). "The geochemistry of salt marshes: Sedimentary ion diffusion, sulfate reduction, and pyritization." Geochimica Acta 47: 1381-1391.

Lovely, D. R. and J. P. Phillips (1994). "Novel processes for anaerobic sulfate production from elemental sulfur by sulfate-reducing bacteria." Appl. Environ. Microbiol. 60: 2394-2399.

Lowe, K. L., T. J. DiChristina, et al. (2000). "Microbiological and geochemical characterization of microbial Fe(III) reduction in salt marsh sediments." Geomicrobiology Journal. 17: 163-178.

Ludwicki, J. K. (1990). "*In vitro* methylation and demethylation of mercury compounds by the intestinal contents." Bulletin of Environmental Contamination and Toxicology 44: 357-362.

Lustwerk, R. L. and D. J. Burdige (1995). "Elimination of dissolved sulfide interference in the flow injection determination of CO2 by addition of molybdate." Limnol. Oceanogr. 40: 1011-1012.

Luther, G. W., P. J. Brendel, et al. (1998). "Simultaneous measurement of O2, Mn, Fe, I⁻, and S(-II) in marine pore waters with a solid-state voltammetric microelectrode." Limnol. Oceanogr. 43: 325-333.

Manz, W., M. Eisenbrecher, et al. (1998). "Abundance and spatial organization of gram-negative sulfate-reducing bacteria in activated sludge investigated by in situ probing with specific 16S rRNA targeted oligonucleotides." FEMS Microbiology Ecology 25: 43-61.

Marvin-Dipasquale, M. C. and R. Ormeland (1998). "Bacterial methylmercury degradation in Florida Everglades peat sediment." Envion. Sci. Technol. 22: 2556-2563.

Mason, R., N. Bloom, et al. (1998). "Investigation of porewater sampling methods for mercury and methylmercury." Environ. Sci. Technol. 32: 4031-4040.

Mason, R. P., W. F. Fitzgerald, et al. (1993). "Mercury biogeochemical cycling in a stratified estuary." Limnology and Oceanography 38(6): 1227-1241.

Matida, Y., H. Kumada, et al. (1971). "Toxicity of mercury compunds to aquatic organisms and accumulation of the compounds by organisms." Bulletin of Freshwater Fish. Res. Lab. Jpn. 21: 197-227.

Mendelssohn, I. A., K. L. McKee, et al. (1981). "Oxygen deficiency in *Spartina alterniflora* roots: metabolic adaption to anoxia." Science 214: 439-441.

Nakamura, K., T. Sakata, et al. (1988). "Volatilization of mercury compounds by methylmercury-volatilizing bacteria in Minamata Bay sediment." Bulletin of Environmental Contamination & Toxicology 41: 651-656.

Newell, R. C., A. S. Linley, et al. (1983). "Bacterial production and carbon conversion based on saltmarsh plant debris." Estuarine, Coastal and Shelf Science 17: 405-419.

Nriagu, J. O. (1979). The Biogeochemistry of Mercury in the Environment. Amersterdam, Elsevier/North-Holland.

Oremland, R. S., C. W. Culbertson, et al. (1991). "Methylmercury decomposition in sediments and bacterial cultures: involvement of methanogens and sulfate reducers in oxidative demethylation." Applied and Environmental Microbiology 57(1): 13--137.

Oremland, R. S., L. G. Miller, et al. (1995). "Methylmercury oxidative degradation potentials in contaminated and pristine sediments of the Carson River, Nevada." Applied and Environmental Microbiology 61(7): 2745-2753.

Ouattara, A. S. and V. A. Jacq (1992). "Characterization of sulfate-reducing bacteria isolated from Sengal ricefields." FEMS Microbiology Ecology 101: 217-228.

Pak, K.-R. and R. Bartha (1998). "Mercury methylation and demethylation in anoxic lake sediments and by strictly anaerobic bacteria." Applied and Environmental Microbiology 64(3): 1013-1017.

Pak, K.-R. and R. Bartha (1998). "Mercury methylation by interspecies hydrogen and acetate transfer between sulfidogens and methanogens." Applied and Environmental Microbiology 64(6): 1987-1990.

Parkes, R. J. (1987). Analysis of microbial communities within sediments using biomarkers. Ecology of Microbial Communities. M. Fletcher, T. R. G. Gray and J. G. Jones. Cambridge, Cambridge University Press: 147-177.

Parkes, R. J., N. J. E. Dowling, et al. (1993). "Characterization of sulphate-reducing bacterial populations within marine and estuarine sediments with different rates of sulphate reduction." FEMS Microbiology Ecology 102: 235-250.

Pereira, M. E., A. C. Duarte, et al. (1998). "An estimation of industrial mercury stored in sediments of a confined area of the Lagoon of Aveiro (Portugal)." Water Science Technology 37: 125-130.

Pomeroy, L. R., W. M. Darley, et al. (1981). Primary Production. Ecology of a Saltmarsh. L. R. Pomeroy and R. G. Wiegert. New York, Springer-Verlag.

Postgate, J. R. (1984). The sulphate-reducing bacteria. Cambridge, England, Cambridge University Press.

Qatibi, A. I., A. Bories, et al. (1991). "Sulfate reduction and anaerobic glycerol degradation by a mixed microbial culture." Current Microbiol. 22: 47.

Ramsing, N. B., M. Kuhl, et al. (1993). "Distribution of sulfate-reducing bacteria, O2, and H2S in photosynthetic biofilms determined by oligonucleotide probes and microelectrodes." Applied & Environmental Microbiology 59(11): 3840-9.

Raskin, L., L. K. Poulsen, et al. (1994). "Quantification of methanogenic groups in anaerobic biological reactors by oligonucleotide probe hybridization." Appl. Environ. Microbiol 60: 1241-1248.

Reddy, K. R. and E. M. D'Angelo (1997). "Biogechemical Indicators to Evaluate Pollutant Removal Efficiency in Constructed Wetlands." Wat. Sci. Tech. 35(5): 1-10.

Regnell, O. (1990). "Conversion and partitioning of radio-labelled mercury chloride in aquatic model system." Can. J. Fish. Aquat. Sci. 47: 548.

Richards, F. A. (1965). Anoxic basins and fjords. Chemical Oceanography. J.P.Riley and G.Skirrow. New York, Academic Press. 1: 611-645.

Ridley, W. P., L. J. Dizikes, et al. (1977). "Biomethylation of toxic elements in the environment." Science 197: 329-332.

Robinson, J. B. and o. H. Tuovinen (1984). "Mechanisms of microbial resistance and detoxification of mercury and organomercury compunds: physiological, biochemical, and genetic analysess." Microbol. Rev. 48: 95-124.

Rochelle, P. A., M. K. Wetherbee, et al. (1991). "Distribution of DNA sequences encoding narrow- and broad-spectrum mercury resistance." Applied and Environmental Microbiology 57(6): 1581-1589.

Rood, B. E. (1996). "Wetland mercury research: a review with case studies." Current Topics in Wetland Biogeochemistry 2: 73-108.

Rooney-Varga, J. N., R. Devereux, et al. (1997). "Seasonal changes in the relative abundance of uncultivated sulfate-reducing bacteria in salt marsh sediment and in the rhizosphere of *Spartina alterniflora*." Applied and Environmental Microbiology 63(10): 3895-3901.

Rudd, J. W. M. (1995). "Sources of methylmercury to freshwater ecosystems." Wat. Air Soil Pollut. 80: 697-713.

Rugh, C. L., J. F. Senecoff, et al. (1998). "Development of transgenic yellow poplar for mercury phytoremediation." Nature Biotechnology 16: 925-928.

Santschi, P. H., M. A. Allison, et al. (1999). "Sediment transport and Hg recovery in Lavaca Bay, as evaluated from radionucleotide and Hg distributions." Environ. Sci. Technol. 33: 378-391.

Schubauer, J. P. and C. S. Hopkinson (1984). "Above- and belowground emergent macrophyte production and turnover in a coastal marsh ecosystem, Georgia." Limnol. Oceanogr. 29: 1052-1065.

Senior, E., E. B. Lindstrom, et al. (1982). "Sulfate reduction and methanogenesis in the sediment of a saltmarsh on the east coast of the United Kingdom." : 987-996.

Shariat, M., A. C. Anderson, et al. (1979). "Screening of common bacteria capable of demethylation of methylmercuric chloride." Bulletin of Environmental Contamination and Toxicology 21: 255-261.

Shea, M. L., R. S. Warren, et al. (1974). "Biochemical and transplantation studies of the growth form of *Spartina alterniflora* on Conmnecticut salt marshes." Ecology 56: 461-466.

Shea, M. L., R. S. Warren, et al. (1975). "Biogeochemical and transplantation studies of the growth form of *Spartina Alterniflora* on Connecticut salt marshes." Ecology 56: 461-466.

Short, F. T., M. W. Davis, et al. (1985). "Evidence for phosphorus limitation in carbonate sediments of the seagrass *Syringodium filiforme*." Estuarine, Coastal and Shelf Science 20: 419-430.

Silverberg, N., J. M. Gagnon, et al. (1995). "A benthic mesocosm facility for maintaining soft-bottom sediments." Netherlands Journal of Sea Research 34(4): 289-302.

Smit, E., P. Leeflang, et al. (1997). "Detection of shifts in microbial community structure and diversity in soil caused by copper contamination using amplified ribosomal DNA restriction analysis." FEMS Microbiology Ecology 23: 249-261.

Smit, E., A. Wolters, et al. (1998). "Self-transmissible mercury resistance plasmids with gene-mobolizing capacity in soil bacterial populations: influence of wheat roots and mercury addition." Applied and Environmental Microbiology 64(4): 1210-1219.

Smith, R. L. and M. L. Klug (1981). "Reduction of sulfur compounds in the sediments of a eutrophic lake basin." Applied Environmental Microbiology 41: 1230-1237.

St. Louis, V. L., J. W. M. Rudd, et al. (1995). "Wet deposition of methylmercury in Northwestern Ontario compared to other geographic locations." Wat. Air Soil Pollut. 80: 405-414.

Steffan, R. J., E. T. Korthals, et al. (1988). "Effects of acidification on mercury methylation, demthylation, and volatization in sediments from an acid-susceptible lake." Applied and Environmental Microbiology 54(8): 2003-2009.

Stein, E. D., Y. Cohen, et al. (1996). "Environmental distribution and transformation of mercury compunds." CRC Crit. Rev. Environ. Sci. Technol. 26: 1-43.

Stookey, L. L. (1970). "Ferrozine - a new spectrophotometric reagent for iron." Analytical Chemistry 42: 779-781.

Sullivan, M. J. and F. C. Daiber (1974). "Response in production of cord grass, *Spartian alterniflora*, to inorganic nitrogen and phosphorus fertilizer." Chesapeake Science(15): 121-123.

Summers, A. O. and S. Silver (1978). "Microbial transformations of metals." Annual Review of Microbiology 32: 637-658.

Tabatabi, M. A. (1974). "A rapid method for determination of sulfate in water samples." Environmental Letters 7: 237-243.

Teal, J. M. and B. L. Howes (1996). "Interannual variability of a salt-marsh ecosystem." Limnol. Oceanogr. 41: 802-809.

Teske, A., C. Wawer, et al. (1996). "Distribution of sulafte-reducing bacteria in a stratified fjord (Mariager Fjord, Denmark) as evaluated by most-probable-number counts and denaturing gradient gel electrophoresis of PCR-amplified ribosomal DNA fragments." Applied and Environmental Microbiology 62(4): 1405-1415.

Thamdrup, B., K. Finster, et al. (1994). "Thiosulfate and sulfite distributions in porewaters of marine sediments related to manganese, iron, and sulfur geochemistry." Geochemica et Cosmochimica 58: 67-73.

Trevors, J. T. (1986). "Mercury resistant bacteria isolated from sediment." Bulletin of Environmental Contamination and Toxicology 36: 405-411.

Trimmer, M., K. J. Purdy, et al. (1997). "Process measurement and phylogenetic analysis of the sulfate reducing bacterial communities of two contrasting benthic sites in the upper estuary of the Great Ouse, Norfolk, UK." FEMS Microbiology Ecology 24: 333-342.

Troelsen, H. and B. B. Jorgensen (1982). "Seasonal dynamics of elemental sulfur in two coastal sediments." Coastal Shelf Science 15: 255-266.

Tseng, C. M., A. d. Diego, et al. (1998). "Cryofocusing coupled to atomic absorption spectrometry for rapid and simple mercury speciation
in environmental matrices." Journal of Analytical Atomic Spectrometry(8): 755-764.

Turner, R. R. and G. R. Southworth (1999). Mercury-Contaminated Industrial and Mining Sites n North America: an Overview with Selected Case Studies. Mercury Contaminated Sites: Characterization, Risk Assessment and Remediation. R. Ebinghaus, R. R. Turner, L. D. de Lacerda, O. Vasiliev and W. Salomons. New York, NY, Springer.

Urban, N. R. and P. L. Brezonik (1993). "Transformation of sulfur in sediment microcosms." Can. J. Fish. Aquat. Sci. 50: 1946-1960.

USDHHS (1992). Toxicological Profile for Mercury: Update, U.S. Department of Health and Human Services.

USDI (1995). Preliminary natural resources survey - LCP chemical site, Glynn County, GA. Memorandum. Washington, D.C., U.S. Department of the Interior.

USEPA (1997). Mercury Study Report to Congress. EPA-452/R-97-009, Office of Air Quality and Standards and Office of Research and Development, United States Environmental Protection Agency, Washington, D.C.

USEPA (1998). Method 1630: Methyl mercury in water by distillation, aqueous ethylation, purge and trap, and cold vapor atomic fluorescence spectrometry. U.S. Environmental Protection Agency Office of Water, Washington, D.C.

USEPA (1999). Draft Method 245.7: Mercury in Water by Cold Vapor Atomic Fluorescence Spectrometry. U.S. Environmental Protection Agency Office of Water, Washington, D.C.

USEPA (1999). Georgia NPL Site Summaries: LCP Chemicals Georgia Inc., U.S. Environmental Protection Agency, Waste Management Division. 1999.

USEPA (1999). Method 1631, Revision B: Mercury by oxidation, purge and trap, and cold vapor atomic fluorescence spectrometry. U.S. Environmental Protection Agency Office of Water, Washington, D.C.

Van Capellen, P. and Y. Wang (1995). Metal Contaminated Aquatic Sediments. H. E. Allen. Chelsea, MI, Ann Arbor Press: 22-64.

Vander Maarel, M. J. E., M. Jansen, et al. (1996). "Demethylation of Dimethylsulfoniopropionate to 3-S-methylmercaptopropionate by marine sulfate-reducing bacteria." Applied and Environmental Microbiology 62(11).

Watras, C. J., N. S. Bloom, et al. (1995). "Methylmercury production in the anoxic hypolimnion of a dimictic seepage lake." Water, Air, and Soil Pollution 80: 735-745.

Webb, D. G. (1998). "Effects of eutrophication on coastal marine systems: Perspectives from 22 years of mesocosm-based research at the Marine Ecosystems Research." Aquatic Ecology.

Weber, J. H. (1993). "Review of possible paths for abiotic methylation of mercury(II) in the aquatic environment." Chemosphere 26: 2063-2077.

Weber, J. H., R. Evans, et al. (1998). "Conversion of mercury (II) into mercury (0), monomethylmercury cation, and dimethylmercury in saltmarsh sediment slurries." Chemosphere 36(7): 1669-1687.

Weis, P., J. Weis, et al. (1986). "Effects of Environmental Factors on Release of Mercury from Berry's Creek (New Jersey) Sediments and its Uptake by Killifish *Fundulus heteroclitus*." Environmental Pollution, Series A: Ecological and Biological 40(4): 303-315.

Wellsbury, P., R. A. Herbert, et al. (1996). "Bacterial activity and production in near-surface estuarine and freshwater sediments." FEMS Micribiology Ecology 19: 203-214.

Wheatley, B. and S. Paradis (1996). "Balancing human exposure, risk and reality: questions raised by the Canadian Aborginal methylmercury program." Neurotoxicology 17: 241-250.

White, C., A. K. Sharman, et al. (1998). "An integrated microbial process for the bioremediation of soil contaminated with toxic metals." Nature Biotechnology 16: 572-575.

Widdel, F. (1988). Microbiology and ecology of sulfate- and sulfur-reducing bacteria. Biology of Anaerobic Microorganisms. A. J. B. Zehnder. New York, John Wiley and Sons.

Widdel, F. and F. Bak (1992). Gram-negative mesophilic sulfate-reducing bacteria. The Prokaryotes: a handbook on the biology of bacteria: ecophysiology, isolation, identification, applications. A. Balows, H. G. Truper, M. Dworkin, W. Harder and K.-H. Schleifer. New York, Springer-Verlag: 3352-3378.

Wiegert, R. G. and R. L. Wetzel (1978). Simulation experiments with a fourteen-compartment model of a *Spartina* salt marsh. Marsh-estuarine systems simulation. R. Dame. Columbia, SC, University of South Carolina Press.

Wind, T. and R. Conrad (1995). "Sulfur compounds, potential turnover of sulfate adn thiosulfate, and numbers of sulfate-reducing bacteria in planted and unplanted paddy soil." FEMS Microbiology Ecology 18: 257-266.

Winfrey, M. R. and D. M. Ward (1983). "Substrates for sulfate reduction and methane production in intertidal sediments." Applied Environmental Microbiology 1983: 193-199.

Winfrey, M. R. and J. G. Zeikus (1977). "Effect of sulfate on carbon and electron flow during microbial methanogenesis in freshwater sediments." Applied Environmental Microbiology 33: 275-281.

Winger, P. V., P. J. Lasier, et al. (1993). "Toxicity of sediments and pore water from Brunswick Estuary, Georgia." Environ. Contam. Toxicol. 25: 371-376.

Zhang, L. and D. Planas (1994). "Biotic and abiotic mercury methylation and demethylation in sediments." Bulletin of Environmental Contamination and Toxicology 52: 691-696.

Zuckerlandl, E. and L. Pauling (1965). "Molucules as documents of evolutionary history." J. Theoret. Biol. 8: 357-366.

Zumdahl, S. S. (1993). Chemistry. Lexington, MA, D. C. Heath.